UTILIZATION OF DRILL - BIT VIBRATIONS AS A DOWNHOLE SEISMIC SOURCE

A DISSERTATION
SUBMITTED TO THE DEPARTMENT OF GEOPHYSICS
AND THE COMMITTEE ON GRADUATE STUDIES
OF STANFORD UNIVERSITY
IN PARTIAL FULFILLMENT OF THE REQUIREMENTS
FOR THE DEGREE OF
DOCTOR OF PHILOSOPHY

By
James Ward Rector III

September 1990

ABSTRACT

A new technique has been developed to provide borehole seismic data. The technique, known as the TOMEX Survey, or drill bit VSP, uses the vibrations produced by a working rotary drill bit as a source of seismic energy at the bottom of a drill hole. The energy produced by a rotary drill bit can be used to seismically image formations around the borehole without using conventional techniques such as velocity surveys or vertical seismic profiling (VSP).

The first chapter describes the fundamental acquisition and data processing used in the technique. A pilot sensor is strapped onto the top of the drillstring and receivers are deployed on the earth's surface. As the drill bit impacts the formation, seismic energy is released into the earth and a longitudinal wave is initiated which travels up the drillstring. To process the drill-bit signals, cross-correlation functions between the pilot sensor response and the receiver responses are computed. The cross-correlation functions are modified to account for the travel of the longitudinal wave from the drill bit up the drillstring to the pilot sensor. The modified data are an approximation to the data that would be recorded if the pilot sensor were located in the drillstring just above the drill bit rather than at the top of the drillstring.

The second and third chapters characterize the S/N and bandwidth of the drill-bit signals recorded at the surface as well as the radiation pattern and seismic wave modes genetrated by the drill bit. The drill-bit signals were found to be wideband, extending from frequencies below 10 Hz to frequencies of 85 Hz and above. The body waves radiated into the earth by the drill bit were found to primarily consist of P-waves along the axis of the borehole and SV waves perpendicular to the axis. Besides these body waves, other waves radiated by the drill bit include rig-generated energy, head waves, and drillstring multiple energy.

The final chapter compares drill-bit data with conventional VSP and checkshot data. The arrival times were found to match closely and the reflected arrivals tied well. The measure-while-drilling nature of the drill bit data was used to monitor and guide the position of the drill bit on the surface seismic time section.

TABLE OF CONTENTS

TABLE OF CONTENTS
(Concluded)

LIST OF ILLUSTRATIONS

LIST OF ILLUSTRATIONS
(Continued)

LIST OF ILLUSTRATIONS
(Continued)

LIST OF ILLUSTRATIONS
(Concluded)

CHAPTER 1

OVERVIEW: UTILIZATION OF DRILL-BIT VIBRATIONS AS A DOWNHOLE SEISMIC SOURCE

1.1 Introduction

Over the past several years there has been a widespread interest within the exploration and production community in the development of a downhole seismic energy source. The interest has primarily come from the emergence of Vertical Seismic Profiling (VSP) as a subsurface imaging tool (Hardage, 1985) and the development of cross-borehole tomography as a reservoir imaging technique (Harris, 1988; Macrides, et al, 1988; and Justice, et al, 1989). In this chapter, a downhole source is introduced whose energy is provided by the drill-bit impacts on the formation. The data acquisition and processing techniques that are used to extract the drill-bit signal from surface measurements is termed seismic-while-drilling, the TOMEX® Survey, or drill-bit VSP. Drill-bit VSP holds several advantages over other downhole energy sources and conventional VSP. Specifically, drill-bit VSP surveys are acquired without any downhole instrumentation. This means there is no interruption to drilling, no lost rig time, and no risk to the borehole or a downhole tool while the seismic data are being acquired. With most other downhole sources or with conventional VSP, drilling must be interrupted and a tool must be lowered into the borehole to acquire the data. In many boreholes, a casing string must be set prior to lowering the tool into the borehole. Moreover, some downhole sources, particularly airguns and explosives, can damage a borehole when activated.

Another advantage to using the drill bit as a downhole source is that measure-while-drill (MWD) seismic surveys are possible. MWD logging and surveying techniques are used by drillers to optimize drilling parameters and to locate the drill bit in terms of spatial position and position within the geologic section. The seismic

data provided by the drill bit can be used to locate the drill bit within a seismic time section (a case study of this use is discussed in Chapter 4). Moreover, unlike other MWD techniques that yield current conditions at the drill bit, the seismic reflections from below the drill bit can be processed to obtain information regarding upcoming formations. This 'look-ahead' feature of the drill-bit energy source can be used to predict upcoming reflectors both directly below the drill bit and laterally away from the drill bit. Based on the MWD drill-bit data, the course of the wellbore can be changed, and drilling parameters such as mud weight or casing and coring depths can be altered, potentially improving the efficiency and the success ratio of drilling wells.

The drill-bit energy source and the techniques used to exploit it in the drill-bit VSP technique have some disadvantages when compared to conventional VSP and other downhole seismic sources. Most obvious is the uncontrolled nature of the drill-bit vibrations. As the drilling process is not altered during the acquisition of the drill-bit data, there is no control over the timing, amplitude, frequency content, or the directivity of the vibrations resulting from the drill bit/formations interactions. Furthermore, since it typically takes weeks or even months to drill a well, multiple drill-bit source positions along the entire length of the well can be very time consuming to obtain. Moreover, the lack of downhole instrumentation means that the drill-bit source signal cannot be directly monitored. Consequently, in examining drill-bit characteristics such as amplitude and frequency content, the source effects may not be separable from the propagation effects.

There are very few published works relating to drill-bit vibrations analysis. The idea of using drill-bit vibrations as an energy source for subsurface imaging was first discussed by Weatherby (1936). He proposed using the discrete impulses generated by a cable-tool drilling assembly as a seismic energy source (rotary drilling was still in its infancy in 1936). A study of drill-bit vibrations recorded downhole was done by Deily, et al (1968). This work, like others published in the drilling engineering

literature (Dareing, 1968; Dareing, 1982), were primarily interested in the effects of drill-bit vibrations on drilling efficiency. In Deily, et al (1968), a downhole recording 'sub' consisting of strain gauges and accelerometers measuring axial, transverse, and torsional vibrations was positioned within the lower section of the drillstring. These recordings indicated that axial vibrations were related to drill bit interactions with the formation, whereas torsional vibrations primarily recorded the rotation of the drillstring. The frequency spectrum of the axial vibrations exhibited a dominant frequency of three times the rotary rate during rough drilling, and a 'random characteristic' in normal drilling. It cannot be ascertained what was meant by a 'random characteristic'. Based on drill-bit VSP data displayed in this thesis, this could mean wideband energy.

Studies by Lutz, et al (1972) and Quichaud (1979) indicated that the amplitudes of an accelerometer recording at the top of the drillstring were also related to drill bit/formation interactions. Out of these measurements a 'SNAP' log was produced which correlated the vibration amplitude with the hardness of the formation being drilled. Higher amplitude vibrations were observed when drilling harder formations. These studies also indicated that the dominant vibrations occurred at a frequency of three times the rotary rate. Higher frequencies thought to be due to the interaction of the individual bit teeth were also observed. The frequency corresponding to three times the rotary rate was interpreted as being related to the interaction of an entire cone with the formation, as a standard rotary drill bit consists of three cones.

1.2 Model of the Drill-Bit Source Signal

A model of the drill-bit signal used in the drill-bit VSP technique is shown in Figure 1-1. In this model, the drill-bit signal is created by the axial impacts of the drill-bit teeth and cones on the formation. A rotary cone roller bit breaks rock through shear and compressive failure of the formation (Adams, 1986). As shown in Figure 1-1, the principal force component of this type of drill-bit action is directed

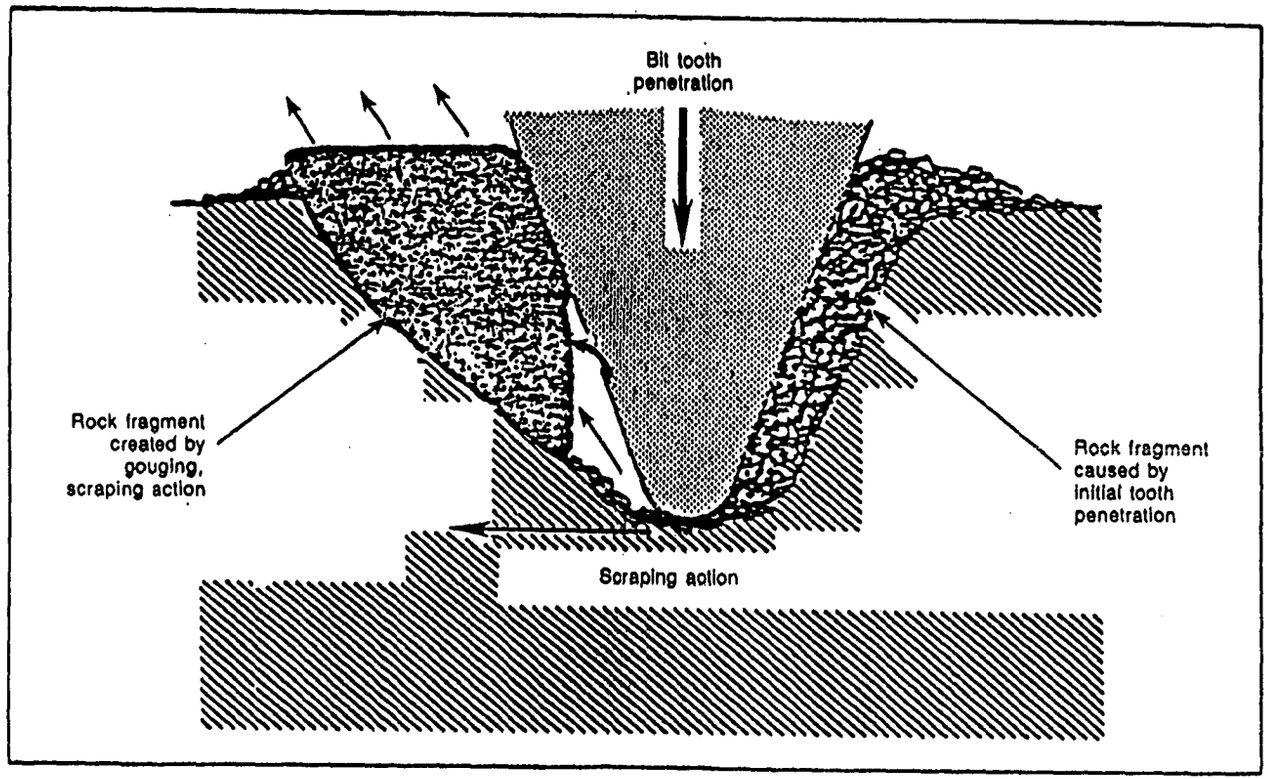

Figure 1-1. (Taken from Adams, 1986). Rock breaking and cutting action of a conventional roller-cone bit tooth.

axially against the formation. A laboratory study by Shepard and Lesage (1988) indicated that the ratio of vertical to tangential force created by the action of a drill bit tooth on the formation was on the order of 10 to 1. In contrast to the roller cone bits, PDC and diamond bits remove rock through a shearing or grinding action (Vennin, 1989) and little axial drill-bit signal would be anticipated. Data recorded on wells drilled with PDC drill bits appear to bear this out, since lower levels of axial energy are detected (Marion, 1990).

The signature of the drill-bit signal is more difficult to model. The previous studies cited (Deily, et al, 1968; Lutz, et al, 1972) showed that low frequencies of three times the rotary rate (3 to 7 Hz) were often the largest signals produced by the drill bit. Besides these frequencies, there did not appear to be a dominant frequency for the drill-bit vibrations. For convenience, we will assume that the drill-bit vibrations are random impulses having a white spectrum. Such a source signature could be generated by axial 'bit bounce' (Dareing, 1984).

1.3 Data Acquisition

Figure 1-2 shows a simple model of the signal paths and the surface recordings used to process drill-bit signals for an inverse VSP geometry. The random axial impulses generated by the bit/formation impacts activate a wave traveling up the drillstring and waves that travel into the earth. These waves are recorded by a sensor positioned at the top of the drillstring and by receivers placed near the earth's surface. As discussed in Section 1.4, the top-of-drillstring sensor output is used as a pilot signal for cross-correlation with the receiver located in the earth. A typical pilot sensor configuration used in the data shown in this thesis is a vertically-oriented accelerometer positioned on the swivel above the rotating part of the drillstring. Another configuration uses horizontal accelerometers as well as a vertical accelerometer. Each of these configurations is discussed in more detail in Chapter 2. The earth-receiver data displayed are primarily from standard 10 Hz vertical geophone

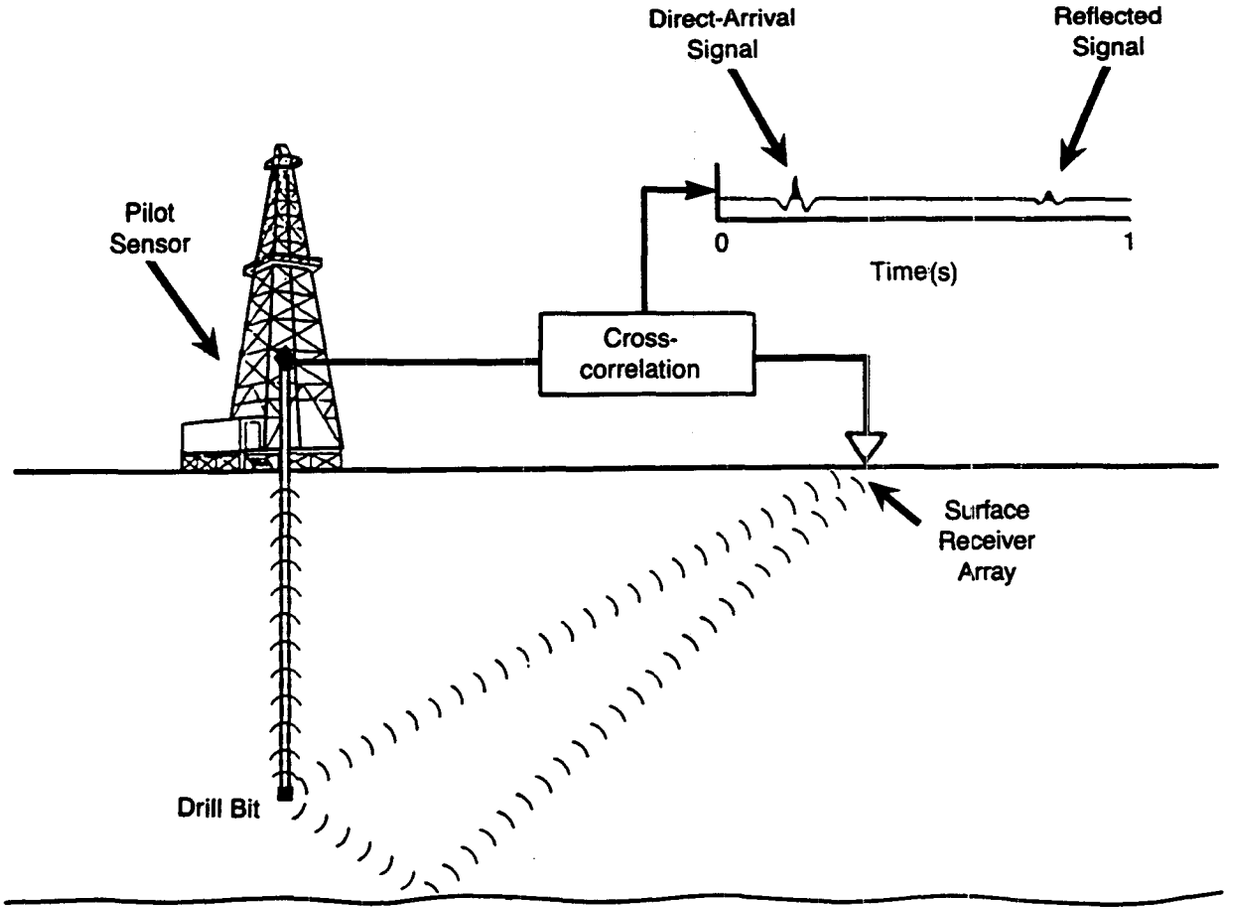

Figure 1-2. Acquisition geometry and cross-correlation processing used in the drill-bit VSP technique.

strings, although examples of horizontal geophone and hydrophone data are also shown.

The monitoring and recording of drill-bit signals is somewhat analogous to mud logging. Drill-bit signals, like cuttings, are available nearly continuously over the well drilling period (with the exception of connections and trips). The data displayed in this thesis were recorded with a system specially constructed for the long periods of well drilling (Rector, et al, 1986). In this system, the data are received by the top-of-drillstring and the earth receivers, and telemetered back to a central recording unit on the drill pad. In the central recording unit, the analog recordings are digitized (with 12 bits/sample) at a 4 ms sample rate and stored on digital tape. The amount of data stored on tape can be quite large if the drilling is monitored continuously. For example, if a well takes 30 days to drill and 40 channels are recorded, the number of samples is 2.6×10^{10} (3.1×10^{12} bits). These sample totals are comparable to 3-D seismic survey data volumes. The continuous signals from the drill bit are compressed to a small fraction of these recording times by computing cross-correlation functions.

1.4 Cross-Correlation

To improve the drill-bit S/N, compress the continuous recordings, and measure traveltimes, a cross-correlation function is computed between the pilot signal recorded at the top of the drillstring and a signal recorded by the earth receiver. This technique was also proposed by Staron, et al (1988). The cross-correlation functions displayed in the following chapters are computed using a linear convolution, 'overlap-add method' (Oppenheim and Schafer, 1975). They are normalized based on the total record length (in samples). The use of cross-correlation to measure arrival times is illustrated by a simple model of the system shown in Figure 1-2. In this model it is assumed that the drill bit acts at a node between two independent, linear, time-invariant systems corresponding to wave propagation in the drillstring and wave

propagation in the earth. (In Chapter 3, this model is expanded to incorporate some of the interactions between the two systems.) Let DS(t) correspond to the response of the top-of-drillstring pilot sensor to an impulse at the drill bit, representing wave propagation in the drillstring, and G(t) correspond to the response of the earth receiver to a drill-bit impulse. If the continuous drill-bit signal is S(t), then the pilot signal is:

$$P(t) = S(t) * DS(t) , \tag{1-1}$$

and the earth receiver signal is:

$$G(t) = S(t) * E(t) . \tag{1-2}$$

The cross-correlation function between these two recordings is:

$$cc(\tau) = P(-t) * G(t) = S(-t) * DS(-t) * S(t) * E(t) \tag{1-3}$$

and we can rearrange terms to get:

$$cc(\tau) = S(-t) * S(t) * DS(-t) * E(t) \tag{1-4}$$

The term S(-t) * S(t) is the autocorrelation of the drill-bit source signal. Assuming that the drill-bit signal is white, the cross-correlation between the pilot and earth recordings becomes:

$$cc(\tau) = DS(-t) * E(t) \tag{1-5}$$

To see how the traveltimes of signals through the earth are represented in the cross-correlation function, assume that $DS(t) \cong \delta(t-t_\rho)$, where t_ρ is the traveltime between the drill bit and the pilot sensor. Then we have:

$$cc(\tau) \cong E(t+t_\rho) . \tag{1-6}$$

Thus, the traveltimes of signals from the drill bit to the earth receiver through the earth are shifted in the cross-correlation by the traveltime of the signal from the drill bit to the pilot sensor. The cross-correlation provides a means to estimate traveltime through the earth without knowing the times that the signals were produced at the drill bit.

In vibroseis cross-correlation, the recording or 'sweep and listen' time is finite, typically from 10 to 30s. The output correlation function is computed with shifts, τ, ranging from $\tau = 0$ to $\tau = 4$ to 8s. When computing drill-bit signal cross-correlations, much longer recording times are available. A typical recording time used in the output cross-correlations shown in this thesis is the time required to drill a 10m 'joint' of drillpipe. For sedimentary rocks at moderate depth, drill-bit penetration rates vary from 1 m/hr to 100 m/hr, resulting in 10m recording times ranging from 6 minutes to 10 hours. The output drill-bit cross-correlation functions are computed for a range of shifts, τ, that is comparable to vibroseis outputs. However, as we shall see in a later section, the term DS(-t) in the drill-bit correlations can create drill-bit arrivals occurring at shifts, τ, less than $\tau = 0$ (i.e., coherent drill-bit signal can arrive at the earth receiver before it arrives at the pilot sensor), requiring that negative as well as positive values of τ be computed.

A drillpipe-joint recording length has several attractive characteristics. For one, the drillstring length, and therefore DS(t), is fixed during the recording time. Assuming the drill-bit signal is stationary, only one filter is applied to each correlation

to remove DS(t) (this filter is discussed in more detail in Section 1.6). Secondly, a 10m vertical source array is typically less than 1/4 λ_z, where λ_z is the smallest apparent vertical wavelength of the drill-bit P-wave arrivals traveling through the earth at seismic frequencies. Arrivals with vertical wavelengths greater than 1/4 λ_z suffer very little attenuation through moveout of the drill bit. (Chapter 3 discusses the apparent vertical wavelengths observed in a series of cross-correlation functions.) Finally, the resulting depth sampling interval is 10m, which is typically less than the nyquist limit (Chapter 3). Although finer sampling intervals could be used, there is no benefit to producing more correlations, since the drill-bit arrivals are adequately represented at 10m intervals. With correlations at finer intervals, the subsequent data volumes are higher. For cross-borehole surveys requiring higher frequencies or shear wave surveys, it may be necessary to shorten the vertical source array and sample the drill-bit wavefield at finer vertical intervals to retain smaller vertical wavelengths.

The data compression achieved in representing a 10m period of drilling with an 8s cross-correlation function ranges from 45 to 4500, depending on the drill-bit penetration rate. The resulting improvement in the ratio of drill-bit signal to stationary, uncorrelated noise is on the order of (data compression)$^{1/2}$ (Aki and Richards, 1980). Thus, signal-to-noise ratios (S/N's) that are much lower than conventional vibroseis S/N's can produce identifiable arrivals in the output cross-correlations. (Chapter 2 gives a more detailed discussion of drill-bit signals in the presence of incoherent noise.)

1.5 Characterization of Top-of-Drillstring Impulse Response and Wave Propagation in Drillstring

The cross-correlation function described in the previous section can be computed between any two sensor outputs. Kostov (1988) showed that drill-bit signals could be detected in the cross-correlation between two geophone recordings. The principal advantage of the top-of-drillstring pilot sensor is that the recorded signal

will be shown to contain primary longitudinal-wave arrivals from the drill bit with a measurable time delay and secondary arrivals that are simple multiples. In contrast, the geophone array response consists of primary arrivals of typically unknown delays. (These delays are often obtained in a checkshot survey performed after a well is completed.) Moreover, as discussed in Chapter 3, the surface geophone response to an impulse at the drill bit is actually much more complicated than the direct and reflected arrivals in Figure 1-2. Other drill-bit arrivals that are not simple multiples of the primary arrivals from the drill bit also exist on a typical geophone response.

To evaluate the impulse response of the top-of-drillstring sensor, it is assumed that wave propagation in a drillstring is analogous to wave propagation along the length of a slender, elastic rod, whose length is much greater than the diameter (Drumheller, 1988). Torsional and dispersive flexural waves (Kolsky, 1963) can also propagate along a slender rod, however these waves exhibit primarily radial and tangential particle motions that do not contribute significantly to the response of an axially-oriented accelerometer. Following Drumheller (1988), the one-dimensional equation for elastic longitudinal wave propagation along a slender, elastic rod of uniform material is:

$$\delta^2 F/\delta t^2 = Z^2(x)\, \delta^2 F/\delta m^2 , \qquad (1\text{-}7)$$

where,

$m = \int_0^x \rho\, a\, (\xi)\, d\xi$,

$Z(x)$ = $\rho\, a(x)c$, and ρ is the density, $a(x)$ is the cross-sectional area, $c = (E/\rho)^{1/2}$, and E is the Young's modulus of the rod material,

x = the position along the rod, and

F = force.

Using common values of E for steel (Roark, 1954), a longitudinal wave velocity in the drillstring between 4960 and 5160 m/s is predicted. Assuming a constant-density rod, the displacement reflection (R) and transmission (T) coefficients at an interface where the cross-sectional area, a(x), changes are:

$$R = a(x_1) - a(x_2) / a(x_1) + a(x_2) , \tag{1-8}$$

and

$$T = 2\, a(x_1) / a(x_1) + a(x_2) \tag{1-9}$$

where x_1 is a position in the incident section of the drillstring and x_2 is a position in the transmitted section.

A drillstring is comprised of two principal sections, the Bottom-Hole-Assembly (BHA) consisting primarily of drill collars and stabilizers, and the drillpipe section consisting of uniform drillpipe separated by threaded tool joints. For longitudinal wave propagation at seismic frequencies (< 100 Hz), the effects of the tool joints and stabilizers are negligible (Drumheller, 1988), and the drillstring can be considered to consist of a uniform BHA section and a uniform drillpipe section. A typical reflection coefficient magnitude at the interface between drill collars of inner diameter 0.1m, thickness 0.067m, and drillpipe of inner diameter 0.1m and thickness 0.008m is 0.77.

The wave propagation between the drill bit and top-of-drillstring pilot sensor can be investigated in the autocorrelation of the pilot signal, $ac_p(\tau)$, where:

$$ac_p(\tau) = [S(-t) * S(t)] * [DS(-t) * DS(t)] . \tag{1-10}$$

For a white drill-bit signal the autocorrelation becomes:

$$ac_p(\tau) = [DS(-t) * DS(t)] \tag{1-11}$$

Figure 1-3 illustrates a series of autocorrelation functions computed from the recordings of the vertical accelerometer taken over an interval of a well where the depths of the drill bit ranged from 1250 to 1550m. The traces in the figure were computed over an average recording time of 30 minutes, creating a vertical drill-bit source array spanning approximately 10m. However, the length of the drillstring did not change during this recording time and hence the array only applies to signals traveling in the earth. The autocorrelations have had a 10 to 45 Hz bandpass filter applied and the display is scaled to the zero lag value.

Either side of the autocorrelation function can be interpreted as approximating the drillstring impulse response, DS(t), if it is assumed that the primary drill-bit arrival at the top of the drillstring is substantially larger than the multiples that follow. (Without this assumption, the events observed in the autocorrelation cannot be attributed to distinct arrivals.) Multiple arrivals traveling in the drillpipe can be identified based on their moveout with drillpipe length. Each time another joint of drillpipe is added, the length of the drillpipe and the traveltime of the drillpipe multiple increases. The events labeled in the figure as 'drillpipe multiples' have this characteristic. Based on the moveout of the multiples, the longitudinal-wave phase velocity in the drillpipe is estimated to be 4758 m/s. Since little dispersion is anticipated in the seismic frequency band (Drumheller, 1988), the group velocity of the drillpipe should be nearly equivalent to the phase velocity.

Assuming a group velocity of 4758 m/s, the travelpath of the drillpipe multiples can be estimated from the autocorrelation times. For example, the delay of the first-order drillpipe multiple at a depth of 1550m predicts a travelpath of about 2650m. This length is about 15 percent less than the two-way travelpath all the way up and down the drillstring, indicating that this arrival is being reflected from an interface before it reaches the bottom. The predicted interface is about 240m above the bottom, about the length of the BHA (254m). The close agreement in these depths is strongly

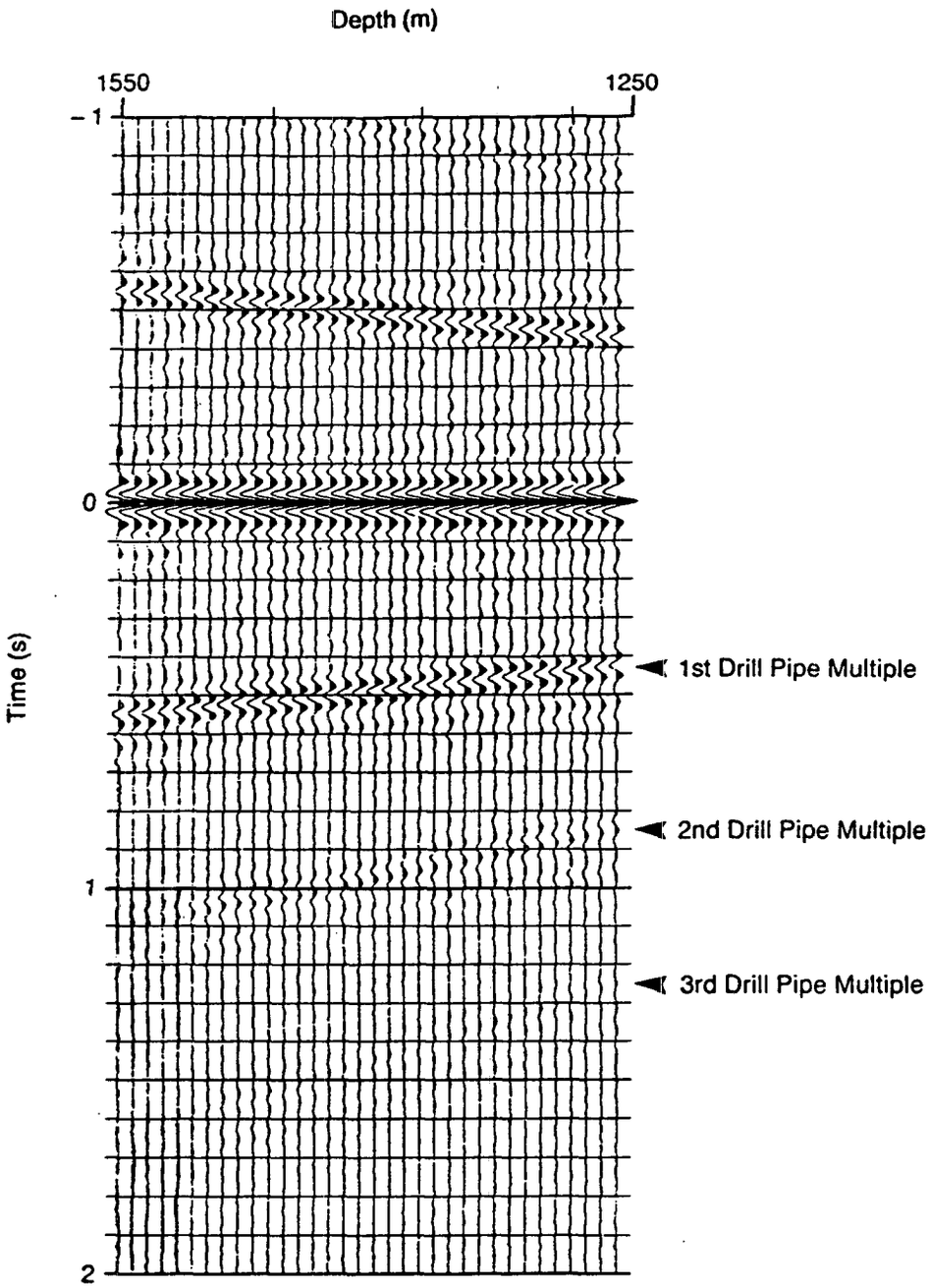

Figure 1-3. Vertical accelerometer pilot signal autocorrelations computed over a drill-bit depth range from 1250 to 1550m. The data have a 10 to 45 Hz bandpass filter applied and are scaled to the zero-lag.

suggestive that the reflecting interface is the BHA/drillpipe interface and that there is little dispersion in the drillpipe. Figure 1-4 summarizes the travelpaths of the primary and first order drillpipe multiple arrivals. If we assume that the velocity in the BHA is equivalent to the velocity in the drillpipe, we can estimate the time shift, t_ρ, in Equation 1-6 as $z_{DS}/4758$, where z_{DS} is the length of the drillstring (in meters). After correcting the correlated data by t_ρ, the traveltimes of drill-bit arrivals through the earth are equal to cross-correlation time.

The measured longitudinal wave velocity of 4758 m/s is approximately 6 percent lower than theoretical values predicted by Roark (1954) and used by Drumheller (1988). One possible explanation for this difference is that the fluid surrounding the drillstring has an effect on the passing longitudinal wave, decreasing its velocity. Samec (1989) found that when the borehole contained a drillstring, the wave velocity of the borehole guided mode was primarily controlled by the drillstring. However the surrounding fluid served to lower the guided mode velocity. As shown in Chapter 2 the interaction of the passing wave with the drilling fluid also appears to introduce an attenuation term into the wave equation.

The drillpipe multiples can also be described in the frequency domain in terms of the resonances they produce. Dareing (1982) modeled the BHA and drillpipe components of the drillstring as two distinct vibrating bars with longitudinal mode resonant frequencies, f_{BHA} and f_{DP}, given by:

$$f_{BHA} = nV_{DS}/4L_{BHA} \qquad n = 1, 3, 5, \ldots \tag{1-12}$$

and

$$f_{DP} = nV_{DS}/2L_{DP} \qquad n = 1, 2, 3, \ldots \tag{1-13}$$

To derive these equations, Dareing assumed that the longitudinal vibration mode in the BHA could be modeled as a bar with a fixed end at the drill bit and a free end at

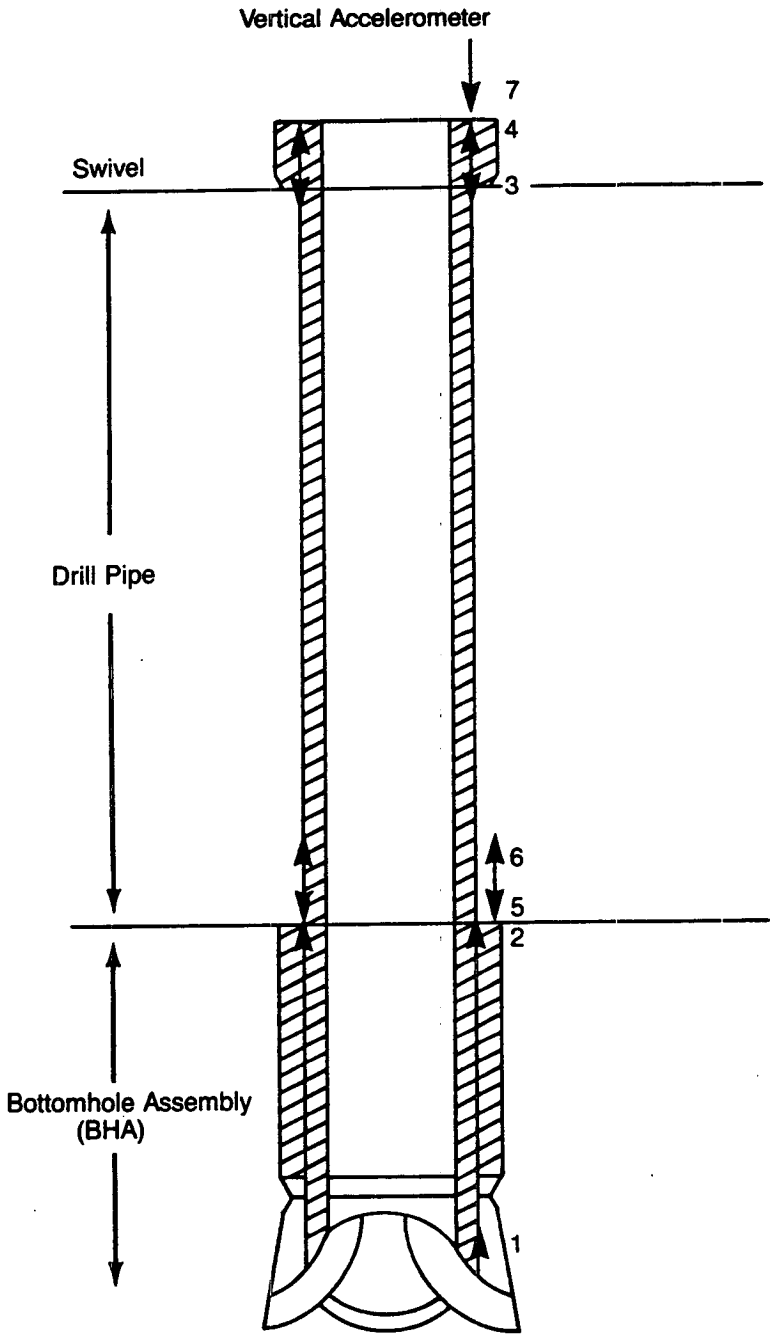

Figure 1-4. Travelpath of first order drillpipe multiple identified in Figure 1-3. The arrival originates 1) at the drillstring travels, 2) through the BHA up the drillstring, 3) is recorded by the vertical accelerometer as the primary drillstring arrival, 4) is reflected at the top of the drillstring and travels back down the drillstring to, 5) the interface between the BHA and the drillpipe, where 6) it is reflected and travels back up the drillstring and is recorded, 7) by the vertical accelerometer at the top.

the drillpipe interface. Likewise, the longitudinal modes of the drillpipe were modeled as a bar that was fixed at both ends. Figure 1-5 shows a frequency spectrum calculated by Fourier transforming an autocorrelation function corresponding to a drillstring length of 1150m. This spectrum was computed on the same well at which the autocorrelation functions in Figure 1-4 were obtained. The rolloff of the data above 70 Hz is due to the 4 ms anti-alias filter. A digital low-cut filter below 10 Hz was also applied. Using a BHA length of 254m and a drillpipe length of 896m, resonant frequency spacings of 4.47 Hz for the BHA and 2.65 Hz for the drillpipe are predicted. In Figure 1-5, drillpipe resonances spaced at approximately 2.73 Hz can be seen up to 100 Hz. The BHA resonances are not easily identified in Figure 1-5. The drillpipe resonances are an indirect measure of the frequency content of the drill-bit impacts on the formation. If a resonance exists at a particular frequency, it means that the arrival is traveling a longitudinal wave up and down the drillpipe before it is recorded. Assuming that there is no other source for longitudinal waves, the arrival comes from the drill bit and thus the drill bit produces energy at the resonant frequency. In the spectrum shown in Figure 1-5, the presence of resonances from 10 to 100 Hz indicate that the drill-bit impacts are probably wideband. The wide, deep valley in the spectrum between 25 and 70 Hz is not predicted by the resonances of the drillstring. This valley is discussed in more detail in Chapter 2, and may be related to travel of the longitudinal wave past the top of the drillstring, into the drill rig.

1.6 Field Examples of Cross-Correlated Data

The field examples of cross-correlated data discussed in this and other chapters are displayed using a vertical axis of correlation time (or in some cases adjusted correlation time to account for the traveltime in the drillstring, t_ρ) and a horizontal axis that represents drillstring length or geophone array offset from the wellhead. As shown in Figure 1-6, when the spatial axis is drillstring length, the surface geophone position is fixed and the data appear like a conventional single-offset VSP display.

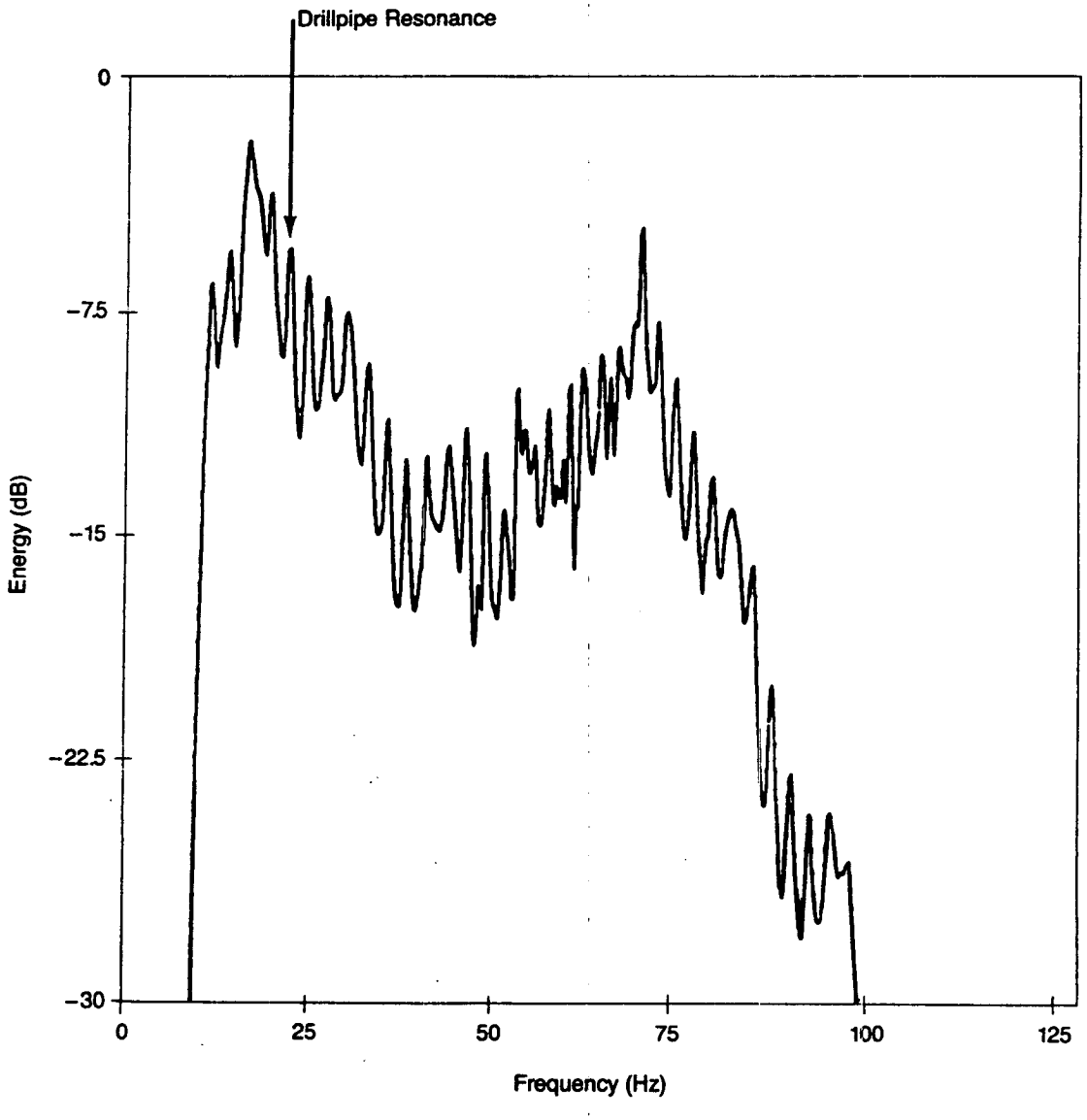

Figure 1-5. Pilot signal spectrum from a drill bit depth of 1150m computed over a recording time of 30 minutes. Resonance spaced at 2.73 Hz correspond to drill pipe multiples.

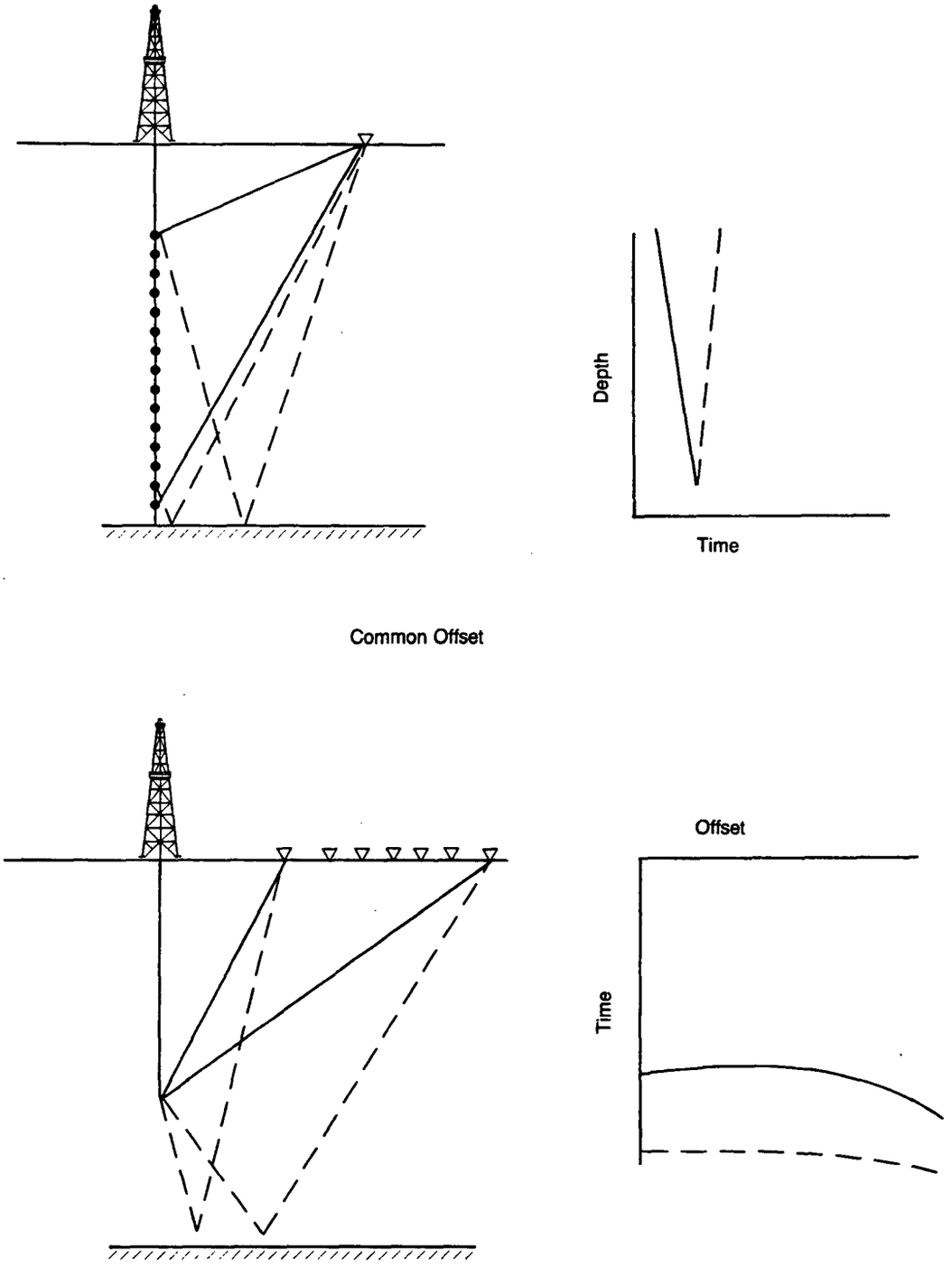

Figure 1-6. Geometries corresponding to correlated data displays.

When the spatial axis is offset, the drill-bit depth is fixed as in walkaway VSP displays. Most of the data examples in the following chapters represent correlation functions computed over a vertical drill-bit movement of about 10m (one joint of drillpipe). Most of the earth receivers were arrays of vertical geophones with the array deployed along a radial from the drill rig as shown in Figure 1-7. As discussed in Chapters 2 and 3, arrays of geophones are used to average coupling variations, attenuate noise from the drill rig, and attenuate coherent drill-bit signal from the drill rig and other sources along the drillstring. The geophone arrays used in recording the data examples shown in this and other chapters were designed to suppress near-surface traveling energy, while preserving P-wave direct arrivals from the drill bit with horizontal wavelengths less than λ_m, where λ_m is approximately given by:

$$\lambda_m \cong V_a/\sin\phi f_m \tag{1-14}$$

V_a is the average compressional velocity, ϕ is the angle of a straight raypath with respect to the vertical, and f_m is the maximum desired frequency. For an average velocity of 3000 m/s and a maximum frequency of 60 Hz, the minimum apparent horizontal direct arrival wavelength for raypath angles of 10 degrees is about 300m. To preserve larger horizontal wavelengths, an array length no longer than about 75m ($1/4\lambda_m$) should be used. Most of the ensuing examples were designed with this criteria in mind, and arrays spanning 30 to 90m were commonly used.

Figure 1-8 is a field data example showing a common-offset series of cross-correlation functions. The geophone array consisted of twenty-four 10 Hz vertical geophones with an array length of 60m, centered 732m from the wellhead. The data are displayed with a time axis of relative time. Hence, traveltimes of drill-bit arrivals through the earth are advanced by the one-way traveltime from the drill bit to the top of the drillstring, t_ρ. In Figure 1-8, the direct arrival is interpreted to be the strong

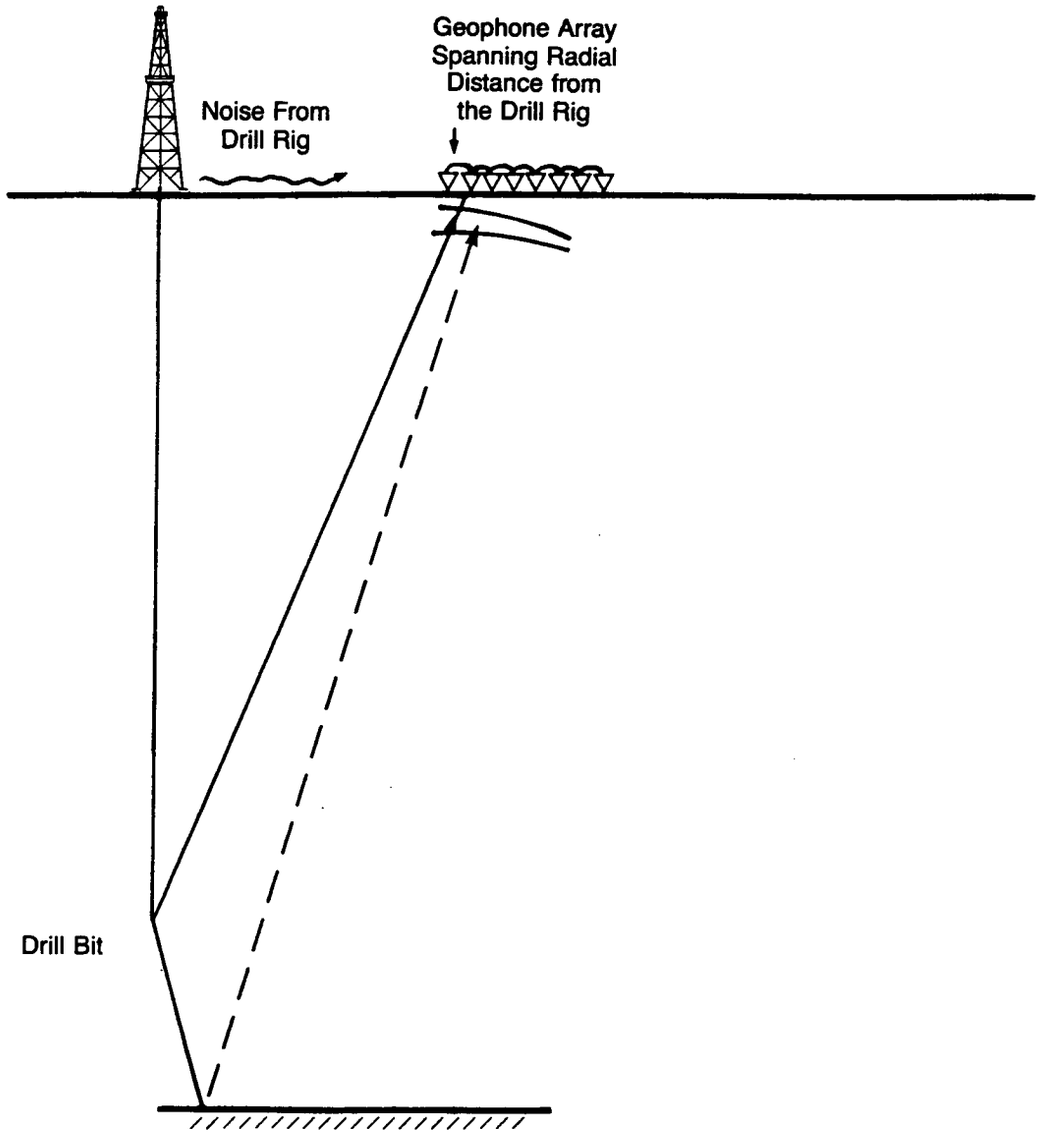

Figure 1-7. Typical geophone array configuration at the surface. The array spans a radial distance from the wellhead to attenuate noise from the rig.

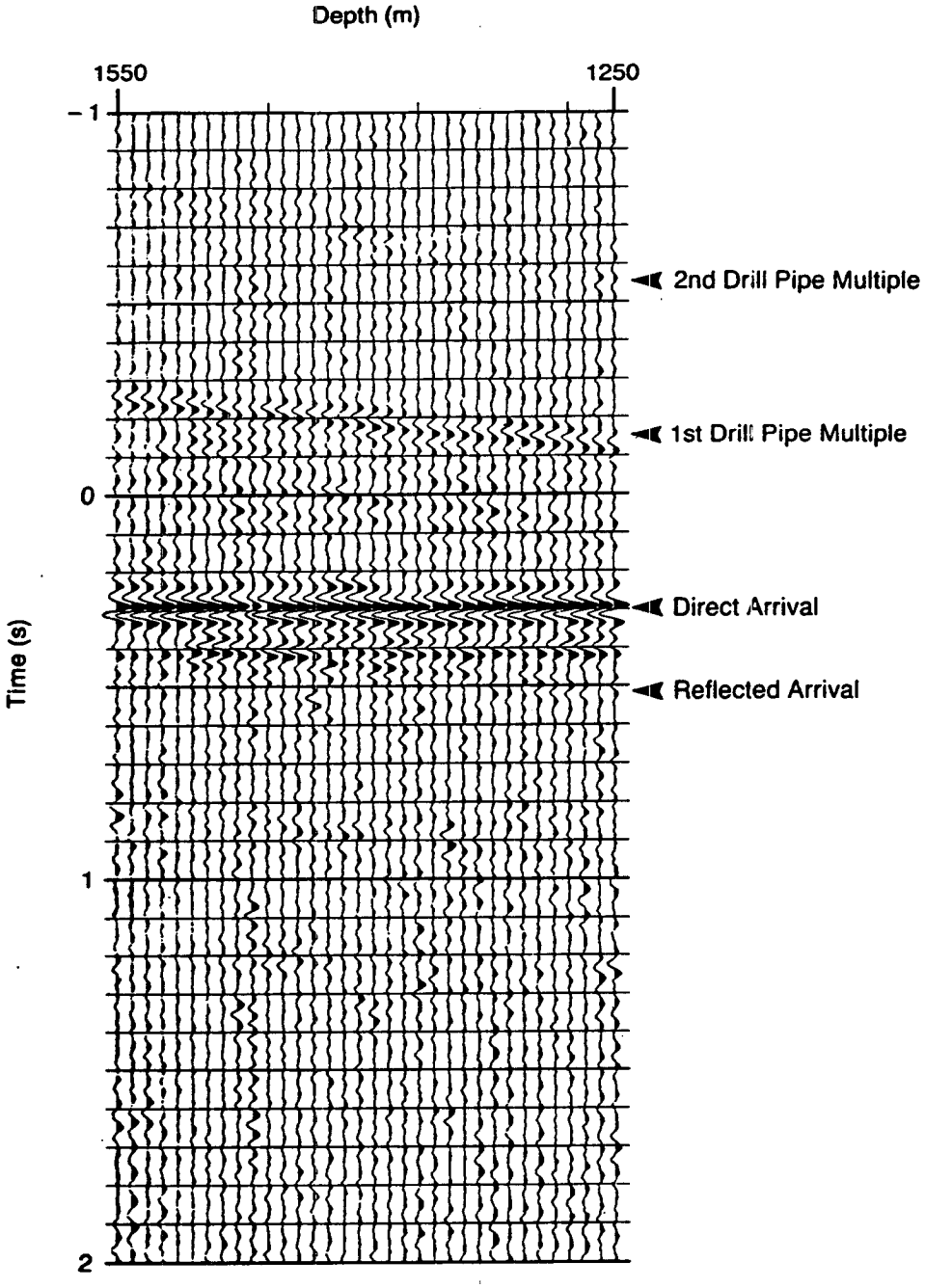

Figure 1-8. Cross-correlated drill-bit VSP field data. Each trace represents a cross-correlation function between the pilot signal and a group of geophones located 732 m from the wellhead. The vertical axis measures the relative traveltime, τ, between coherent energy sensed at the pilot sensor and at the group of geophones.

broadband arrival at 285 ms. This event occurs at the correlation time and moveout of a primary longitudinal arrival in the drillstring with the primary direct P-wave arrival from the drill bit to the geophone array at the surface. The reflected arrival labeled in Figure 1-8 occurs at a correlation time and moveout of the same drillstring arrival with a reflected arrival that appears to originate at a depth of 1600m (its intersection with the direct arrival). These arrivals correspond to travelpaths depicted in Figure 1-2. They are identified based on their correlation time and moveout as described in Chapter 3. Other events following the direct arrival in Figure 1-8 are also discussed in Chapter 3. Figure 1-9 shows the data after adding the drillstring traveltime, t_p, to the time axis of each of the cross-correlated traces in Figure 1-8. The data in Figure 1-9 are now positioned with a time axis where the primary events have traveltimes of the type that would be recorded by a conventional VSP. As shown in Chapter 4 after correction for the drillstring traveltime, the traveltimes of the drill-bit direct arrival closely match conventional VSP direct-arrival traveltimes.

1.7 Reference Deconvolution

Besides the primary arrivals traveling up the drillstring and in the earth, there are strong secondary arrivals labeled in Figure 1-8 that are related to the drillstring multiple arrivals detected in the pilot-signal autocorrelation. These secondary arrivals are associated with the term DS(-t) in Equation 1-5. They appear to be auticausal because the cross-correlation process time reverses the pilot signal prior to convolution with the receiver signal. These multiples pose a slightly different deconvolution problem from conventional surface seismic deconvolution in that an auticausal filter must be applied to the cross-correlation function to attenuate the drillstring multiples of the pilot signal. Alternatively, a causal deconvolution filter can be applied to the pilot signal prior to cross-correlation. The resulting correlation function from this deconvolution process, known as reference deconvolution, is

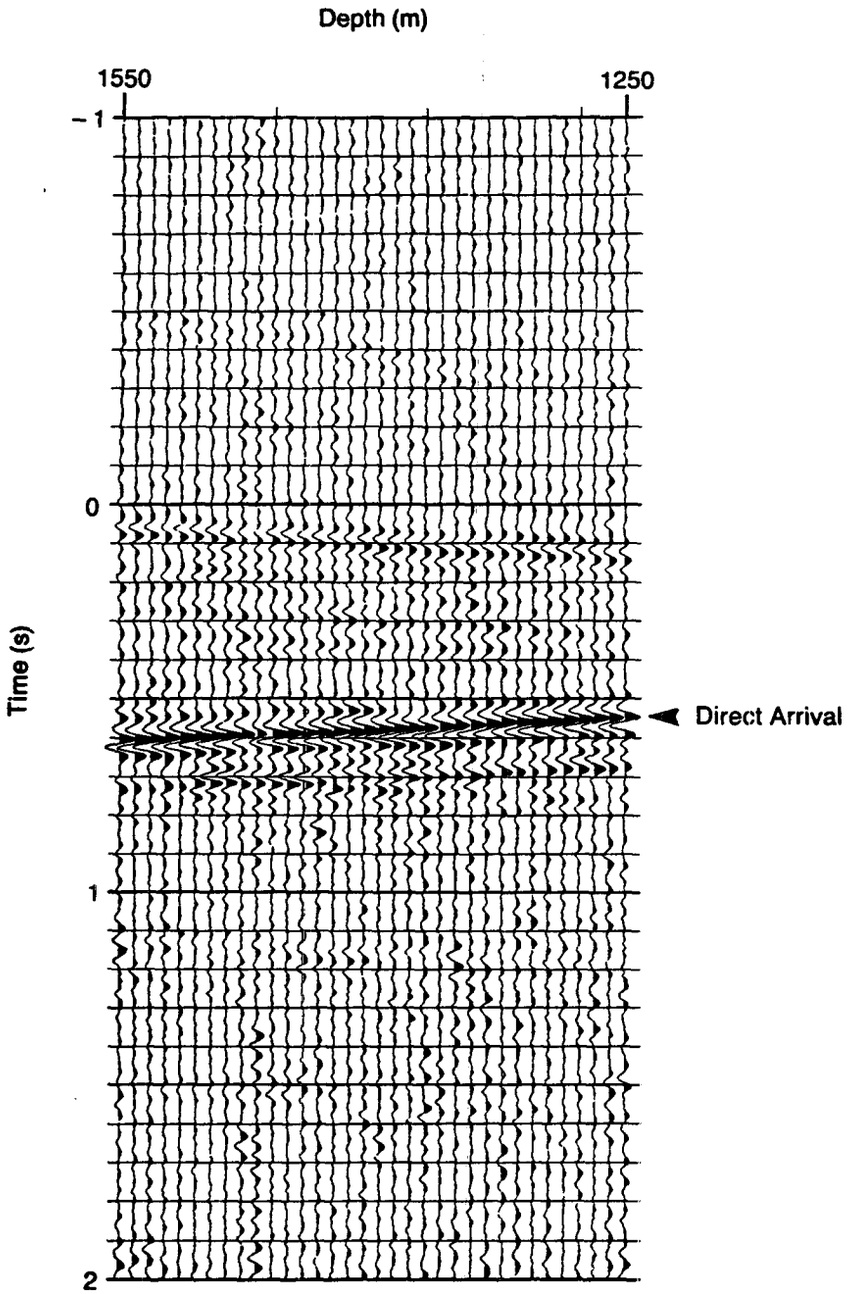

Figure 1-9. Cross-correlated drill-bit VSP data after correcting for the traveltime within the drill string. The data are now positioned in earth traveltime where the primary arrivals occur at the same traveltimes as a conventional VSP.

representative of the cross-correlation between a whitened pilot signal and the geophone signal.

Referring to Equation 1-3, if the pilot signal were white and the drillstring were an all pass (purely phase shift filter), the cross-correlation function could be written as:

$$cc(\tau) = S(-t+t_\rho) * S(t) * E(t) . \qquad (1\text{-}15)$$

Except for the time shift, t_ρ, this is the typical representation of vibroseis cross-correlation. Assuming that DS(t) is minimum phase, the recorded pilot signal can be filtered to obtain S(t) by performing predictive deconvolution on the pilot signal with unit prediction distance (Peacock and Treitel, 1969). The filter obtained is $DS^{-1}(t)$, the minimum-phase inverse of the drillstring response. If this filter is time-reversed and convolved with the cross-correlated data, we obtain the desired result shown in Equation 1-15, the cross-correlation between the whitened version of the pilot signal, S(t), and the signal received through the earth:

$$W_{cc}(\tau) = DS^{-1}(-\tau) * cc(\tau) = S(-t+t_\rho) * S(t) * E(t) . \qquad (1\text{-}16)$$

It is much less computationally intensive to apply the minimum phase inverse of the pilot signal to the cross-correlated data rather than to apply the inverse to the pilot signal prior to cross-correlation. However, if there is any non-stationarity in the signals, the latter approach would be more accurate.

Figure 1-10 shows the data in Figure 1-9 after application of the reference deconvolution filter. The drillstring multiples preceding the direct arrival are substantially attenuated, and the remaining arrivals consist of primary, top-of-drillstring arrivals correlated with drill-bit arrivals recorded by the geophone array.

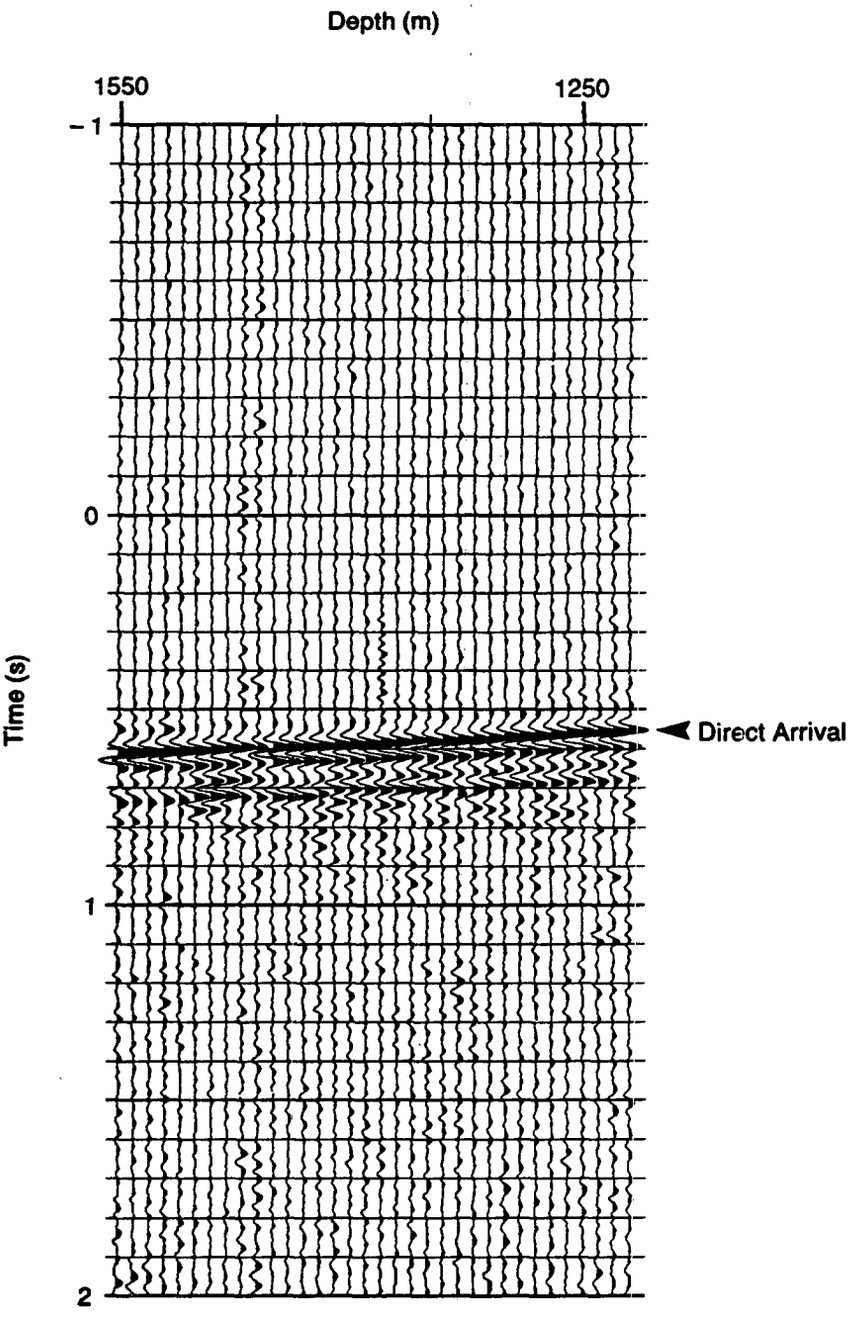

Figure 1-10. Cross-correlated drill-bit VSP data corrected for traveltime within the drill string and applying reference deconvolution.

From the effectiveness of the reference deconvolution process in Figure 1-10, it is inferred that the minimum phase and stationarity assumptions made in deriving the filter were valid for this example.

1.8 Conclusions

Wideband vibrational signals originating at the drill bit can be detected at the surface by cross-correlating a top-of-drillstring pilot signal with geophone-array signals. By repeating this process for a series of depths, a VSP-like data section is obtained. The long periods of drilling mean that much longer recording times are available to drill-bit signal cross-correlation functions than are used in conventional vibroseis. Consequently, much weaker signals can be detected. The travel from the drill bit to the top of the drillstring introduces time shifts and anti-causal multiple arrivals into the cross-correlated data. The time shift is equivalent to the drillstring length/drillstring velocity.

From the delay and moveout of multiple arrivals in the pilot signal autocorrelation, the drillstring velocity was estimated to be 4758 m/s. The multiple arrivals can be substantially attenuated by finding an inverse filter from the pilot signal and convolving the time-reversed inverse with the cross-correlated data.

Chapter 1: References

Adams, N.J., 1986, Drilling Engineering: a complete well planning approach, PennWell Publishing Co., 960p.

Aki, K. and Richards, P.G., 1980, Quantitative seismology, theory and methods: W.H. Freeman & Co..

Dareing, D.W., 1982, Drill collar length is a major factor in vibration control, 57th Annual Fall Technical Conference of Society of Petroleum Engineers of AIME, SPE 11228.

Dareing, D.W., 1984, Vibrations increase available power at the drill bit, Oil and Gas Journal, Nov. 12, 67-70.

Deily, F.H., Dareing, D.W., Paff, G.H., Ortloff, J.E., and Lynn, R.D., 1968, Downhole measurements of drill string forces and motions: Trans. Am. Soc. Mech. Eng. of Eng. for Ind., May, 217-225.

Drumheller, D.S., 1988, Acoustical properties of drillstrings, J. Acoust. Soc. Am., 85(3), 1048-1064.

Hardage, B.A., 1985, Vertical seismic profiling Part A: Principles, 2d edition, Pergammon Press, 517p.

Harris, J.M., 1988, Cross-well seismic measurements in sedimentary rocks: Presented at the 58th Ann. Internat. Mtg., Soc. Expl. Geophys., Expanded Abstracts, 147-150.

Justice, J.H., Vassiliou, A.A., Singh, S., Logel, J.D., Hansen, P.A., Hall, B.R., Hutt, P.R., and Solanti, J.J., 1989, Acoustic tomography for monitoring enhanced oil recovery: The Leading Edge, 8, no. 2, 12-19.

Kolsky, H., 1963, Stress waves in solids, Dover Publications, 208p.

Kostov, C., 1988, Drill-bit signal: Stanford Exploration Project, 59, 11-34.

Lutz, J., Raynaud, M., Stalder, S.G., Quichaud, C., Raynal, J., and Muckelroy, J.A., 1972, Instantaneous logging based on a dynamic theory of drilling: J. Pet. Tech., 10, 750-758.

Macrides, G.G., Kanasewich, E.R., and Bharata, S., 1988, Multiborehole seismic imaging in steam injection heavy oil recovery projects, Geophysics, 53, 65-75.

Marion, B.P., 1990, personal communication.

Oppenheim, A.V. and Schafer, R.W., 1975, Digital signal processing, Prentice-Hall, 585p.

Peacock, K.L. and S. Treitel, 1969, Predictive deconvolution: theory and practice, Geophysics, 34, 155-169.

Quichaud, C., Raynal, J., Roux, C., and Feneyrou, G., 1979, SNAP and VA logs pass 2-year offshore, onshore field test, Oil and Gas Journal, March 12, 55-60.

Rector, J.W., Marion, B.P., and Widrow, B., 1986, Seismic borehole tomography: Final Report 1983-1986, GRI Contract Number 5083-211-0833.

Roark, R.R., 1954, Formulas for stress and strain: McGraw-Hill Book Co. (Div. of McGraw-Hill, Inc.), 384p.

Samec, P., 1989, Modeling of downhole sources radiation pattern using the finite element method, Stanford Rock Borehole Annual Report, Paper G.

Shepard, M.C. and Lesage, M., 1988, The forces at the teeth of a drilling rollercone bit: theory and experiment, Presented at the 63rd Annual Technical Conference and Exposition of the Society of Petroleum Engineers, Houston, TX.

Staron, P., et al, 1988, Method of instantaneous acoustic logging within a wellbore: U.S. Patent 4718048.

Vennin, H.C., 1989, Drilling bits optimized for the Paris Basin, Oil and Gas Journal, July 31, 93-96.

Weatherby, B.B., 1936, Method of making sub-surface determinations: U.S. Patent no. 2,062,151.

CHAPTER 2

CHARACTERIZATION OF DRILL-BIT SIGNAL AND NOISE ON SURFACE RECORDINGS

ABSTRACT

Drill-bit signal and noise are characterized in recordings of top-of-drillstring accelerometers and geophone arrays. From the signal-to-noise ratio (S/N) of drillpipe multiples in the vertical accelerometer autocorrelations, the S/N of drill-bit energy in the vertical accelerometer recordings is estimated. The S/N decreases with increasing frequency, possibly due to dissipation of longitudinal wave energy traveling up the drillpipe. The primary noise on vertical accelerometer recordings is wideband and is predominantly polarized in a horizontal direction. The geophone array recordings consist of noise that is primarily due to equipment on the drill rig. The rig noise present on geophone array recordings is not recorded at the top of the drillstring and thus is attenuated in cross-correlation functions between the two recordings.

The noise on the vertical accelerometer is linearly related to the noise on a horizontal accelerometer oriented appropriately. This linear relationship allows component filtering to be used to obtain an improved estimate of drill-bit signal at the top of the drillstring, improving the identifiable bandwidth of the drill-bit signal, and resulting in an improved pilot signal for cross-correlation with geophone array recordings.

2.1 Introduction

The vibroseis method cross-correlates geophone recordings with the recording of an artificially-generated sweep of frequencies that is imparted into the earth through the baseplate of the vibroseis truck. The vibroseis sweep signal is often called a pilot signal because it corresponds closely to the signal imparted into the earth. In the drill-bit signal acquisition method outlined in Chapter 1, an analog to the vibroseis pilot

signal is the recording of a vertical accelerometer at the top of the drillstring. As shown in Chapter 1, the top-of-drillstring pilot signal consists of multiple arrivals as well as the primary arrivals of interest. It was also shown that the cross-correlation functions contain both causal multiples from earth reverberations and anticausal multiples related to the drillstring impulse resonance (due to the time reversal of the pilot signal in cross correlation). Similarly, the cross-correlation function exhibits noise due to noise in the pilot recording as well as noise in the geophone array recording. To improve the quality of the cross-correlated data, it is important to characterize the nature of the noise on both recordings. With a knowledge of the noise characteristics and their relation to the cross-correlated data, data acquisition and processing techniques can be optimized for noise attenuation.

2.2 Characterization of Drill-Bit Signal and Noise From the Vertical Accelerometer Recording Autocorrelation

As shown in Chapter 1, the vertical accelerometer recording at the top of the drillstring, P(t), can be considered to consist of drill-bit signal, S(t), that undergoes filtering by the drillstring, DS(t). If we also include noise, N(t), then we can write P(t) as:

$$P(t) = S(t) * DS(t) + N(t). \tag{2-1}$$

Assuming that both drill-bit signal and noise are wideband and random, it is difficult to distinguish signal and noise in a time domain analysis of a single vertical accelerometer recording. However, the autocorrelation function provides both a means to distinguish coherent drill-bit signal from incoherent noise and a means to estimate S/N.

We can write the autocorrelation function of the vertical accelerometer recording over a finite recording time, $ac_p(\tau)$, as:

$$ac_p(\tau) = [S(-t)*DS(-t)] * [S(t)*DS(t)] + [N(-t)*N(t)] + \text{estimator noise}, \quad (2\text{-}2)$$

where τ is the autocorrelation time lag and the estimator noise represents the cross terms, S*N. The relationship between coherent signal and estimator noise in a correlation function having a finite recording time is derived in Appendix 2-A.

Provided that the drill-bit impacts and the noise are both stationary, random functions, Equation 2-2 becomes:

$$ac_p(\tau) = \beta K_\beta(0) * [DS(-t)*DS(t)] + \eta K_\eta(0) + \text{estimator noise}, \quad (2\text{-}3)$$

where β is proportional to the variance of the drill-bit signal, η is proportional to the variance of the noise, and K is a Klauder wavelet that has a width inversely proportional to the bandwidth of the signal or the noise. From Equation 2-3, we can see that both drill-bit signals as well as noise are concentrated around $\tau = 0$. At other values of τ, the autocorrelation represents the Klauder wavelet resulting from the drill-bit signals convolved with the autocorrelation of the drillstring impulse response and estimator noise. As shown in Chapter 1, drillpipe multiple arrivals are major contributors to the drillstring impulse response. Drillpipe multiples provide an excellent mechanism for distinguishing drill-bit signal from noise because of their known delay and moveout characteristics in the autocorrelation functions. As shown in Appendix 2-A, the ratio of drillpipe multiple to estimator noise provides one method to estimate the S/N of the vertical accelerometer recording.

Another method for estimating the vertical accelerometer S/N compares the zero-lag amplitude of the autocorrelation and the amplitudes of the first and second order drillpipe multiples. The ratio of the zero lag of the autocorrelation, $ac_p(0)$, to the 'first-order' drillpipe multiple, $ac_p(\tau_{dp})$, is:

$$\frac{ac_p(0)}{ac_p(\tau_{dp})} \cong \frac{\sigma_b^2+\sigma_n^2}{A\sigma_b^2}, \qquad (2\text{-}4)$$

where τ_{dp} is the two-way time of the drillpipe multiple, σ_b^2 is the variance of the drill-bit signal, σ_n^2 is the variance of the incoherent noise, and A is the ratio of the $N+1^{th}$ to the N^{th} order drillpipe multiple ($N \geq 1$). The S/N of the vertical accelerometer recording, $\sigma_b^2/\sigma_n 2$, is then

$$\frac{\sigma_b^2}{\sigma_n^2} \cong \left(\frac{ac_p(0)}{ac_p(\tau_{dp})} - \frac{1}{A} \right)^{-1}. \qquad (2\text{-}5)$$

A typical series of autocorrelations containing drillpipe multiples was shown in Chapter 1 (Figure 1-4). Using Equation 2-5, and a measured A of 0.4, a drill-bit S/N of +3 dB in the raw vertical accelerometer recording is estimated.

For high drill-bit S/N's, the estimate in Equation 2-5 is very sensitive to measurement error. For example, a S/N of +3 dB (2/1) could be misestimated as a S/N of $+\infty$ with a 30 percent error in each of the measured terms in Equation 2-5. When the drillpipe multiple cannot be detected above the estimator noise, the S/N cannot be estimated at all from Equation 2-5. However, the absence of a drillpipe multiple is not necessarily due to a low S/N in the raw recordings. Low values of A, resulting from travelpath attenuation of the drillpipe multiple could also result in a multiple arrival below the estimator noise threshold, even with a high primary drill-bit S/N. Consequently, the primary use of Equation 2-5 is as a constraint on the lower bound of the recording S/N.

Figure 2-1 illustrates a series of vertical-accelerometer autocorrelations that have been bandpassed filtered into different frequency ranges. The data are plotted with a 0.5s agc to enhance the higher-order drillpipe multiples. The first-order

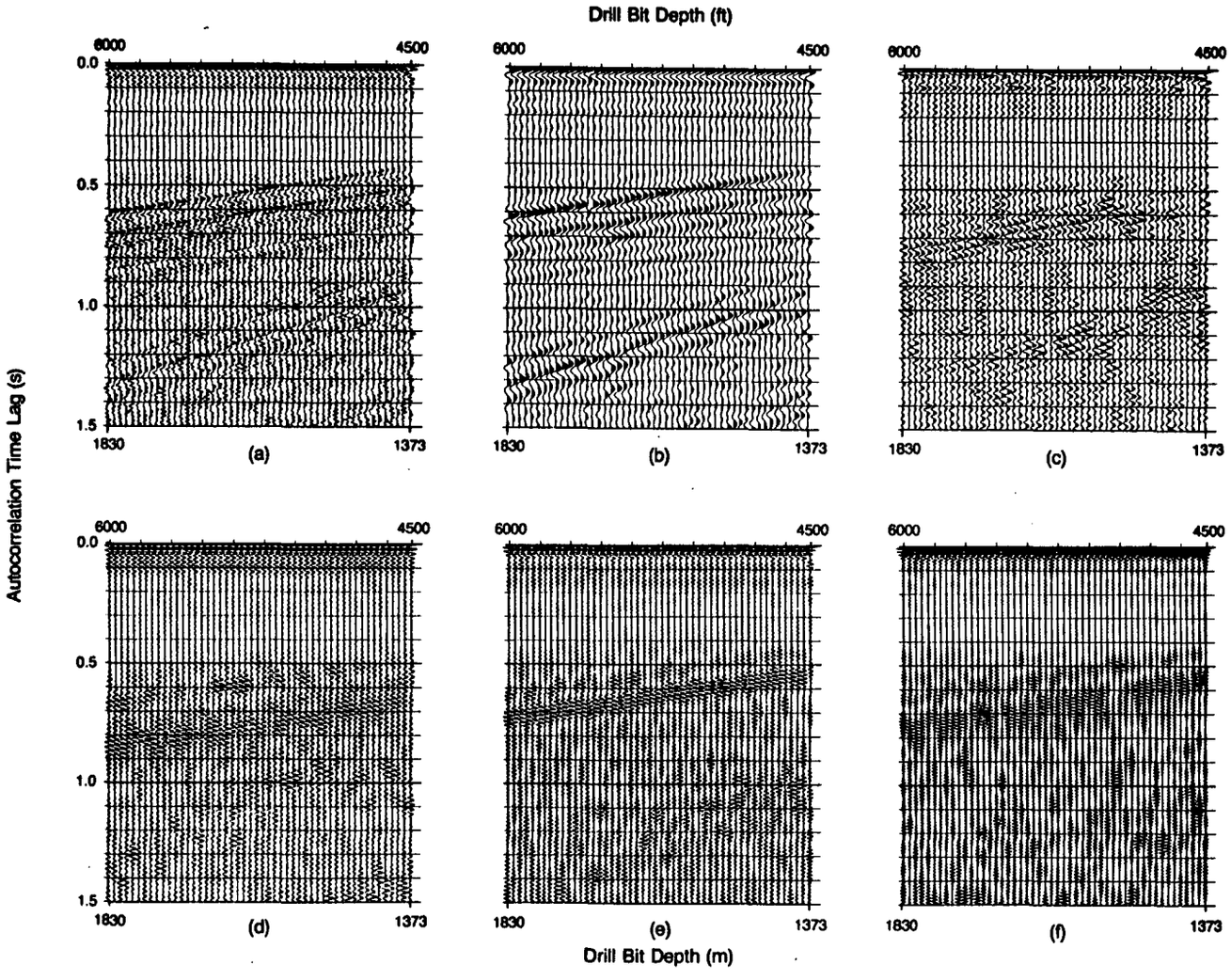

Figure 2-1. Frequency dissects of a series of vertical accelerometer autocorrelations computed over an average precorrelation recording time of 500s. (a) 10-85 Hz, (b) 10-25 Hz, (c) 25-40 Hz, (d) 40-55 Hz, (e) 55-70 Hz, (f) 70-85 Hz.

multiples are apparent at all frequencies whereas the second-order multiples are only apparent at the lower frequencies. The S/N for the first-order multiple arrival is lowest in the 25 to 40 Hz band, corresponding to a deep notch in the frequency spectrum. Figure 2-2 is the frequency spectrum corresponding to the tenth trace from the right in Figure 2-1. Drillpipe resonances, evident throughout most of the seismic band, are somewhat obscured in the deep notch at about 35 Hz. (Appendix 2-B investigates the causes of the spectral notch.)

There are several potential causes for the decrease in S/N of the second-order drillpipe multiple with increasing frequency observed in Figure 2-1.

1) The drill bit may output less vibrational energy at these frequencies.
2) The noise may be colored.
3) The transmission effects between the drill bit and the top of the drillstring may attenuate the drill-bit signal differently at different frequencies.

The second possibility is unlikely, since as we shall see in Section 2.3, the noise present at the top of the drillstring has a practically white spectrum. The first possibility is at odds with the model of the drill-bit signal production as a random signal having a white spectrum (Chapter 1). However, this model has not been confirmed. Other studies (Lutz, et al, 1972; Deily, et al, 1968) observed much larger vibrations at the very low frequencies (3 to 7 Hz) related to the third harmonic of the rotary rate. Presumably, the S/N variations with frequency could be due to increased drill-bit signal production at higher harmonics of the rotary rate such as the sixth and ninth. This possibility cannot be verified from harmonic spectral peaks because the rotary rate (nominally at 2 Hz for the data in Figure 2-1) varied by up to 40 percent over the depth zone displayed. The variation in the rotary rate resulted in harmonics spread over a wide range of frequencies.

Another way to explain the S/N variations with frequency is to include an attenuation term in the model for longitudinal wave propagation along a drillstring.

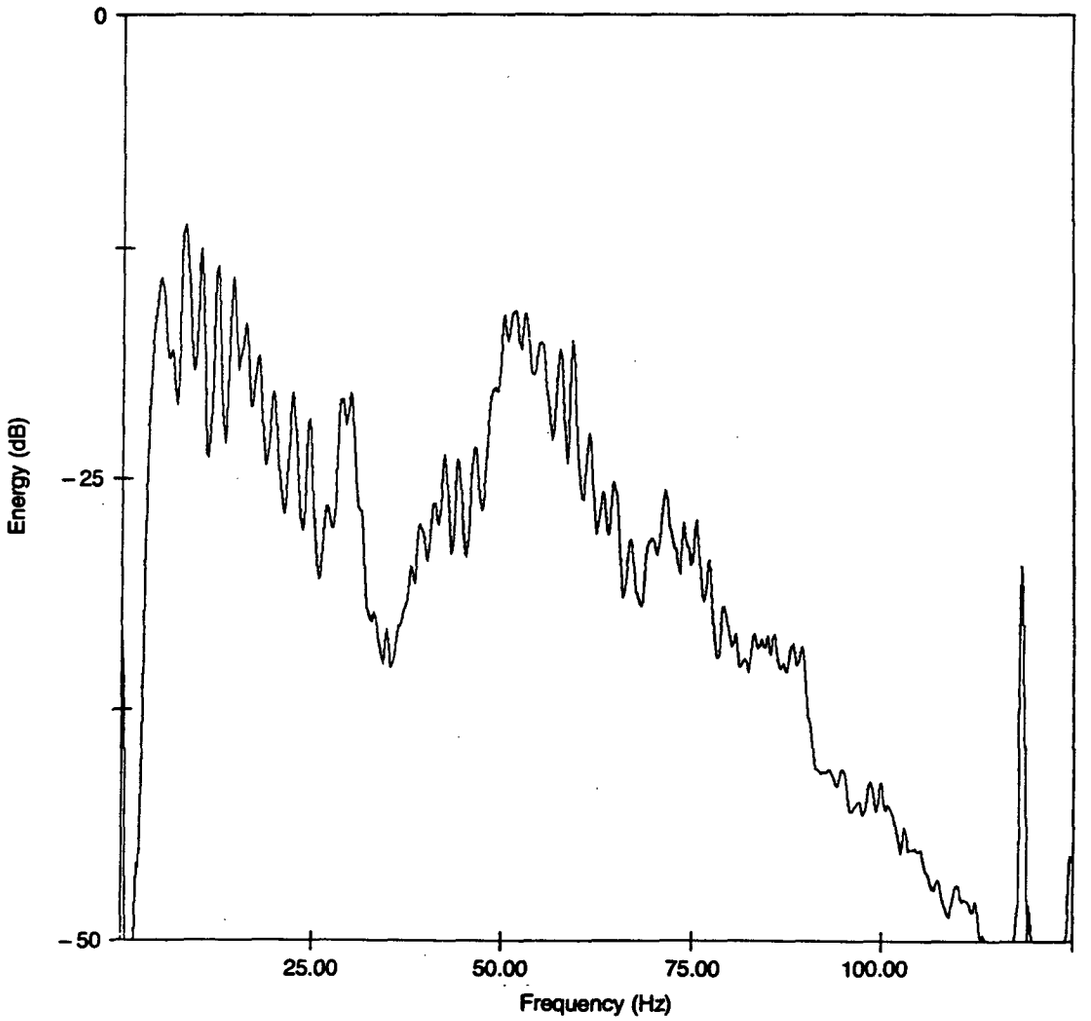

Figure 2-2. Vertical acceleration spectrum corresponding to the tenth autocorrelation function in Figure 2-1.

The model described by Drumheller (1988) and used in Chapter 1 did not include attenuation due to absorption. Like seismic wave propagation in porous rock, longitudinal waves traveling in a drillstring suspended in drilling fluid could be dissipated by attenuation terms. Studies by Sun Oil in 1948 and 1968 reported signal losses ranging from 12 dB to 30 dB/300m (Cox and Chaney, 1981). Moreover, longitudinal wave velocities obtained in Chapter 1 were 15 percent lower than theoretical values, indicating that the drilling fluid may also be involved in the longitudinal wave propagation.

A study by Squire and Whitehouse (1979) enumerated three principal mechanisms for attenuation of waves propagating along a drillstring immersed in drilling fluid:

1) Intrinsic drillstring absorbtion (very small)
2) Viscous losses due to motion of the drillstring surface in the drilling fluid (small)
3) Dissipation into the fluid surrounding the drillstring (large)

Dissipation (or radiation losses) only exist in longitudinal waves (or more accurately, extensional waves) traveling along a bounded medium. Squire and Whitehouse used the analog of a transmission line immersed in fluid to obtain exponential attenuation with distance traveled and frequency, with a drillstring quality factor, Q_{DS}, given by:

$$Q_{DS} = 1 / [(\pi\rho_f / \rho_s)\mu^2 \; 1/1-(r_i/r_o)^2] \,, \qquad (2\text{-}6)$$

where ρ_f is the drilling fluid density, ρ_s is the drillstring density, μ is Poissons ratio for the drillstring, r_i is the inner radius of the drillstring, and r_o is the outer radius of the drillstring. For the drillpipe, typical values for these parameters result in calculated Q's of 10 to 20.

The model of Squire and Whitehouse can be investigated by computing the amplitude ratio of drillpipe multiples and their variation with depth. Figure 2-3 shows another series of vertical accelerometer autocorrelations each computed over about 1 hour of recording time. First-, second-, and third-order drillpipe multiples are all apparent. The traces are displayed after scaling to the amplitude of the first-order multiple peak and applying an 8 to 50 Hz bandpass filter. The autocorrelations have had reference deconvolution applied (Chapter 1) to remove one side of the drillstring response (DS(-t)). Hence, these traces are no longer symmetric anymore. They can be viewed as a shifted version of the drillstring impulse response, with additive noise also present at the zero lag. To show this we return to the definition of the autocorrelation in Equation 2-3. If we assume there is no noise, then convolution of the minimum phase inverse of the drillstring impulse response ($DS^{-1}(-t)$), with the autocorrelation of the pilot signal results in:

$$DS^{-1}(-t) * ac_p(\tau) \cong \beta K_B * DS(t) \cong DS(\tau) \qquad (2\text{-}7)$$

In Figure 2-3, the second-order multiple is about one third the first-order amplitude at a depth of 1400m. The ratio decreases to about one fifth at 2100m. Since the BHA/drillpipe reflection coefficient is about 0.77 (Chapter 1), a dissipation mechanism is needed in order to explain the ratios observed. Assuming a BHA length of 200m, and a center frequency of 30 Hz, a Q of 63 is estimated from the change in the ratio with depth, and a Q of 58 is estimated from the value of the ratio at any particular depth. Similar Q values (50 to 70) have been computed on other wells (Marion, 1990).

The Q values estimated from real data both in this study and the reports of Cox and Cheney are significantly greater than the Q's predicted by Squire and Whitehouse. As will be shown in Chapter 3, the drillstring wave does dissipate energy into the

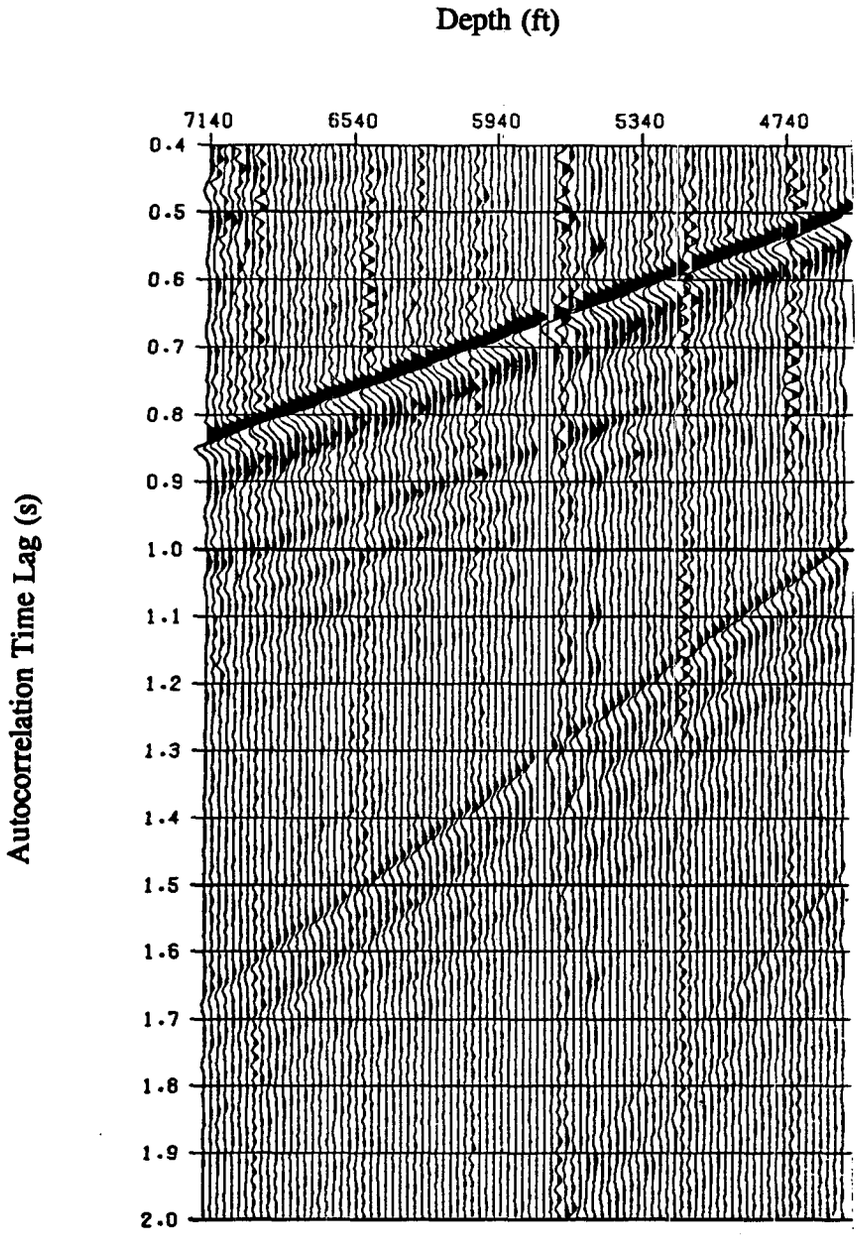

Figure 2-3. Series of accelerometer autocorrelations after applying reference deconvolution (Chapter 1) and an 8 to 50 Hz bandpass filter. The traces are displayed after scaling to the first-order drillpipe multiple peak.

formation. However, the dissipation is organized, often resulting in a conical seismic wavefront. Consequently, the loss of drillstring amplitude with distance could be due to the increase in aperture of the conical wavefront with distance traveled. The model proposed in Chapter 3 would also accommodate a decrease in amplitude with increasing frequency. As the aperture of the conical wavefront is dependent on the formation velocities adjacent to the drillstring, the attenuation with distance is probably controlled by the formation velocities as well.

2.3 Multi-Component Analysis and Filtering of Drill-Bit Signals

To investigate the causes and characteristics of noise on the vertical accelerometer recording, multiple-component accelerometer recordings were made at several wells. The motivation behind these recordings was the assumption that drill-bit signal resulting from drillstring longitudinal waves would have primarily axial accelerations. Other signals (i.e., noise) were expected to have larger non-axial components. The multi-component data were acquired with accelerometers positioned on the swivel above the rotating drillstring. Figure 2-4 shows a diagram of a drill rig with an insert showing the orientations of the accelerometers used in the analysis. As discussed in Chapter 1, the vertical accelerometer was oriented along the axis of the drillstring to record the longitudinal waves resulting from the axial drill-bit impacts. The horizontal accelerometers H_1 and H_2 were oriented perpendicular and parallel to a vertical plane containing the bail.

Figure 2-5 shows typical spectra from the three acceleration components computed over a recording time of 10 minutes at a drill-bit depth of 1550m (the BHA length was 200m). The vertical accelerometer signal had a 60 Hz notch filter applied. The 1.5 Hz resonances in the vertical spectrum are at the predicted spacing of drillpipe multiples (Chapter 1). The resonances begin to disappear above 40 Hz, indicating that the S/N of the drillpipe multiples is lower in this band.

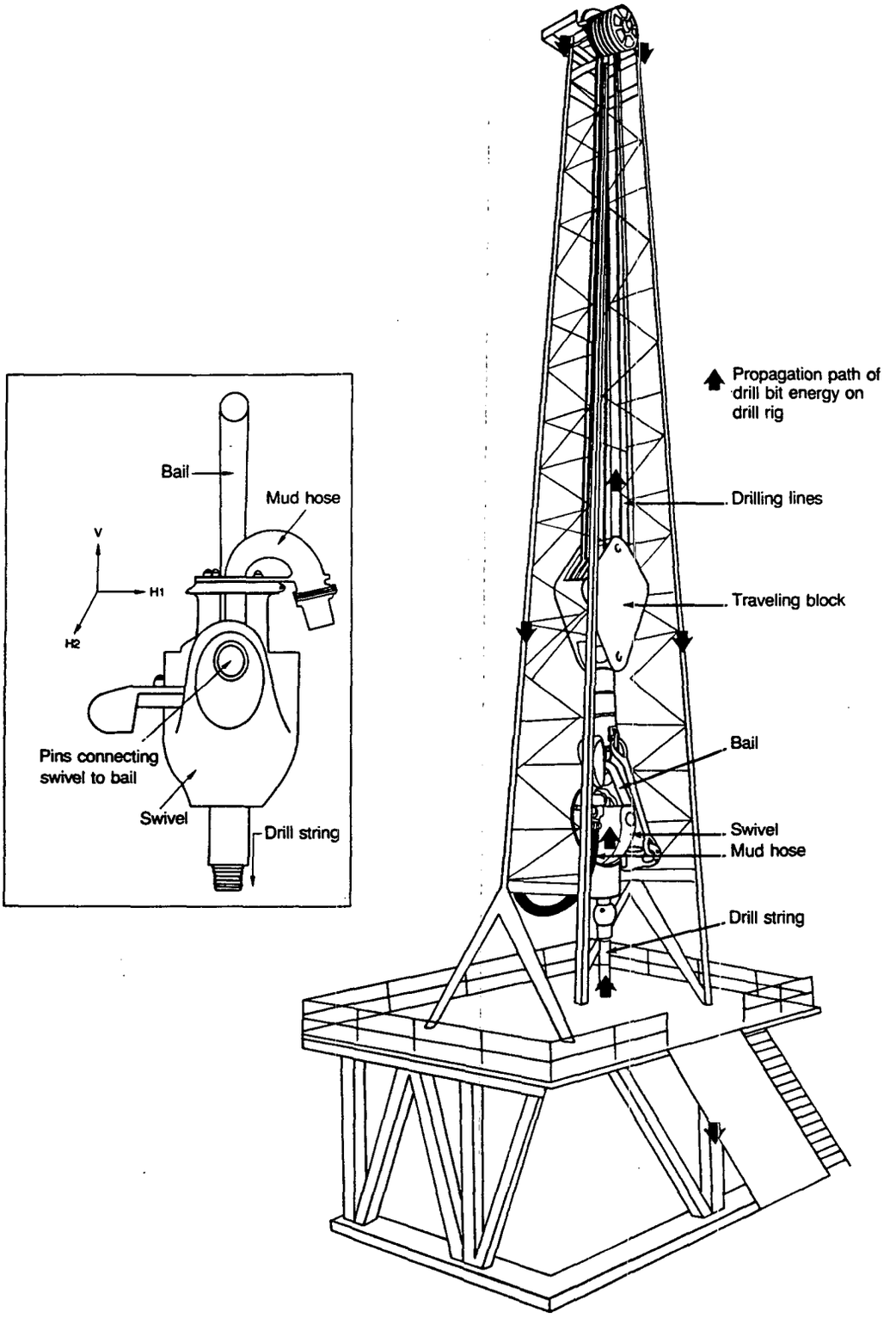

Figure 2-4. Hypothetical path by which drill-bit energy is transmitted from the drillstring into the earth. The insert shows the vertical accelerometer location at the top of the drillstring and the orientation of horizontal accelerometers H_1 and H_2.

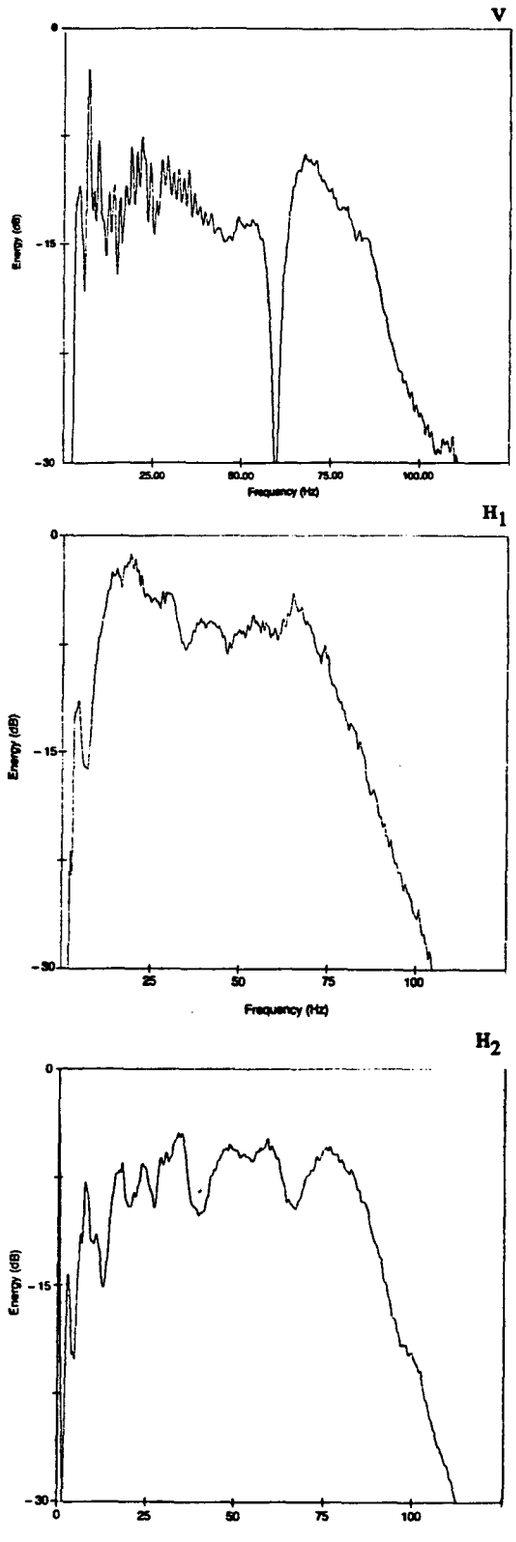

Figure 2-5. Spectra of three accelerometer components computed at a depth of 1550m.

Unlike the vertical spectrum, the horizontal specta do not exhibit resonances due to longitudinal-wave drillpipe multiples. Instead, these components are nearly white. It is believed that the absence of drillpipe resonances is due to both higher noise levels on these components and less axial drill-bit signal. However, these two effects cannot be decoupled because the drill-bit signal cannot be identified on the horizontal spectra. The signals observed on the horizontal components have an unknown origin. Their spectra cannot be caused by torsional or flexural wave drillpipe multiples. As shown by Kolsky (1963), these multiples would be expected to have resonances spaced about one half the longitudinal wave drillpipe resonances. The horizontal signals do appear to be related to the drilling process, because their amplitude has been observed to decrease when the drill bit is off bottom (Marion, 1990).

The interrelationship between the different components was investigated by computing coherence functions and by cross plotting the recordings. The coherence function, C(f), is a measure of the similarity between two signals. It is defined (Jenkins and Watts, 1968) as the cross-spectrum between two signals x and y divided by the autospectra of the individual signals.

$$C(f) = S_{xy}(f)S^{*}_{xy}(f)/|S_{xx}(f)|\ |S_{yy}(f)| \qquad (2\text{-}8)$$

where $S_{xy}(f)S^{*}_{xy}(f)$ is the cross spectrum, and S_{xx}, S_{yy} are the autospectra of the individual recordings. From Schwarz's inequality, the coherence function lies between 0 and 1. A high coherence near 1 indicates that the signals are identical to within a constant. A low coherence near zero indicates that the recordings are not alike.

Figure 2-6 shows coherence functions between the vertical and the H_1 and H_2 recordings. The coherence functions were computed from the raw signals used to compute the spectra in Figure 2-5. The vertical and H_1 signals have coherences

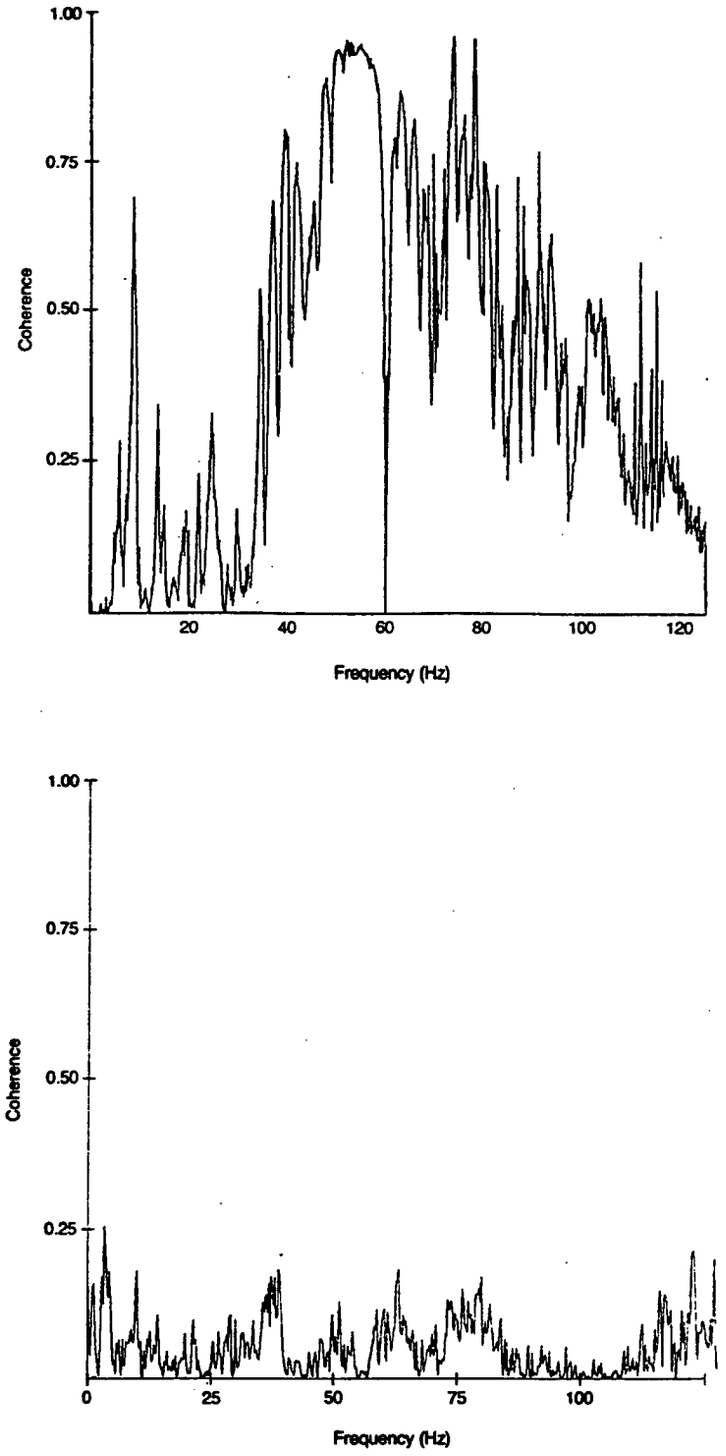

Figure 2-6. Coherence functions between vertical accelerometer and a) H_1; b) H_2 accelerometer recordings. The coherence function is defined as the cross-spectrum normalized by the individual autospectra. The coherence functions were computed over a recording time of 10 minutes.

greater than 0.5 in the 40 to 80 Hz band. This indicates that the predominant energy recorded on both sensors is coherent. By contrast, the frequencies below 40 Hz have low coherence indicating that at least one of the recordings contains signals that are not present on the other. The vertical and H_2 recordings exhibit low coherence at all frequencies. The slight peaks at 36, 60, and 78 Hz are correlated with peaks in the H_2 spectra. Thus, there may be some small coherence between the two recordings. Since the coherence functions in Figure 2-6 do not show much coherence at the low frequencies, where the drill-bit signal was most evident on the vertical spectrum, the frequency bands with high coherence are probably associated with noise rather than axial drill-bit signal. Moreover, if the nearly white H_1 spectrum corresponds to the noise spectrum, then the lower coherence between H_1 and V at the low frequencies is due to the drill-bit signal recorded on the vertical accelerometer rather than to a decrease in the noise level at the low frequencies.

Once the frequency bands of high noise coherence have been identified, the noise can be further characterized by computing cross plots between the recordings over a frequency band where the coherence is high. Figure 2-7 shows typical cross plots between the vertical recording and the H_1 and H_2 recordings. These plots represent samples every 4 ms over a 1s interval. Prior to cross-plotting, the recordings were bandpass filtered from 40 to 80 Hz, to isolate the frequency range where the coherence between the vertical and H_1 recordings was high. In Figure 2-7, the vertical and H_1 recordings have a predominantly linear polarization, with a slope of about 0.2; whereas the vertical and H_2 recordings have a random polarization as expected from their low coherence. The linear relationship between the vertical and H_1 recordings in this band is used in the next section to derive a filter that removes noise from the vertical accelerometer.

The extreme difference in the noise coherence between the two accelerometers, and the linear polarization of the noise, indicates that the noise is primarily polarized

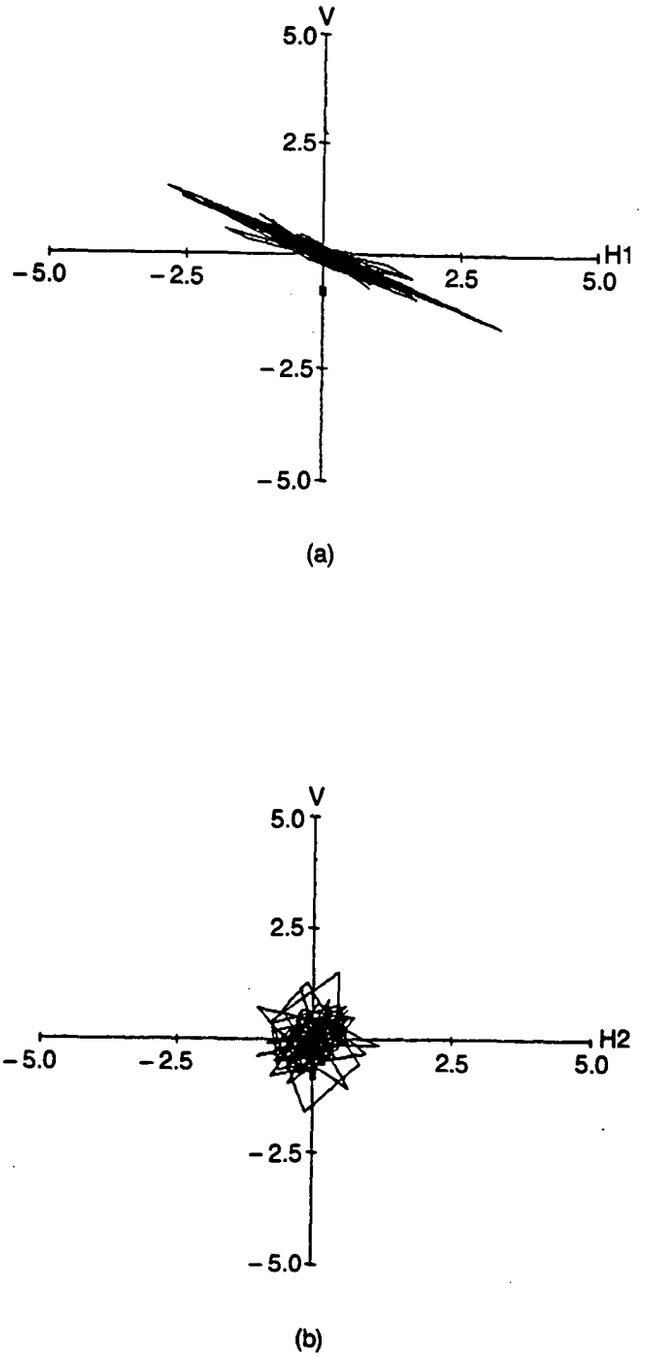

Figure 2-7. Cross-plot of vertical accelerometer and a) H_1; b) H_2 horizontal accelerometer recordings. The data have been bandpassed from 40 to 80 Hz. The cross-plots represent 1 second of recording time.

normal to a vertical plane containing the bail. The polarization of the noise can be explained by the construction of the swivel/bail assembly shown in Figure 2-4. The pins connecting the swivel to the bail allow horizontal motion perpendicular to the vertical plane of the bail, while restricting motion parallel to this plane. Thus, the swivel will respond to accelerations with a horizontal component by pivoting perpendicular to the bail plane, resulting in noise cross feed. Since the swivel cannot pivot parallel to the plane of the bail, there is little cross feed of the noise into the H_2 recording. This characteristic is important because it means that the noise on the vertical accelerometer can only be estimated and removed with an accelerometer oriented in the H_1 direction.

2.4 Attenuation of Vertical Accelerometer Noise Through Component Filtering

The coherent relationship between the noise recorded on the vertical and H_1 accelerometers can be used to component-filter the vertical accelerometer signal, reducing the level of coherent noise. By reducing the noise level, the S/N of the cross-correlation function is improved (Appendix 2-A) and the S/N of the pilot signal autocorrelation is also improved. This latter result means that better reference deconvolution filters (Chapter 1) can be obtained.

The component filtering process takes recordings from two components containing the same noise, and through weighted subtraction obtains a pilot signal, P'(t), with the noise substantially reduced. In terms of the vertical accelerometer signal, P(t), and the H_1 accelerometer signal, $H_1(t)$, the component filtering process can be written as:

$$P'(t) = P(t) - K\, H_1(t) \tag{2-9}$$

where K is a scalar weight. To obtain a good estimate of the weight, the drill-bit signal is bandpassed to a frequency range where the noise coherence is high. Within

this frequency range the weight is computed by determining a best least squares straight line fit to the cross-plotted recordings. The slope of the straight line is the weight. Inspection of Equation 2-9 shows that the component filter does not significantly attenuate drill-bit signal if the weight is constrained to be less than 1, because the drill-bit signal amplitude will be higher on the vertical accelerometer than on the H_1 accelerometer. If the H_1 signal is corrupted by other types of noise, the weight will be misestimated and the other noise may be introduced into the vertical signal. In most instances it appears that the H_1 signal primarily consists of a single wideband noise that is also recorded by the vertical accelerometer (Marion, 1990).

Figure 2-8 shows the pilot signal spectrum after component filtering using Equation 2-9. The input vertical and H_1 recordings correspond to the spectra in Figure 2-5. The weight was computed from the accelerometer signals after applying a 40 to 80 Hz bandpass filter. Figure 2-8 is scaled to the same peak value as Figure 2-3A so that the relative amplitudes of the different frequencies can be compared. The component-filtered spectrum is virtually identical to the vertical accelerometer spectrum at the low frequencies, but above 25 Hz the component-filtered spectrum has lower amplitude. Between 40 and 80 Hz, where the noise coherence was highest, approximately 15 dB of noise has been removed. Drillpipe multiple resonances can be seen up to 90 Hz. Additionally, a 45 Hz 'notch' (Appendix 2-B) is apparent that had been completely filled in by noise prior to component filtering.

The improvement in pilot signal quality after component filtering translates into improved S/N and improved wavelet character in the cross-correlation functions. Figure 2-9A shows a series of cross-correlation functions computed using the vertical recording as the pilot signal and Figure 2-9B shows the same correlation functions using a component-filtered pilot signal. The traces were computed over a recording time of 20 minutes at a depth of 1677m. The direct arrival in Figure 2-9B is the event

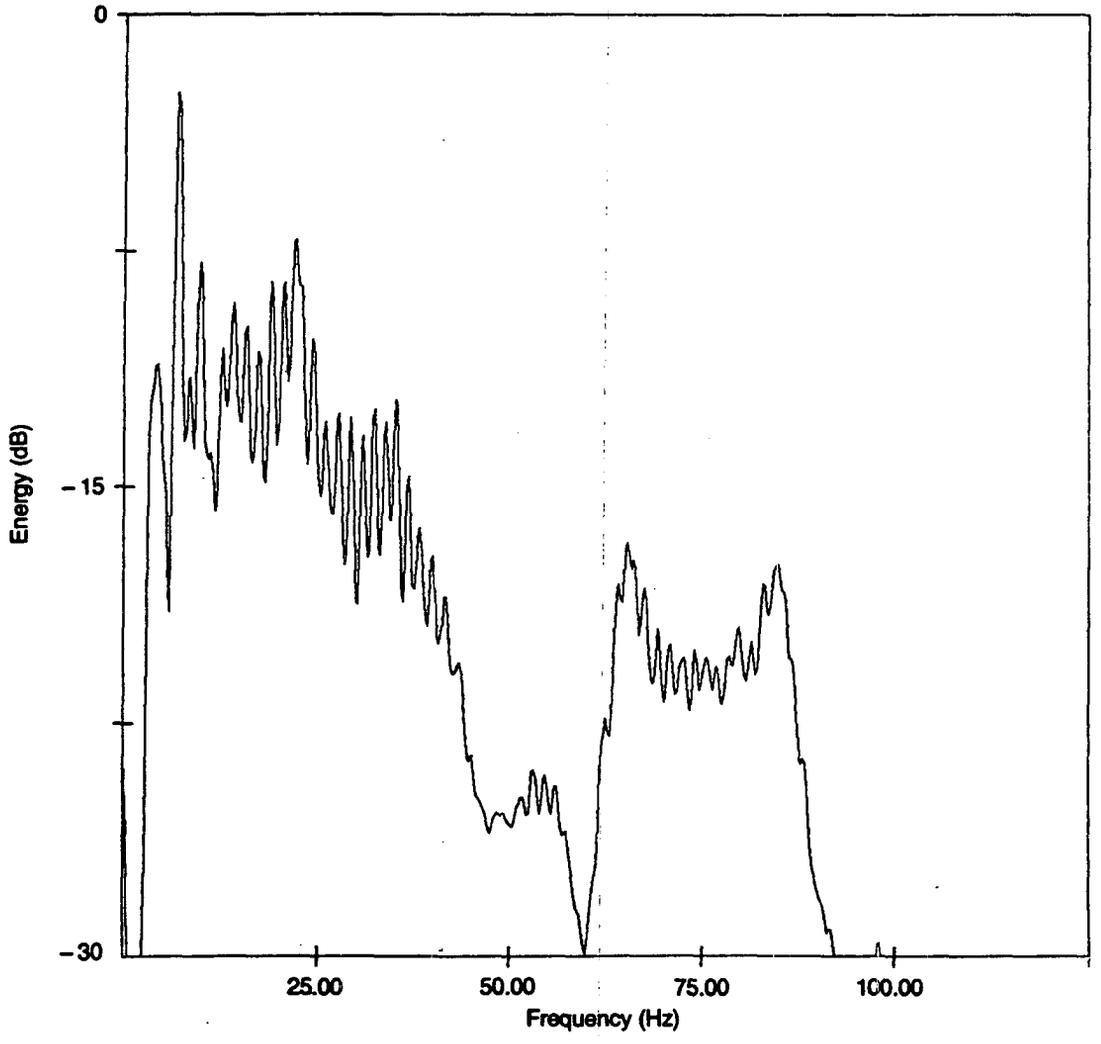

Figure 2-8. Vertical acceleration spectrum of Figure 2-5 after weighted subtraction of H_1 recording from vertical accelerometer recording.

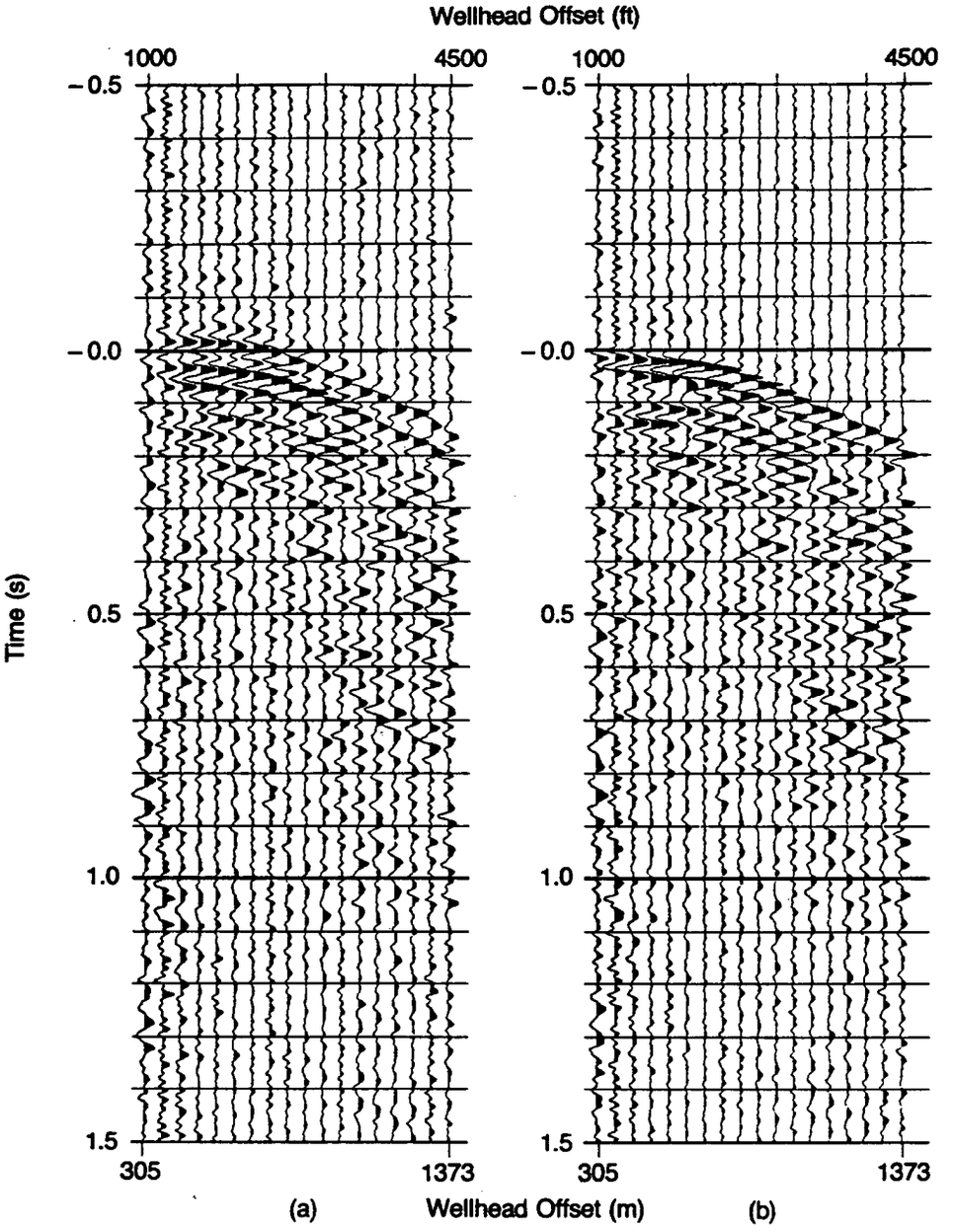

Figure 2-9. Cross-correlation functions between geophone array recordings and a) the vertical accelerometer recording pilot signal and b) the component-filtered pilot signal were computed over a recording time of 20 minutes. The component-filtered pilot signal results in a clearly superior direct-arrival wavelet.

with a correlation delay of 10 ms at the nearest geophone offset and increasing delay with offset. The events that follow the direct arrival are rig arrivals (Chapter 3). The direct arrival in Figure 2-9A is more difficult to identify. Is it the first event or the second, 50 ms later? The improved direct-arrival wavelet obtained through component filtering is important for obtaining a zero phase reflectivity function to compare with synthetic seismograms. An 'ugly' wavelet of the type observed in Figure 2-9A would be much more difficult to deconvolve properly. The improved wavelet is also important for using the technique as a checkshot method (as discussed in Chapter 4). In Figure 2-9A, there is as much as 50 ms of uncertainty in the timing of the wavelet peak, resulting in a potential depth uncertainty of up to 150m. In Figure 2-9B, there is virtually no uncertainty in the peak timing.

2.5 Characterization of Signal and Noise on Geophone Array Recordings

As described in Chapter 1, a typical configuration used to record the drill-bit signal path through the earth is a linear array of geophones of uniform spacing, with the array oriented toward the drill rig. The array is oriented toward the drill rig because the primary noise component on a single geophone comes from the drill rig engines and mud pumps (Rector, et al, 1986; Kostov, 1988). By spanning a distance encompassing a noise wavelength, the noise energy can be reduced much like shot noise is reduced through source and receiver arrays. The linear, uniformly-spaced array has a well-known response that will not be repeated here. Coupling and spacing pertubations serve to reduce the noise attenuation provided by the array, particularly for the higher-wavelength noise (Berni and Roever, 1989; Levin, 1989). The average attenuation provided by the linear array spanning a noise wavelength is usually assumed to be about 12 dB. Hence, the array output may still contain appreciable amounts of rig noise.

Assuming that the pilot signal noise is uncorrelated with the geophone array noise, the remaining noise on the geophone array recording can be characterized by

examining the S/N of the cross-correlated traces as a function of distance from the drill rig. If the pilot signal noise were correlated with the geophone array noise we would see correlated events unrelated to the drill-bit signal. (As shown in Chapter 3 the correlated events can all be interpreted as originating at the drill bit.) Figure 2-10 is a display of cross-correlation functions computed over a 10 minute interval between the component-filtered pilot signal and a series of geophone arrays beginning at 153m and ending at 915m from the wellhead. The geophone arrays consisted of twenty-four 10 Hz vertical geophones having a total span of 70m. The arrays were oriented toward the drill rig to attenuate rig noise. The traces have had reference deconvolution (Chapter 1) and an 11 to 39 Hz bandpass filter applied. The arrival with a correlation time of 500 ms at the near offsets and hyperbolic moveout with wellhead offset has a delay and a moveout that identify it as a P-wave direct arrival from the drill bit (Chapter 3). The arrival preceding the direct arrival with linear moveout as a function of wellhead offset is a head wave arrival from the drillstring (the arrival is discussed at length in Chapter 3). The low-frequency energy at the near offsets with correlation times between 0.6 and 1.5s is drill-bit signal secondarily radiated from the drill rig and traveling to the geophones via ground roll modes. This arrival is also discussed in more detail in Chapter 3.

Figure 2-11 is a S/N estimate of the P-wave direct arrival shown in Figure 2-10. The S/N was estimated by calculating the ratio of the direct arrival peak amplitude to the rms amplitude of the correlation function over a time window from -400 to 0 ms, where no correlated drill-bit signals were anticipated. To compare the S/N's between the traces and relate the differences to a particular noise source, several assumptions must be made. From Appendix 2-A we observe that the correlation S/N is a complex combination of the S/N's on the input recordings. The correlation S/N is only dependent on the precorrelation geophone array S/N for array S/N's less than 0 dB. Secondly, it must be assumed that the P-wave direct arrival has uniform

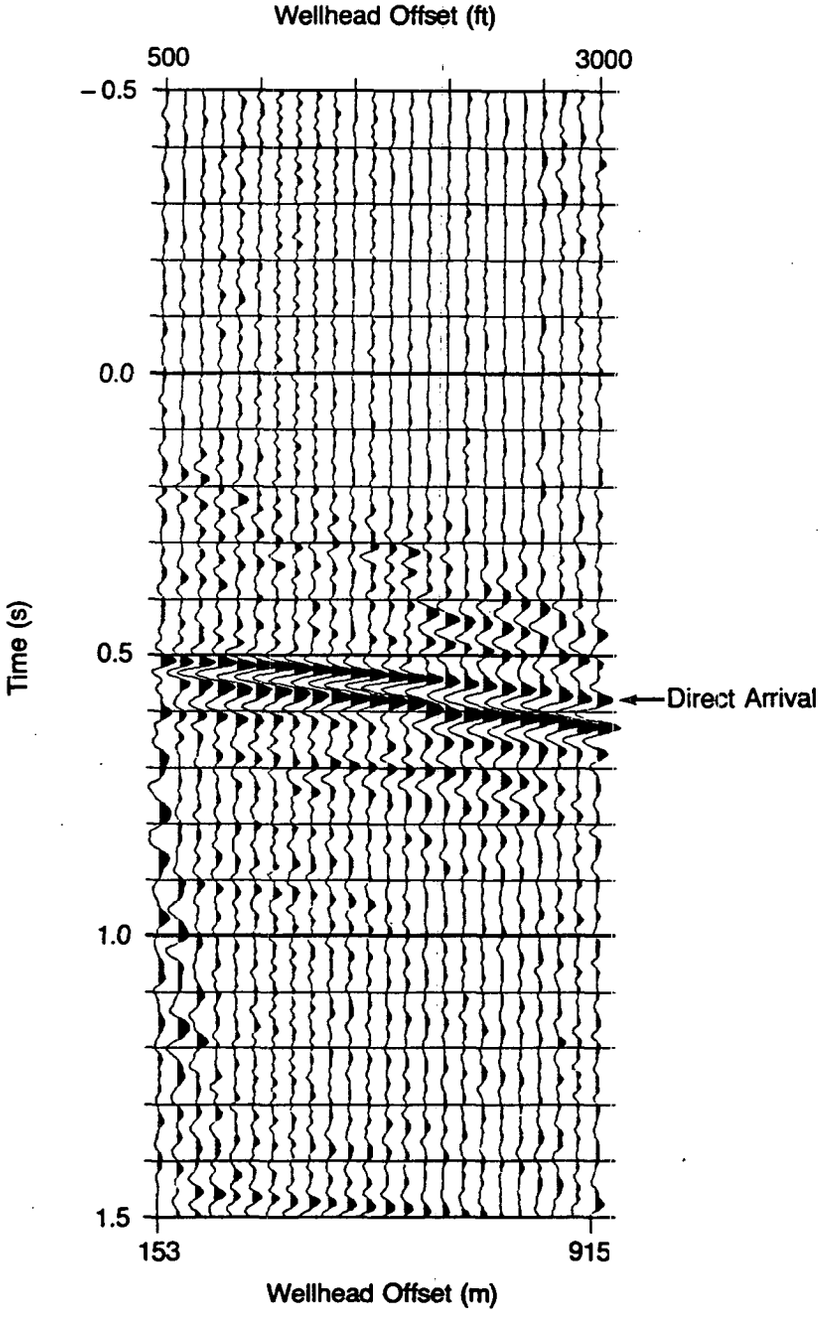

Figure 2-10. Cross-correlated traces using the recording of a component-filtered accelerometer pilot signal. The data are bandpassed from 11 to 39 Hz.

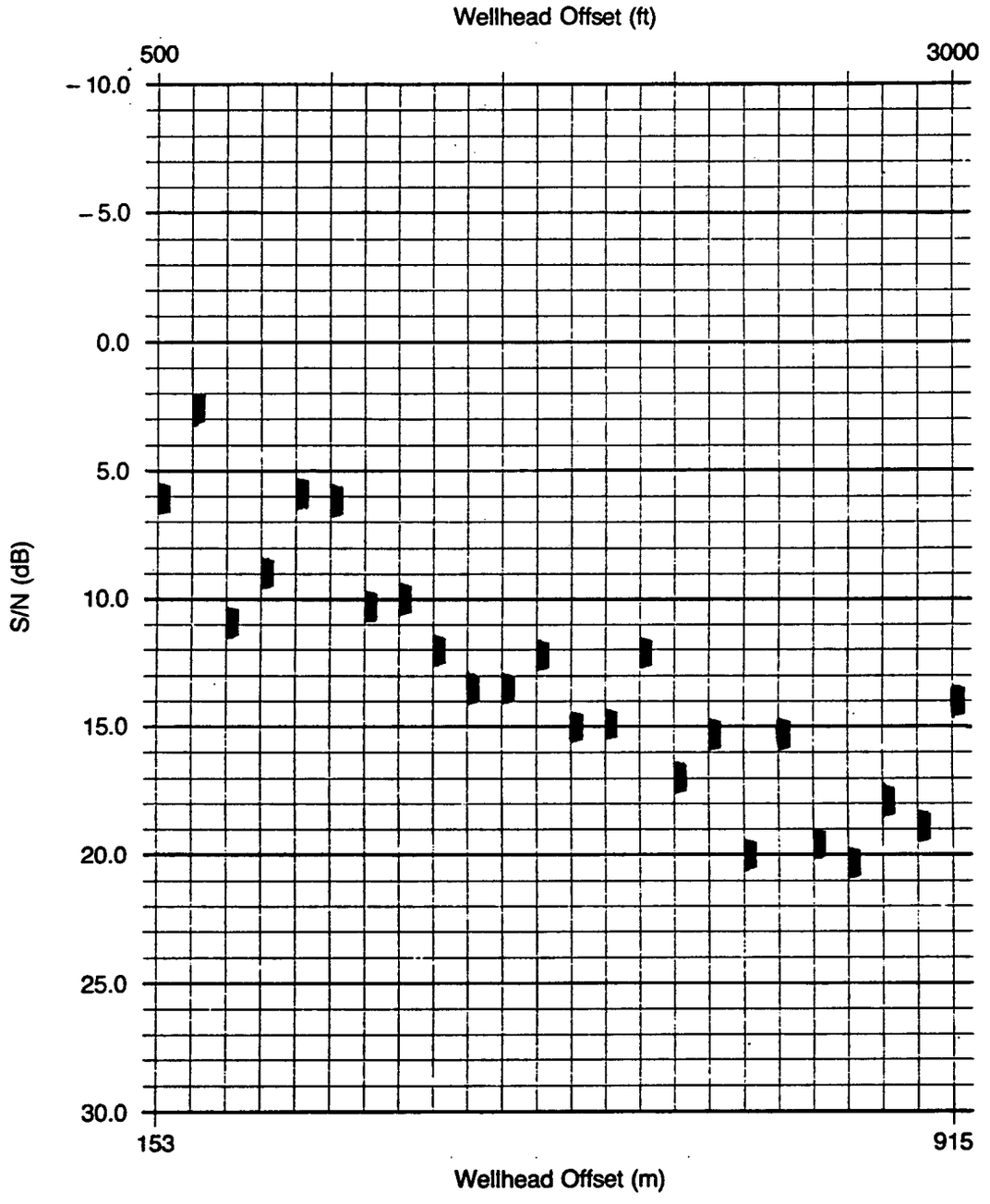

Figure 2-11. The computed direct arrival S/N for each of the traces shown in Figure 2-10 (in dB). The average absolute noise amplitude in the cross-correlation function was computed over a time window from -0.4 to 0s.

amplitude as a function of offset. Theoretically, the amplitude of the direct arrival should decrease with offset due to geometric spreading, absorption, source radiation (Chapter 3) and receiver antenna effects. In the example shown, these effects resulted in a very slight (about 15 percent) reduction in the direct arrival amplitude across the series of arrays. The improvement in S/N observed in Figure 2-11 confirms that the geophone array S/N is less than 0 dB. If this were not so, the S/N would not change dramatically as a function of offset (Appendix 2-A). Since both assumptions are met, we can conclude that the geophone array noise is primarily coming from noise sources on the drill rig.

From the S/N variations in the correlation function of Figure 2-10, we can also infer that the rig noise recorded on the geophone array is uncorrelated with the pilot signal. A possible mechanism for the decoupling is obtained from Figure 2-12. Figure 2-12 shows a series of cross-correlation functions between the component-filtered pilot signal and accelerometers located at various positions on the rig mast and on the principal rig noise sources (the rig engines and the mud pumps). The data have had reference deconvolution and a 12 to 80 Hz bandpass filter applied. The data are displayed in true relative amplitude. In our formulation of correlation, the correlation function is not normalized to the autocorrelations of the input recordings. Thus, the relative amplitudes of correlated signals between a common pilot signal and different geophone (or accelerometer) signals are equivalent to the relative amplitudes of the signals prior to correlation. As shown by Figure 2-12, the drill-bit signal propagates with little attenuation throughout the rig mast. The interface between the mast and the earth (and the interface between the rig engines and the earth) substantially attenuate the drill-bit signal. Using reciprocity, these interfaces would also substantially reduce the level of engine noise recorded on the pilot signal.

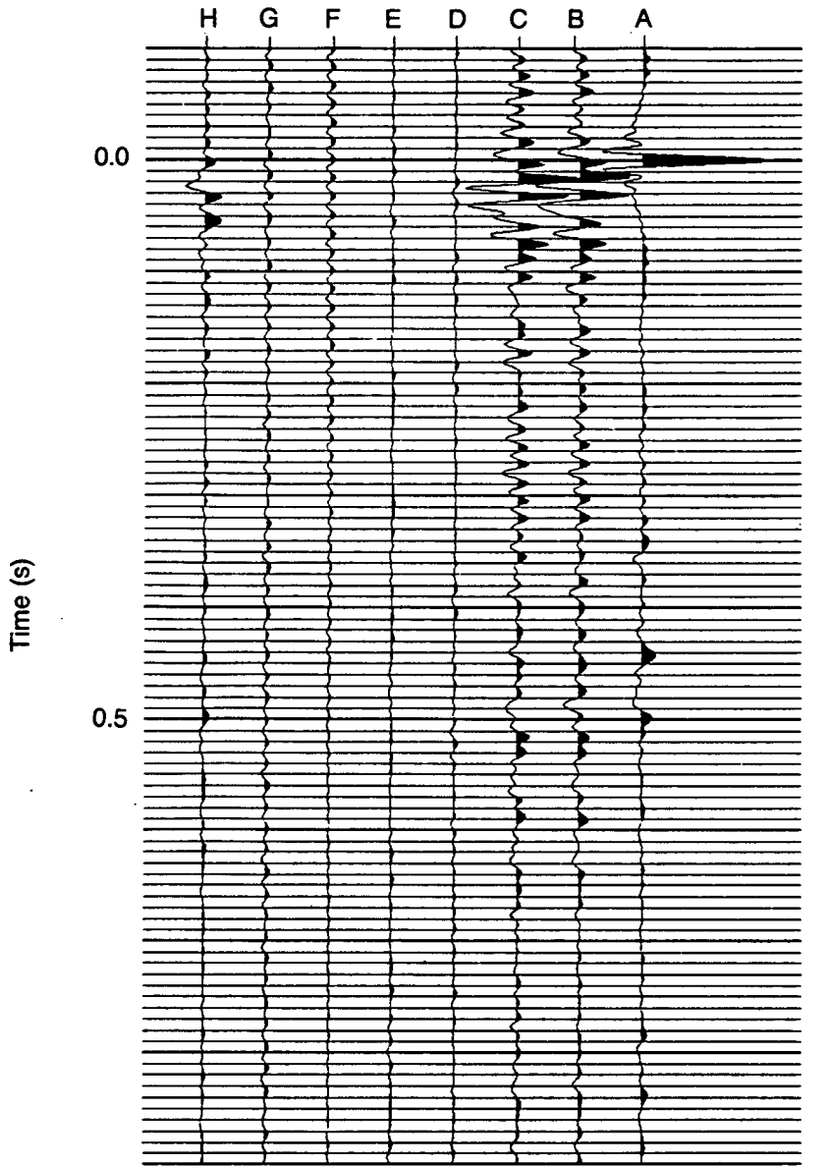

Figure 2-12. Cross-correlation functions between the vertical accelerometer (after application of spiking deconvolution) and a) itself; b) an accelerometer strapped to the top of the mast; c) an accelerometer strapped to the middle of the mast; d) and e) accelerometers strapped to the mud pump; f) an accelerometer strapped to the diesel engines; g) an accelerometer strapped to the bottom of the mast. The data are plotted so that the relative amplitude between the traces is preserved.

2.6 Summary

Both the vertical accelerometer and the geophone array record noise as well as drill-bit signal. The noise recorded on one of these responses is uncorrelated with the drill-bit signal and with the noise recorded on the other response. Consequently, it is attenuated in the cross-correlation function between the two recordings by a factor roughly proportional to the square root of recording time.

The drill-bit S/N of the vertical accelerometer varies with frequency partially due to a signal 'notch' between 25 and 50 Hz. Dissipation of the drill-bit signal caused by travel of the longitudinal wave up the drillstring also causes attenuation of higher frequencies. The noise on the vertical accelerometer was found to be wideband.

With an understanding of the causes of the noise on the individual recordings, the S/N of the drill-bit signal can be improved in cross-correlation functions by improving the S/N of the individual recordings. The vertical-accelerometer noise is reduced by component filtering with a noise estimate from a horizontal accelerometer oriented perpendicular to the bail. The geophone array noise can be reduced through offset spatial filtering. Although only simple linear arrays were described here, more sophisticated beamformers could also be used to improve the geophone array S/N.

Chapter 2: References

Aki, K. and Richard, P.G., 1980, Quantitative seismology, theory and methods, W.H. Freeman and Co.

Backus, M.M., 1959, Water reverberations-their nature and elimination, Geophysics, 24, 2, 233-261.

Berni, A.J. and Roever, W.L., 1989, Field array performance: theoretical study of spatially correlated variations in amplitude coupling and static shift and case study in the Paris Basin, Geophysics, 54, 4, 451-459.

Cox, W.H. and Chaney, P.E., 1981, Telemetry System, U.S. Patent No. 4293936.

Dareing, D.W., 1982, Drill collar length is a major factor in vibration control, 57th Annual Fall Technical Conference of Society of Petroleum Engineers of AIME, SPE 11228.

Deily, F.H., Dareing, D.W., Paff, G.H., Ortloff, J.E., Lynn, R.D., 1968, Downhole measurements of drillstring forces and motions: Trans. Am. Soc. Mech. Eng. Journal of Eng. for Ind., May, 217-225.

Drumheller, D.S., 1988, Acoustical properties of drill strings, J. Acoust. Soc. Am., 85 (3), 1048-1064.

Jenkins, G.M. and Watts, D.G., 1968, Spectral analysis and its applications, Holden-Day, Oakland.

Kolsky, H., 1963, Stress waves in solids, Dover Publications.

Kostov, C., 1988, Drill-bit signal, Stanford Exploration Project, 59, 11-34.

Levin, F.K., 1989, The effect of geophone arrays on random noise, Geophysics, 54, 11, 1466-1473.

Lutz, J., Raynaud, M., Stalder, S.G., Quichand, C., Raynal, J., and Muckelroy, J.A., 1972, Instantaneous logging based on a dynamic theory of drilling, J. Pet. Tech., 10, 750-758.

Marion, B.P., 1990, personal communication.

Squire, W.D. and Whitehouse, H.J., 1979, A new approach to drillstring acoustic telemetry, Presented at the 34th Annual Fall Technical Conference and Exhibition of the Society of Petroleum Engineers of AIME, Las Vegas, NV.

White, J.E., 1965, Seismic waves: radiation, transmission, and attenuation, McGraw-Hill.

APPENDIX 2-A

COHERENT SIGNAL AND ESTIMATOR NOISE IN A CORRELATION FUNCTION

An estimate of the cross-correlation function between two recordings, p(t) and g(t), in discrete time, t, is:

$$cc(\tau) = \frac{1}{N} \sum_{t=1}^{N} p(t)\, g(t+\tau)\, \Delta t \qquad (2\text{-}1A)$$

where N is the number of samples in the estimate, Δt is the sampling interval, and τ is the cross-correlation lag. If each of the recordings consist of coherent signal, b(t), and incoherent noise, $n_i(t)$, then:

$$p(t) = \alpha_1 b(t) + n_1(t)\,,$$

and (2-2A)

$$g(t) = \alpha_2 b(t) + n_2(t)\,,$$

where α_1 and α_2 are the amplitudes of the coherent signal.

Let us assume that the signal and the incoherent noise are time stationary, have zero mean, and variances σ_b, σ_{n1}, and σ_{n2}. If there is a single coherent, wideband signal in the cross-correlation function, then the amplitude of this event, C_1, is approximately given by:

$$C_1 \cong \frac{1}{N} \alpha_1\, \alpha_2\, \sigma_b^{\,2} \qquad (2\text{-}3A)$$

An estimate of the cross-correlation signal-to-noise ratio, $CC_{S/N}$, is the ratio of the coherent signal amplitude to the expected estimator noise absolute amplitude, η:

$$CC_{S/N} = \frac{C_1}{E[\eta]} . \tag{2-4A}$$

Since the estimator noise in the cross-correlation occurs at all delays, τ, $E[\eta]$ can be estimated from the cross-correlation amplitude over a time window that does not include the coherent signal. Jenkins and Watt (1968) showed that two stationary, uncorrelated signals x and y have a cross-correlation variance, σ^2_{xy}, where

$$\sigma^2_{xy} \cong \frac{k\sigma_x^2\sigma_y^2}{N} \tag{2-5A}$$

The scalar k is related to the estimator bias in two uncorrelated signals. If both inputs are narrowband, then k may significantly change the variance of the cross-correlation. If one of the two input signals is broadband, then $k \sim 1$ and the variance of the cross-correlation function is only related to the variances of the input signals and the recording time, N. In this case, the estimator noise variance, σ^2_η, can be written as:

$$\sigma_\eta^2 \cong \frac{1}{N} (\alpha_1^2 \sigma_b^2 + \sigma_{n1}^2) (\alpha_2^2 \sigma_b^2 + \sigma_{n2}^2) \tag{2-6A}$$

The expected absolute value of a normally distributed random variable, x, is:

$$E\{|x|\} = \sigma \frac{2}{\pi} e^{-m^2/2\sigma} + 2\,\mathrm{merf}(m/\sigma) \quad , \tag{2-7A}$$

where σ^2 is the variance and m is the mean. Plugging (9) into (10) the expected absolute noise amplitude E[η], becomes:

$$E[\eta] = - \frac{2}{\pi N^{1/2}} (\alpha_1^2 \sigma_b^2 + \sigma_{n1}^2)\,(\alpha_1^2 \sigma_b^2 + \sigma_{n2}^2)^{1/2}, \qquad (2\text{-}8A)$$

and Equation 2-5A then becomes:

$$CC_{S/N} \cong \frac{\pi}{2} \left(\frac{N \alpha_1^2 \alpha_2^2 \sigma_b^4}{(\alpha_1^2 \sigma_b^2 + \sigma_{n1}^2)\,(\alpha_1^2 \sigma_b^2 + \sigma_{n2}^2)} \right)^{1/2}. \qquad (2\text{-}9A)$$

Like CDP stacking, the improvement in S/N is proportional to the square root of recording time. As shown in Figure 2-1A, the drill-bit signal and the noise exhibit behavior that is nearly stationary over short (< 10 minute) recording times. The S/N of the coherent drill-bit energy in the cross-correlation functions improves by a factor roughly proportional to the square root of the recording time.

Several simplifications can be made to Equation 2-9A provided certain assumptions are made. If the drill-bit S/N on each input is greater than 0 dB, then Equation 2-9A reduces to:

$$CC_{S/N} \cong \left(\frac{\pi N}{2} \right)^{1/2}. \qquad (2\text{-}10A)$$

In this case, the S/N in the cross-correlation function is not dependent upon the S/N of the input signals. If the S/N is much less than 0 dB on both inputs then Equation 2-9A becomes:

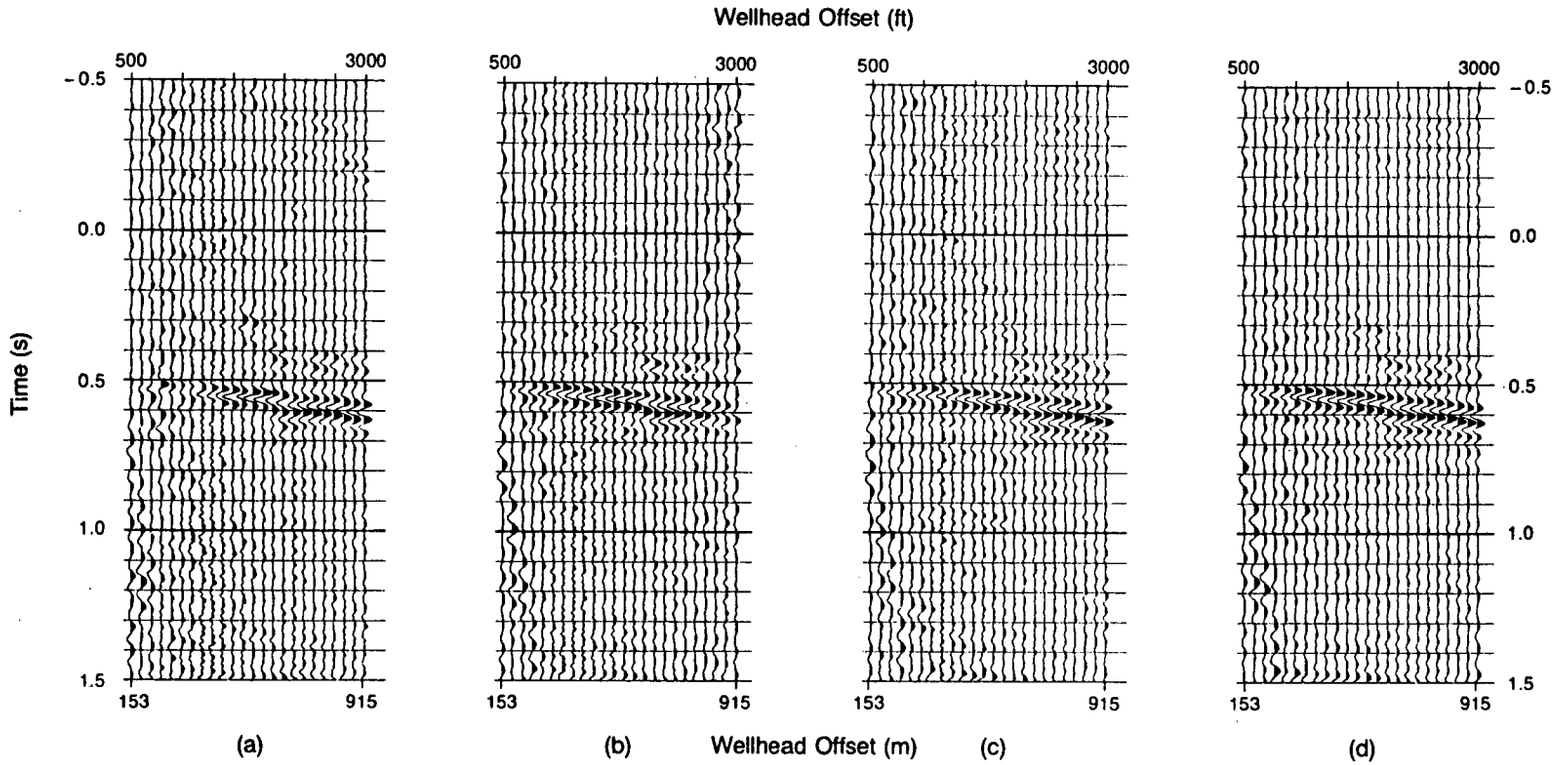

Figure 2-1A. Cross-correlated data computed using fractions of the recording time used in Figure 2-10.
a) 1/16; b) 1/9; c) 1/4; d) 1/2.

$$CC_{S/N} \cong \frac{\pi(N)^{1/2}}{2} \left(\frac{\alpha_1^2\sigma_b^2}{\sigma_{n1}^2}\right) \left(-\frac{\alpha_2^2\sigma_b^2}{\sigma_{n2}^2}\right)^{1/2} . \qquad (2\text{-}11A)$$

Equation 2-11A shows that provided N is large enough, the $CC_{S/N}$ can be greater than 0 dB even though the input S/N's are much less than 0 dB.

The autocorrelation estimate is a particular subset of the cross-correlation. If there is a time delay in the autocorrelation where only coherent signal is concentrated, then Equation 2-9A becomes:

$$AC_{S/N} \cong \frac{\pi}{2} (N)^{1/2} \left(\frac{\alpha_1^2 \sigma_b^2}{\alpha_1^2 \sigma_b^2 + \sigma_n^2}\right) . \qquad (2\text{-}12A)$$

In the particular case of the TODS vertical accelerometer autocorrelation function we can estimate $AC_{S/N}$ from the ratio of the drillpipe multiple to the estimator noise:

$$AC_{S/N} \cong \frac{\pi (N)^{1/2}}{2} \left(\frac{A}{1-A^2}\right) \frac{\alpha_1^2 \sigma_b^2}{(\alpha_1^2 \sigma_b^2 + \sigma_{n1}^2)} , \qquad (2\text{-}13A)$$

where A is the ratio of the $N + 1^{th}$ to the N^{th} order drillpipe multiple.

APPENDIX 2-B

INVESTIGATION INTO SPECTRAL NOTCH CAUSES

A wide, often deep, spectral valley between about 25 and 50 Hz has been observed in several examples of drill-bit signal recorded at the top of the drillstring. It is unlikely that lower drill-bit signal amplitude or drillstring resonances produce this spectral valley or notch. The model of drill-bit signal production proposed in Chapter 1 provides no known mechanism for reducing the drill-bit signal amplitude in this band and the maximum spacing of drillstring resonances is about 10 Hz.

Another possible explanation for the notch is that the accelerometer location at the top of the drillstring is not at a system node, as modeled in Chapter 1. A notch could be created as drill-bit arrivals travel past the top of the drillstring, are reflected, and return to the swivel where they behave as a ghost reflection of the primary. Observations on several wells indicate that the notch center frequency is fixed over the entire drilling period and appears to be correlated with rig size. Lower notch frequencies (about 30 Hz) are observed with larger drill rigs (Marion, 1990).

After Backus (1959), the spectrum resulting from the superposition of a primary and drill rig ghost reflection can be written as:

$$P(\omega) = [1 - \cos\omega t_g]\, S(\omega)\, DS(\omega)\,, \qquad (2\text{-}1B)$$

where $S(\omega)$ is the fourier transform of the drill-bit source signal, $DS(\omega)$ is the fourier transform of the drillstring impulse response, and t_g is the two-way time delay of the ghost. It is assumed for now that the ghost is a displacement reflection from a 'fixed' boundary (a free boundary would be written as $2[1 + \cos\omega t_g]$. To obtain a fixed-boundary notch at 30 Hz, the two-way traveltime of the ghost would have to be about 30 ms.

To determine a suitable reflecting interface for a 'notch-producing' multiple arrival, the travelpaths and velocities above the top of the drillstring must be known. These can be obtained from the correlation time delay of drill-bit signal recorded by accelerometers located on different parts of the drill rig (Figure 2-12). From the correlation time delays in Figure 2-12, it is observed that after traveling past the swivel, the drill-bit signal is received first by an accelerometer at the top of the rig mast. Lower positions on the rig mast have progressively longer correlation times. The delays in Figure 2-11 are in qualitative agreement with the drill-bit signal path on the drill rig previously shown in Figure 2-4. The drill-bit signal continues from the swivel through the bail, the traveling block, and the drilling lines into the rig mast and down the rig mast to the base of the rig.

The complicated structure of the drill-bit arrivals on the rig mast accelerometers indicates that multiple reflected arrivals and/or multiply transmitted arrivals are being received. The relative amplitudes of these correlations to the autocorrelation (which also contains some amount of noise at the zero lag) indicates that the drill-bit travels relatively unattenuated between the swivel and the upper portions of the drillstring. Hence, the 'fixed' interface is most likely somewhere between C and H (in Figure 2-12). Using this logic, the rig floor could be the reflecting interface on this rig. Since rigs are not constructed uniformly, the depth and frequency of the notch would be expected to vary from rig to rig.

CHAPTER 3

RADIATION PATTERN AND SEISMIC WAVES GENERATED BY A WORKING ROTARY DRILL BIT

ABSTRACT

The seismic body wave radiation pattern of a working rotary drill bit can be characterized by theoretical modeling and field data examples. Our model of drill-bit signal generation is a pseudo-random series of impacts directed into the formation along the axis of the drillstring. Each axially-directed drill bit impact creates a longitudinal wave that travels up the drillstring and body waves that radiate into the earth. The model predicts that P-waves radiate primarily along the axis of the borehole, and SV waves radiate primarily perpendicular to the borehole axis. In a vertical hole the largest P-waves will be recorded directly above and below the drill bit; whereas, the largest SV waves will be recorded in a horizontal plane containing the drill bit. In a deviated borehole, the radiation patterns are rotated by the inclination angle of the drill bit. This seismic body wave radiation pattern is investigated with several field data examples.

The presence of the drillstring in the borehole creates other wave modes that are not observed when conventional vertical seismic profiles (VSPs) are conducted in fluid-filled boreholes. The longitudinal wave traveling up the drillstring is expressed in the earth as a head wave traveling away from the drillstring provided the formation velocities adjacent to the borehole are less than the drillstring velocity. When the longitudinal wave traveling up the drillstring reaches the drill rig, some of the energy continues through the drill rig structure and re-enters the earth. Secondary events are radiated at the drill bit after they travel up the drillstring as a longitudinal wave, reflect off drillstring discontinuities, and travel back down the drillstring to the bit. Each of these drill bit arrivals has a characteristic moveout as a function of wellhead

offset and drill bit depth. A knowledge of the radiation patterns and the wave modes generated by the drill bit is essential to interpreting drill bit wavefields.

3.1 Introduction

In Chapter 1 we modeled the drill-bit source as an impact source acting axially at the bottom of the borehole. Since conventional borehole seismic techniques are performed after the well is drilled, other investigations of borehole source radiation patterns have been concerned primarily with sources acting on the walls of the borehole (Heelan, 1953; White and Sengbush, 1963; Lee and Balch, 1982; Paulsson, 1988; Kennedy, et al, 1988, and Winbow, 1989). The closest analog found to the drill-bit source model discussed in Chapter 1 was a weight-drop source acting on the bottom of a cylindrical borehole. The weight-drop source can be approximated as a monopole force acting at the bottom of the borehole (White, 1965), which produces P and SV waves with unique radiation patterns. In Section 3.2, a model of the drill bit radiation pattern is introduced and its implications for surface recordings are discussed. In Section 3.3, real data examples are used to investigate the accuracy of the modeled radiation patterns.

When recording conventional VSP and acoustic logs, the presence of the borehole creates guided waves, such as Stoneley waves, that travel up and down the borehole. With the drill-bit energy source, the partial replacement of borehole fluid with steel drillstring changes the boundary conditions of the borehole system, modifying wave propagation inside the borehole and in the earth outside the borehole. In Section 3.4, theoretical models of wave propagation along a cylindrical borehole (White, 1965) and longitudinal wave propagation in a drillstring (Chapter 1) are used to characterize the wave types created when a drillstring occupies the borehole.

Conventional VSP data processing and analysis use the time moveout over receiver depth and source offset as a means to distinguish and filter different wave modes (Hardage, 1985). Direct and reflected P-wave arrivals can be distinguished

from shear wave arrivals and Stoneley waves by identifying the relative moveouts. This type of analysis can also be used with correlated drill bit wavefields. However, the presence of the drillstring and the use of a pilot sensor at the top of the drillstring change the time and moveout characteristics of drill-bit arrivals in a series of cross-correlated traces. In Section 3.5 and 3.6, the correlation times and moveouts of the different arrivals with depth and offset are characterized. The moveouts can be used to separate the different drill-bit wave modes with spatial filters.

3.2 Radiation Pattern of the Drill Bit

The radiation pattern of the axial drill-bit impact source described in Chapter 1 can be modeled as a transient point force acting along the axis of the borehole (White, 1965). White (1965) and Heelan (1953) showed that the far-field radial displacement resulting from a point force, g(t), applied along the axis of a cylinder embedded in a homogeneous solid is:

$$U_r(r,\phi,t) = \frac{A_1 \cos\phi}{\rho\alpha^2 r} g\left(t - \frac{r}{\alpha}\right), \tag{3-1}$$

and the far-field angular displacement is:

$$U_\phi(r,\phi,t) = \frac{A_2 \sin\phi}{\rho\beta^2 r} g\left(t - \frac{r}{\beta}\right), \tag{3-2}$$

where ρ is the formation density, r is the straight line distance from the source to the wavefront, α and β are the formation compressional and shear velocities, A_1 and A_2 are scalars, and the angle ϕ is measured relative to the direction of the point force (i.e., relative to the direction of drill bit impacts at the bottom of the borehole). U_r represents P-wave radiation since it is a component of motion that is oriented radially away from the source. U_ϕ represents SV-wave motion since its particle displacement

is in a plane containing the cylinder axis, perpendicular to U_r. There are no SH waves radiated by an axial source, and the radiation patterns have rotational symmetry about the cylinder axis. When the wavelengths of the body waves are much greater than the borehole radius, the far-field displacements are not influenced by the presence of the borehole.

The calculated P-wave and SV wave displacements corresponding to Equations 3-1 and 3-2 are shown in Figure 3-1. P-waves are radiated along the direction of the applied force; whereas no P-wave energy is radiated perpendicular to the force direction. SV waves are radiated perpendicular to the force axis, and no SV energy is radiated along the axis. The relative amplitudes of the P and SV radiation lobes are determined by the Poisson ratio of the formation being impacted by the drill bit. If the formation has a Poisson's ratio of 0.25 the SV displacement at an angle of 45° from the force axis will be three times the P-wave displacement and the displacements will be equal when $\phi = 18°$.

This model predicts that in a vertical well drilled in a horizontally-layered earth, vertical geophones deployed on the earth's surface directly above the drill bit will receive only P-body wave energy from the drill bit. At positions offset from the borehole, the SV radiation lobe begins contributing to the vertical geophone response at the surface. When a well is deviated, the radiation pattern observed on the surface is theoretically a rotated version of the vertical borehole radiation pattern, with the angle of rotation equal to the inclination angle of the drill bit. In such a case, receivers positioned at certain surface positions will not record a P-wave direct arrival from the drill bit. The geometry shown in Figure 3-2, taken from an offshore case study (Chapter 4), shows an example of this phenomenon. When the drill bit is working at the depth shown in Figure 3-2, there is a zone on the surface where the P-wave direct arrival will be very weak. In this zone, a direct raypath to the drill bit intersects the drill bit within a null between the two lobes of the P-wave radiation

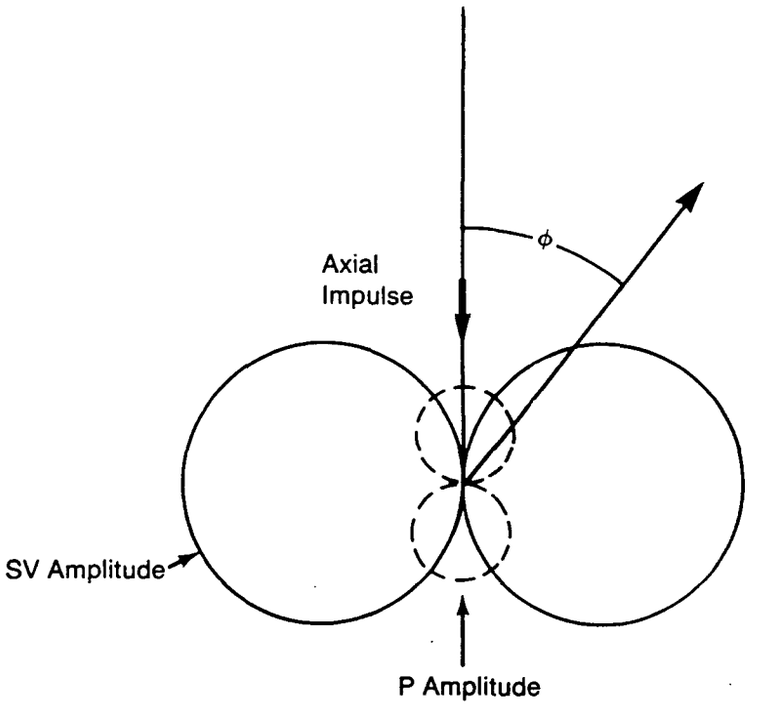

Figure 3-1. Far-Field P and SV wave amplitude distributions produced by an axial drill bit impulse on the formation at the bottom of the borehole. The relative amplitude of the P-wave radiation lobe to the SV wave radiation lobe is drawn for a formation with a Poisson's ratio of 0.25.

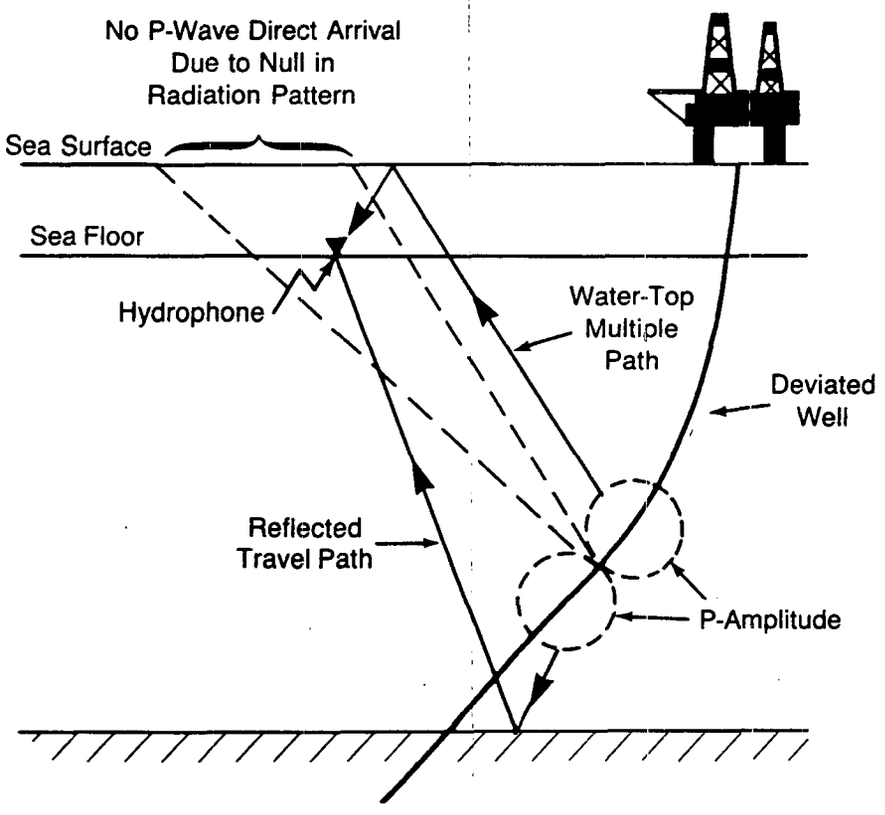

Figure 3-2. Theoretical drill bit P-wave radiation distribution in a deviated borehole drilled from an offshore platform. There is a zone on the seafloor where P-wave direct arrivals will not be received.

distribution. If the well is horizontal, receivers deployed directly above the drill bit in a horizontally-layered earth will theoretically record only shear body wave energy from the drill bit, polarized along the axis of the drillstring.

3.3 Field Data Investigations of the Drill-Bit Radiation Pattern

Figure 3-3 shows drill bit data that were recorded with a series of vertical geophone arrays extending away from the wellhead. Geophone arrays were deployed at 100 ft (30.5m) intervals on the surface beginning at a distance of 1300 ft (396m) from the wellhead and ending 4600 ft (1402m) from the wellhead. Each array consisted of four 4.5 Hz geophones placed 25 ft (7.6m) apart. The cross-correlated traces were computed on a vertical well was drilling at a depth of 3290 ft (1003m), over a recording time of 30 minutes. The traces in Figure 3-3 are displayed with a fixed gain so that the relative amplitudes between traces can be estimated. After cross-correlation, the data processing consisted of reference deconvolution (Chapter 1), and a bandpass filter from 12 to 40 Hz. The P-wave direct arrival in Figure 3-3 is identified based on its hyperbolic moveout with offset and its correlation time (as discussed in Section 3.5). The other hyperbolic moveout events are drillstring multiples, and the linear moveout that crosses the direct arrival is a rig arrival (discussed in Section 3.4). The amplitude of the direct arrival is a maximum at the near offsets and decreases uniformly as the offset distance and the takeoff angle, ϕ, increases. This behavior qualitatively agrees with the amplitude response of the upward traveling P-wave depicted in Figure 3-1. The anomalous amplitudes at 3100, 3200, 4500, and 4600 ft (945, 975, 1370, and 1400m) were due to malfunctioning equipment and noise. These offsets were not used in the radiation pattern analysis.

In order to use the direct arrival amplitudes to estimate the P-wave radiation pattern, the data must be corrected for the effects of wave propagation between the drill bit and the surface and for the vector response of the vertical geophone. The vertical geophone vector response is theoretically equivalent to the shape of the

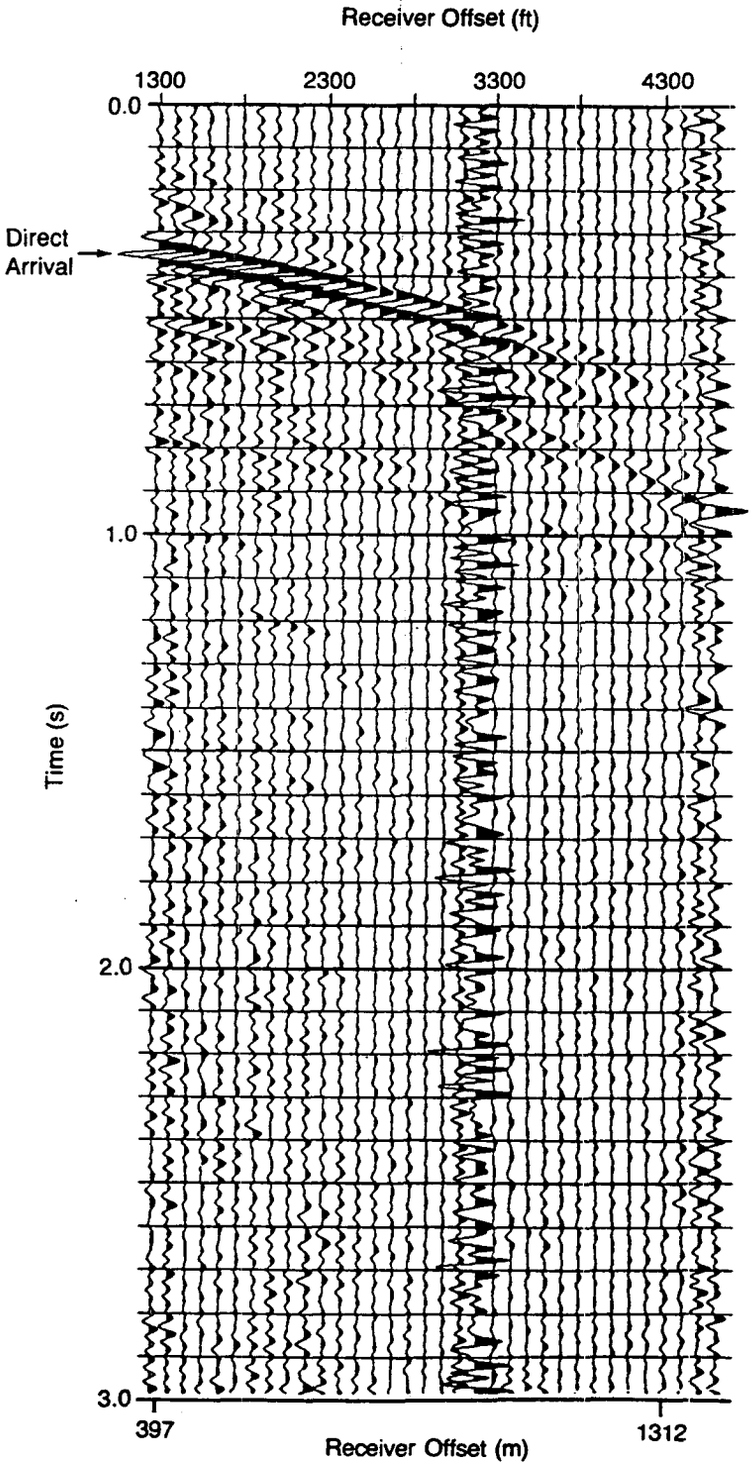

Figure 3-3. Wavefield recorded when the drill bit was drilling in a vertical well at a depth of 3290 ft (1003m). Each trace represents the cross-correlation function between the pilot signal recorded at the top of the drillstring and a different geophone array on the earth's surface. The direct arrival amplitude decreases with increasing offset from the wellhead.

P-wave radiation pattern illustrated in Figure 3-1. The array response had little effect on P-wave direct arrival wavelengths, which were generally greater than 250 ft (76m). Combining the effects of the geophone vector response and the attenuation of the P-wave direct arrival due to geometric spreading and absorbtion gives a scale factor, s(x), with which to correct the P-wave direct arrival amplitudes in Figure 3-3:

$$s(x) = \frac{x}{\sin\phi\cos\phi} \; e^{\frac{\pi f x}{QV \sin\phi}} \qquad (3\text{-}3)$$

where f is the frequency, V is the formation velocity (assumed homogeneous), and Q is the quality factor.

Figure 3-4 compares the magnitude of the theoretical drill-bit P-wave radiation (obtained from Equation 3-1) with the measured P-wave radiation as a function of ϕ. The measured radiation was obtained by computing the P-wave direct-arrival peak amplitude for each trace and scaling this value for each trace using s(x) defined in Equation 3-3 (assuming f = 30 Hz, Q = 50, and V = 8000 ft/sec (2430 m/s)). The measured values were scaled to the median amplitude computed from the first five offsets. The computed amplitudes exhibit a great deal of scatter, but the general trend with offset is similar to the theoretical curve. The high frequency data scatter is probably due to coupling variations and overlapping rig and head wave arrivals (discussed in Section 3.5).

Figure 3-5 is a three-component drill bit wavefield recorded on a vertical well at an offset of 3500 ft (1067m) from the wellhead. The vertical component was recorded as an array of twenty-four 10 Hz vertical geophones with a total length of 250 ft (76.9m). The two horizontal components were oriented transverse and radially inline to the wellhead. The horizontal components were recorded by an array of

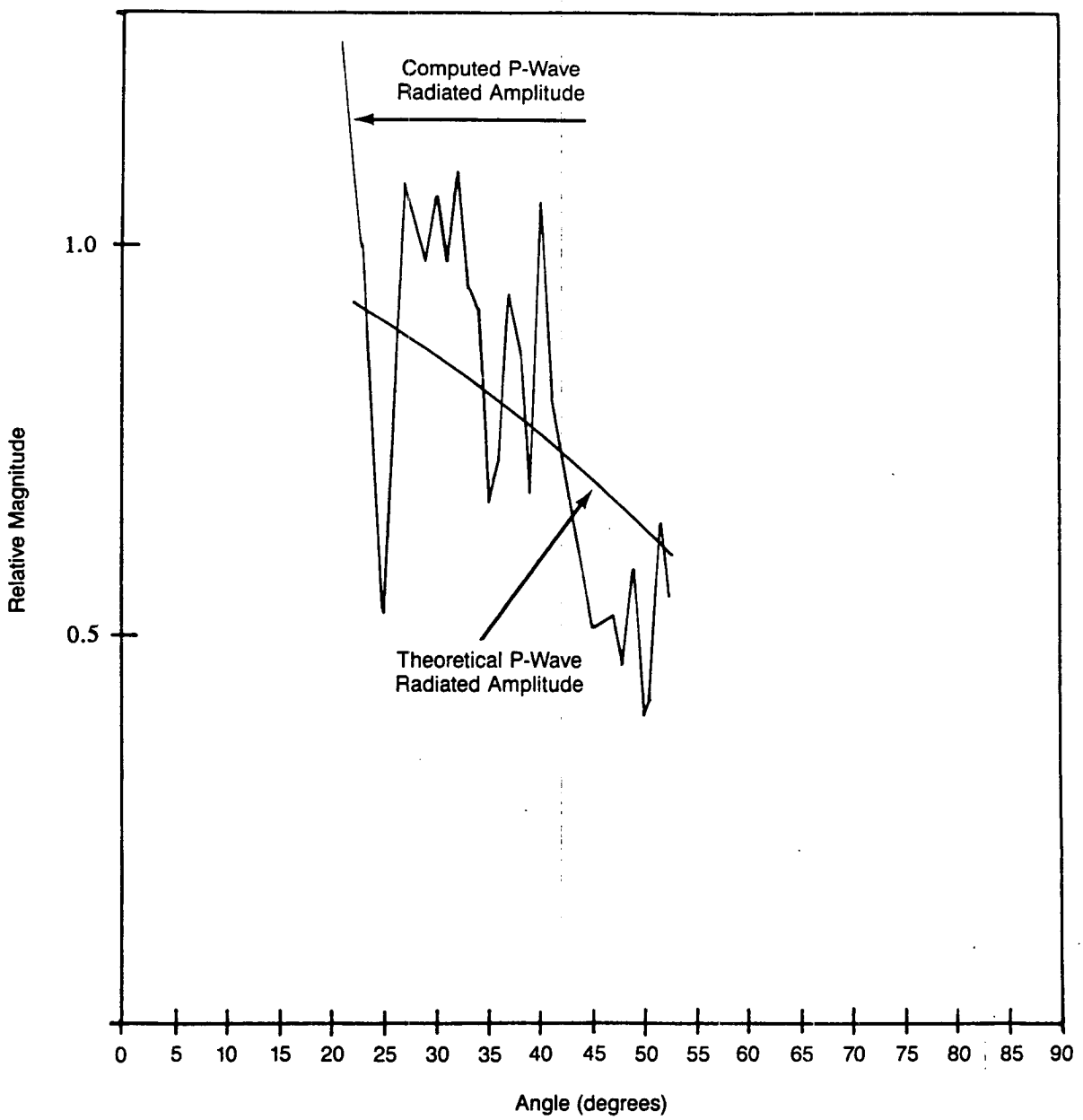

Figure 3-4. Measured versus theoretical P-wave radiation as a function of angle ϕ. The measured values were taken from the data in Figure 3-3 after correcting for attenuation and receiver response.

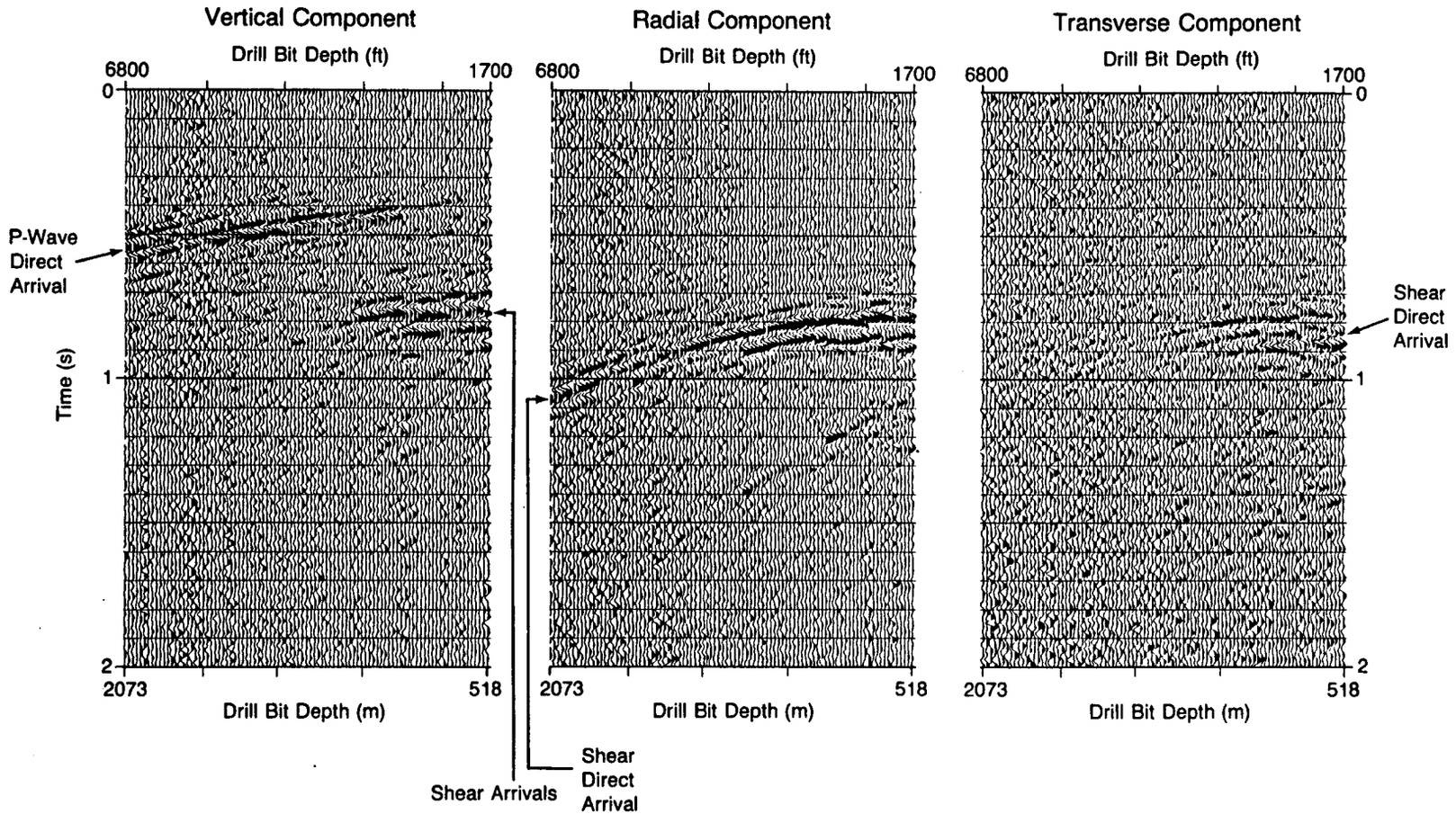

Figure 3-5. Drill bit wavefields recorded at a three-component geophone group located 3500 ft (1067m) from the wellhead of a vertical well. The traces represent drilling depths from 1700 to 6800 ft (518 to 2073m). The P-wave direct arrival from the drill bit to the geophone array as well as a shear direct arrival are labeled.

twelve 10 Hz horizontal geophones 100 ft (30.5m). Each of the three arrays spanned a radial distance away from the wellhead to attenuate incoherent noise from the drill rig (Chapter 2). The vertical array length was chosen to preserve P-waves from the bit at frequencies below 60 Hz at a depth of 6000 ft. The horizontal array length was less than the vertical array length to preserve shorter wavelength shear waves at the same frequencies.

Each trace in Figure 3-5 was computed over a 30 ft (9.1m) drilling interval representing approximately 1 hour of recording time. After cross-correlation, the data processing consisted of reference deconvolution (Chapter 1), a bandpass filter from 12 to 60 Hz, and correction of the traveltime from the drill bit up to the pilot sensor (Chapter 1). The P and shear direct arrivals labeled in Figure 3-5 are identified based on their traveltimes and moveout (Section 3.5). Both the P and shear direct arrivals exhibit a wavelet that is quite broad, encompassing over 100 ms. The reverberatory nature of the wavelet is probably due to near-surface multiples and residual drillstring multiples remaining after reference deconvolution. (As discussed in Chapter 2, noise present on the pilot signal can result in misestimation of the reference deconvolution filter, leaving residual drillstring multiples that appear as anticausal events before the primary direct arrival event.) Besides the direct arrivals, higher-moveout drillstring multiples (discussed in Section 3.4) and negative-moveout P and shear reflections are also apparent. The linear moveout events with an apparent velocity of 15600 ft/s (4758 m/s) are rig and head wave arrivals (Section 3.4) that would have zero moveout with depth if the traveltime of the drill bit up to the pilot sensor had not been corrected.

The display in Figure 3-5 was scaled by normalizing each trace to its peak rms amplitude. Thus, the relative amplitudes of the arrivals cannot be estimated. However, the improvement in direct S/N and the degradation of direct shear with depth are in qualitative agreement with Equations 3-1 and 3-2. The radial component

records direct shear arrivals with higher S/N than the transverse component, indicating that the radiated shear energy from the drill bit is primarily polarized as an SV wave, with particle motion in the borehole/surface array plane. The lower S/N shear arrival on the transverse component may be due to anisotropy in a zone above the drill bit (Crampin, 1985). The transverse component records the shear arrival approximately 10 ms before the radial component. The shear arrival on the transverse component may also be due to the weaker component of tangential force created by the drill bit impacts (Chapter 1).

Figure 3-6 shows a 3-component trace from a depth of 4440 ft (1353m) displayed in true relative amplitude. As predicted by the S/N's in Figure 3-5, the shear wave direct arrival on the radial component is much larger than the arrival on the transverse component, confirming the primary radiation of SV energy by the drill bit. The vertical component direct arrival has an amplitude that is approximately equivalent to the shear wave direct arrival on the radial component. By contrast, the modeled radiation patterns would predict a shear wave direct arrival about three times the P amplitude. Assuming these arrivals traverse the same earth path, the discrepancies between observation and theory are either due to coupling differences between the geophones or higher shear wave absorbtion. The latter is more likely since the use of multiple geophones should average out the coupling differences. The lower frequency character of the shear arrival is also indicative of greater absorbtion. High shear wave absorbtion is very common in travel through unconsolidated sediments near the earth's surface. The near surface in this region was unconsolidated glacial till which would be expected to be highly absorptive of shear wave energy.

A quantitative estimate of the drill bit radiation pattern can be obtained from the measured direct arrival amplitudes in several ways. Like the analysis with offset, the direct arrival amplitudes can be scaled for attenuation and receiver vector response and then compared with curves defined by Equations 3-1 and 3-2. However, this

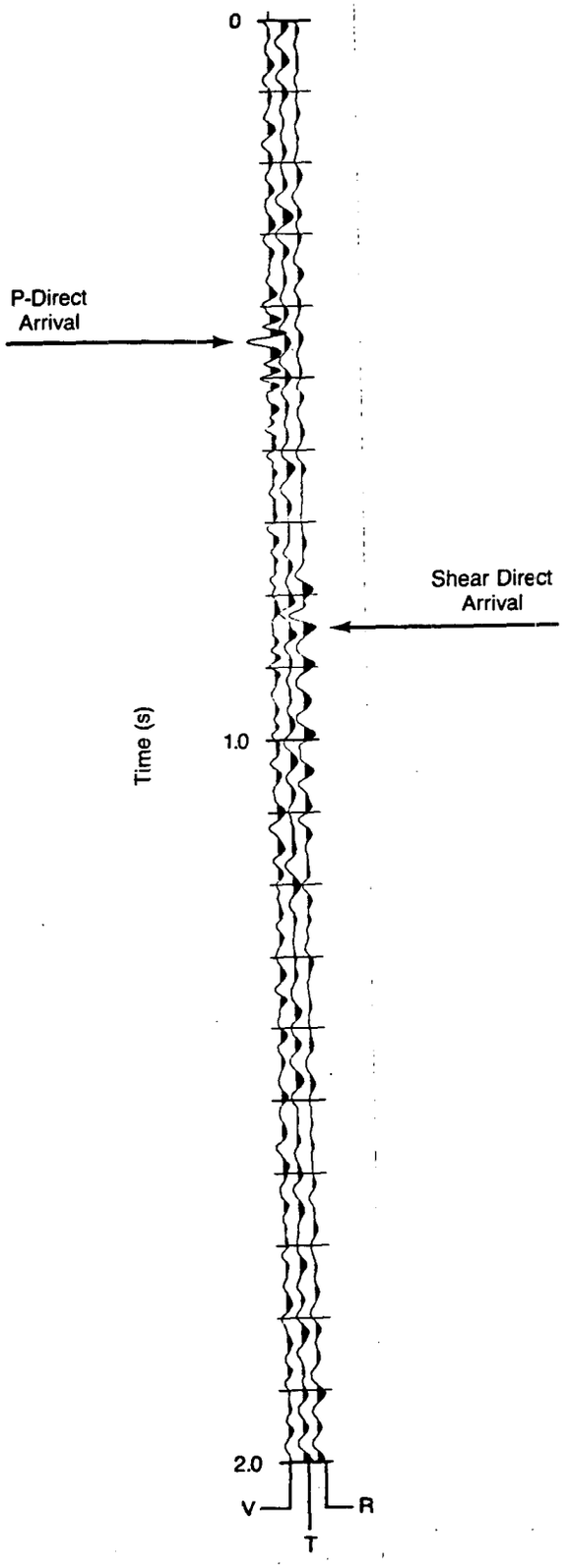

Figure 3-6. Three component (Vertical (V), Radial (R), and Transverse (T)) response corresponding to a depth of 4440 ft (1354m) in Figure 3-5, displayed in true relative amplitude.

method assumes that the drill bit source amplitude is constant over depth. Scatter in the measurements could be introduced if the drill bit source amplitude varied over depth.

A more robust method to estimate the drill bit radiation is to analyze the variation in the ratio of shear to P wave direct arrival amplitude with depth. Since, at each depth the shear and P waves have the same source amplitude and similar raypaths, there is no need to apply a depth dependent scaling factor to the data. Figure 3-7 shows a comparison of this measured ratio and an adjusted theoretical curve. The theoretical curve was adjusted to incorporate the differences between the measured and the theoretical amplitude ratios observed in Figure 3-6. The ratios were measured at particular depths where the S/N of both arrivals was high. After adjustment, the theoretical and measured curves give generally good agreement.

3.4 Other Wave Modes Generated by the Drill Bit

Besides the primary P and SV body waves radiated into the earth at the drill bit, there are other mechanisms by which drill bit vibrations are theoretically transferred into the earth and recorded by surface geophones. These other wave modes are caused by energy transfer between the wave traveling in the drillstring and the formation. This is similar to the secondary energy radiated by tube waves traveling in a fluid filled borehole (Hardage, 1981), however the presence of the drillstring changes the characteristics of secondary arrivals recorded in drill bit wavefields. Before discussing correlated field examples we model a few of the principal travelpaths taken by these other wave modes.

In conventional VSP, the principal non-body waves are Stoneley waves (or 'Tube waves') created at the wellhead by ground roll arriving from the surface energy source (Hardage, 1981). Classical Stoneley waves have not been observed in correlated drill bit wavefields recorded at the surface. (In all the data examples shown in this thesis, none of the arrivals observed have a moveout with depth near the fluid

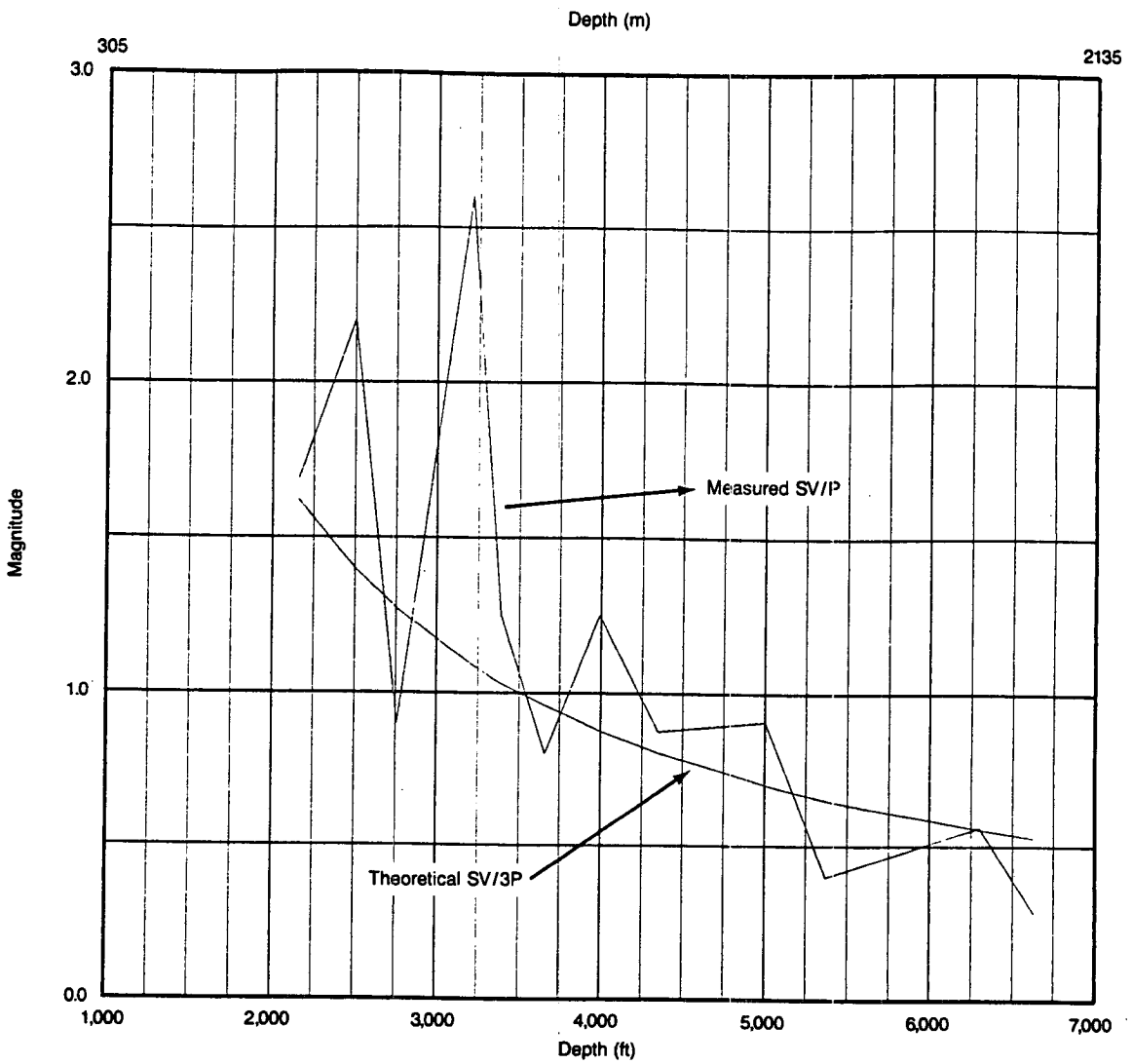

Figure 3-7. Measured versus theoretical SV to P-wave radiation as a function of depth. The theoretical curves were corrected for the higher absorbtion of the shear waves observed in Figure 3-6.

velocity.) The absence of tube wave arrivals in drill bit wavefields may be due to the recording of drill bit wavefields with receiver arrays offset from the wellhead (Chapter 2). Hardage (1981) showed that tube wave interference in a conventional VSP was signficantly reduced when the source/wellhead offset increased. Alternatively, the lack of tube wave arrivals may be due to the presence of the drillstring in the borehole. Finite-element modeling results (Samec, 1989a) indicated that the borehole guided wave mode is primarily controlled by the higher density drillstring and only slightly modified by the borehole fluid.

Rig Generated Arrivals

In correlated drill bit wavefields recorded by surface geophones, one of the principal arrivals has a delay and a moveout with depth and offset (Sections 2.5 and 2.6) that identify it as having a source location at the drill rig. As shown in Figure 3-8, this rig generated arrival is modeled as traveling from the drill bit up the drillstring, entering into the rig mast via the drilling lines, and traveling into the earth through the feet of the rig mast. A group of surface geophone arrays extending away from the wellhead would be expected to record rig-generated arrivals similar to a 'shot' gather in conventional surface seismic acquisition, with the shot position at the drill rig. The data shown in Chapter 2 appear to support this model for transfer of energy through the drill rig. In Chapter 2 it was noted that drill bit signals recorded at progressively lower positions on the rig mast exhibited progressively longer time delays.

Head Wave Arrivals

Besides the drill rig, the drillstring itself can appear to act as a secondary radiator of drill bit energy. When the velocity of the longitudinal wave traveling up the drillstring is greater than the formation velocity, the longitudinal wave traveling in the drillstring can theoretically travel into the earth, away from the drillstring, with characteristics that are similar to 'head waves' observed in conventional seismic

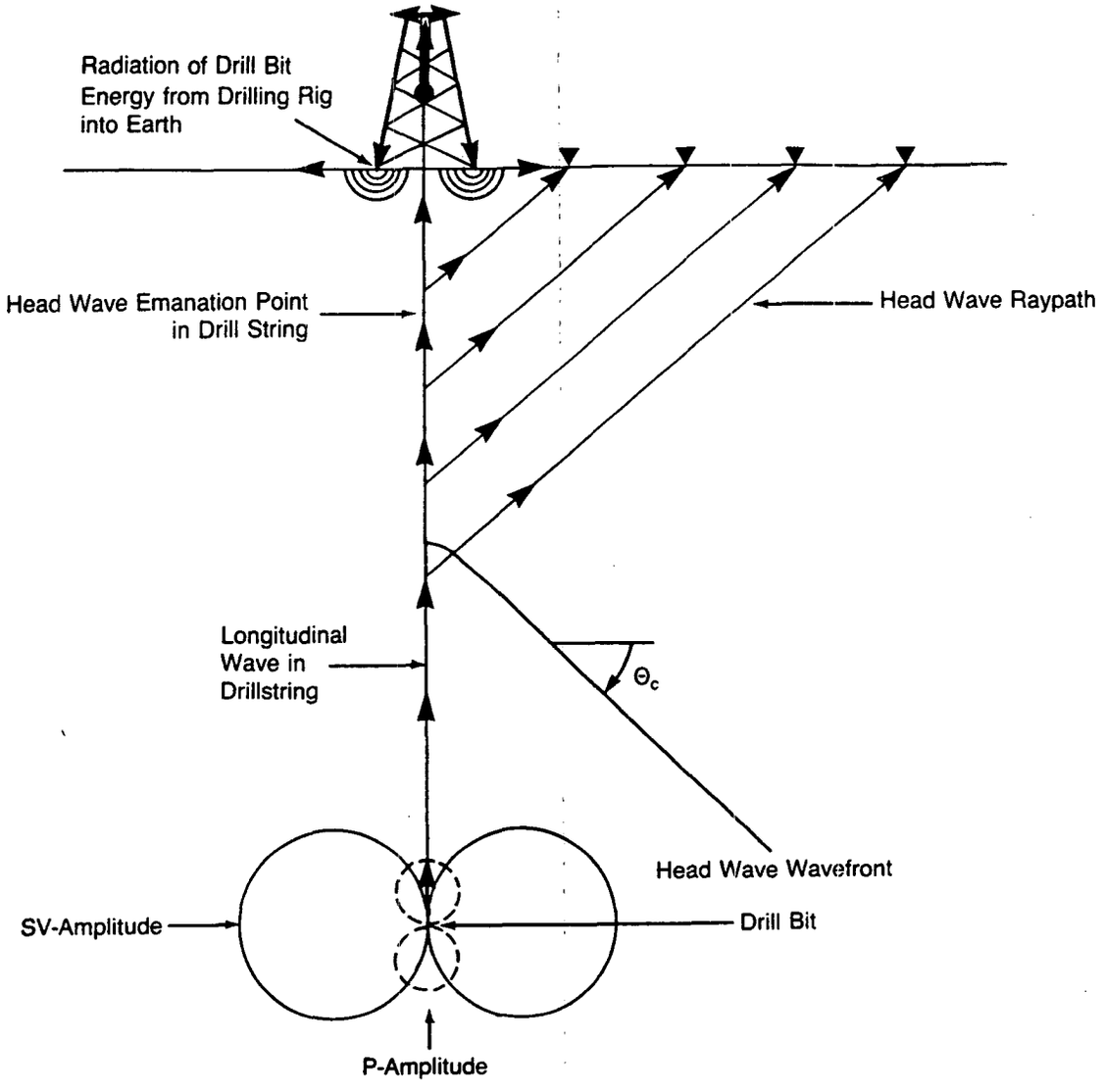

Figure 3-8. Drill bit energy radiated by the drill rig and the drillstring. The impacts of the drill bit at the bottom of the borehole create longitudinal waves that travel up the drillstring. As they travel up the drillstring, these waves create head waves traveling in the earth provided that the formation velocity adjacent to the drillstring is less than the drillstring velocity. The longitudinal waves also travel into the earth through the drill rig and then travel to geophone arrays via near-surface travelpaths.

recordings. As typical longitudinal wave velocities are 15600 ft/s (4758 m/s), head waves would be expected to be an extremely common occurrence in wells drilled in sedimentary rock. Head waves were predicted by White (1965) who described them in three dimensions as conical waves. In conventional VSP where the borehole does not contain a drillstring, the propagation velocity in the borehole (i.e., the fluid velocity) is generally less than the formation velocities and no head waves are produced.

As with energy partitioning in conventional tube wave analysis (Cheng and Toksoz, 1981), the impedance mismatch between the drillstring, the fluid, and the formation would be expected to produce a head wave displacement in the earth that is only a small fraction of the longitudinal wave displacement in the drillstring. However, unlike tube waves, whose amplitude decreases exponentially away from the borehole wall, the head wave amplitude theoretically decreases as the square root of the distance from the borehole. Thus, in theory, head waves can be recorded with geophone arrays on the surface a long distance from the wellhead. Finite element modeling (Samec and Kostov, 1988) of an axial force at the bottom of a borehole, and steel drillstring surrounded by fluid has also predicted these head waves. Samec (1989b) obtained head waves at the surface that were of comparable magnitudes to primary body waves from the drill bit. In the examples that follow, we will be discussing head waves that propagate into the earth as compressional waves, although shear modes also exist.

As shown in Figure 3-8, in the far-field of a homogeneous solid, the head wave wavefront is linear, with a wavefront normal that makes an angle with respect to the borehole axis of φ_c, where:

$$\varphi_c = \sin^{-1} \frac{V_f}{V_{DS}} \qquad (V_f < V_{DS}). \qquad (3\text{-}4)$$

In Equation 3-4, V_f is the formation velocity of the solid V_{DS} is the velocity of the drillstring longitudinal wave. Near the borehole, the wavefront is defined by a modified Hankel function (Appendix 3-A) and at the borehole, the head wave has a wavefront normal that parallels the drillstring axis. The raypaths taken by the head wave from the drillstring to the earth's surface are depicted in Figure 3-8 for a formation velocity of 10000 ft/s (3048 m/s) in a vertical borehole. Receivers placed at the surface near the rig would record head waves that intersect the drillstring near the surface, while at longer surface offsets head waves arrive from deeper portions of the drillstring. For more details of head wave propagation, refer to Appendix 3-A.

In most formations, the longitudinal wave traveling up the drillstring propagate with a velocity that is higher than the formation velocities adjacent to the drillstring. However in a few situations, i.e., hard limestones, anhydrites, evaporites, and granite, the formation P-wave velocity can be higher than the velocity of the longitudinal wave in the drillstring. In this situation, the critical angle, φ_c, in Equation 3-4 is undefined, and a compressional head wave is not predicted to exist (a shear head wave would still exists in these situations). Instead, a guided wave would theoretically be generated such as the one depicted in Figure 3-9. This wave travels along the borehole at the velocity of the longitudinal wave in the drillstring; however, like a tube wave, its amplitude decreases exponentially away from the borehole wall, and very little of its energy reaches the surface geophone arrays via direct paths through the earth. Like tube wave arrivals in conventional VSP, significant transfer of the guided wave energy into the earth may result after mode conversion at borehole discontinuities.

Drillstring Multiples Radiated at the Drill Bit

In Chapter 1 it was observed that the impulse response of the drillstring consisted primarily of multiple arrivals caused by reflections at the ends of the drillstring and at the interface between the BHA and the drillpipe. Since the waves

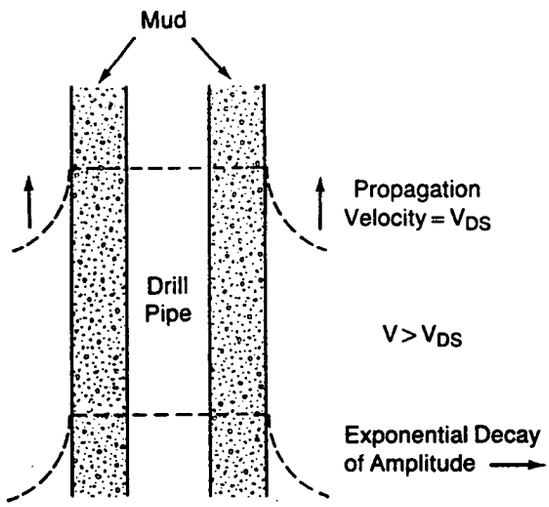

Figure 3-9. Guided waves are generated by the longitudinal wave traveling up the drillstring when the formation velocity adjacent to the drillstring is greater than the drillstring velocity.

traveling in the drillstring can theoretically transfer energy into the formation, these multiple arrivals also have the ability to transfer energy into the formation. We can write a simplified surface response, G(t), to an impulse produced at the drill bit as:

$$G(t) = E_o(t,0) + \sum_i K_i DS(t-t_i,Z_i) * E(t,Z_i) \qquad (3\text{-}5)$$

where $E_o(t,0)$ is the response of the earth to an impulse at the drill bit (this is the principal term were interested in with conventional VSP), $E(t,z_i)$ is the earths impulse response between a secondary radiation point, z_i, along the drillstring, $DS(t,z_i)$ is the response of the drillstring to an impulse at z_i, t_i is the traveltime of the primary impulse from the drill bit to the secondary radiation point, and k_i is the coupling coefficient between the secondary radiation point and the earth. Equation 3-5 is an oversimplification, because it does not take into account the nature or directivity of the impulse, however it does provide insight into the character of the surface response. Of particular interest in the data examples that follow in Sections 3.5 and 3.6, are body waves that are secondarily radiated at the drill bit after undergoing reflection at drillstring discontinuities. Figure 3-10 shows a few of the many possible multiple arrival paths. A 'BHA' multiple is radiated at the bit after traveling up the drillstring to the bottom-hole assembly/drillpipe interface, where a portion is reflected and travels back down to the bit. The 'drillstring' multiple is radiated at the drill bit after traveling up, and then down, the entire length of the drillstring. Only a fraction of the multiple energy is reradiated at the drill bit. The remainder is reflected back up the drillstring and can create secondary rig-generated arrivals, secondary head wave arrivals, and higher order multiples.

3.5 Identification of Arrivals Based on Traveltime and Offset Moveout

The arrivals obtained in a cross-correlation function of a geophone recording with a top-of-drillstring recording results in events that are shifted with respect to their

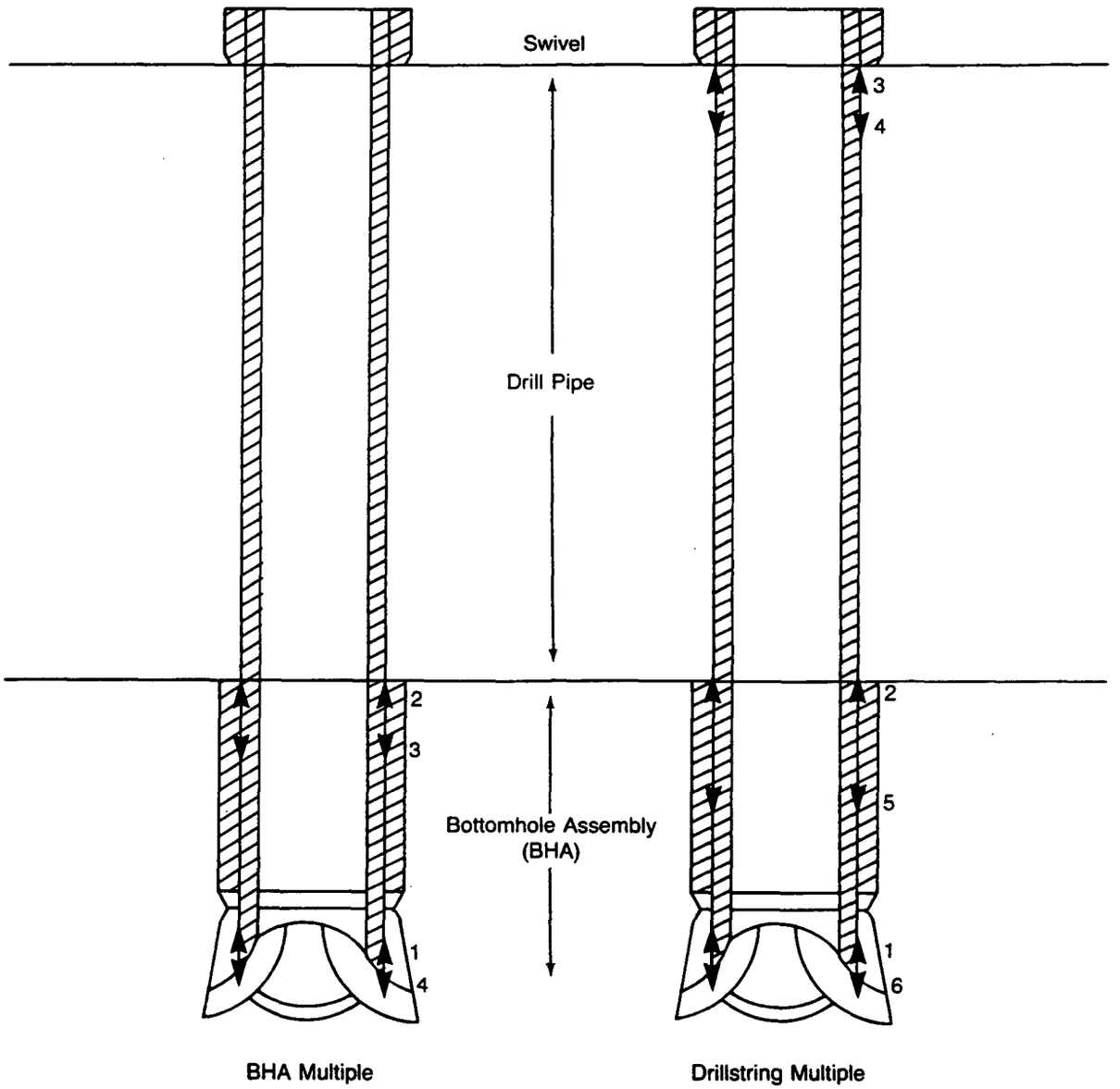

Figure 3-10. Drillstring travelpaths taken by a) BHA multiples and b) drillstring multiples of the primary body wave energy radiated into the earth at the drill bit. a) The BHA multiple is generated as follows: 1) the longitudinal wave travels up the BHA, 2) reflects off the BHA/drillpipe interface, 3) the reflected wave travels back down the BHA, and 4) is radiated into the earth at the drill bit. b) The drillstring multiple is generated in the following manner: 1) the longitudinal wave travels up the drillstring, 2) transmits through the BHA/drillpipe interface and continues up the drillpipe where it 3) reflects off the base of the swivel, 4) travels down the drillpipe, 5) transmits through the drillpipe into the BHA, and 6) is radiated into the earth.

earth traveltime (Chapter 1). In Sections 3.5 and 3.6, we show how arrivals can be identified based on their 'correlation' time and their moveout with offset and depth. Figure 3-11a through 3-11d show four drill bit wavefields recorded at the same vertical well where the data in Figure 3-3 were recorded (Figure 3-11a is a duplicate of Figure 3-3). In these displays, the depth of the drill bit increases from 3290 ft (1003m) in Figure 3-11a to 6515 ft (1986m) in Figure 3-11d. Each of the traces were computed over a drilling span of 30 ft (9.1m). The recording times input into the cross-correlation process were 30 minutes on average. The sediments encountered by the drill bit were clastics ranging in age from late Tertiary to late Cretaceous. Figure 3-12 shows the regional P-wave velocity function (derived from checkshot data on a nearby well) along with some sample raypaths. In addition to the primary P-wave direct arrival, four other arrivals are labeled in Figure 3-11: a head wave arrival, a rig generated arrival, and BHA/drillstring multiples radiating from the drill bit as secondary P-wave direct arrivals. Inspection of the wavefields shows that each of the arrivals exhibits a characteristic moveout and arrival time as a function of offset from the wellhead.

The P-wave direct arrival in a vertical well drilling at a depth, z, exhibits a correlation time, t_D, that can be approximated by:

$$t_D = \frac{(x^2+z^2)^{1/2}}{V_f} - \frac{z}{V_{DS}} \qquad (3\text{-}6)$$

where V_f is the average formation P-wave velocity, and a straight raypath between the drill bit and the geophone offset, x, is assumed. The moveout of this arrival with offset, $\Delta t_D/\Delta x$, is then:

$$\frac{\Delta t_D}{\Delta x} = \frac{\sin\phi}{V_f} \; . \qquad (3\text{-}7)$$

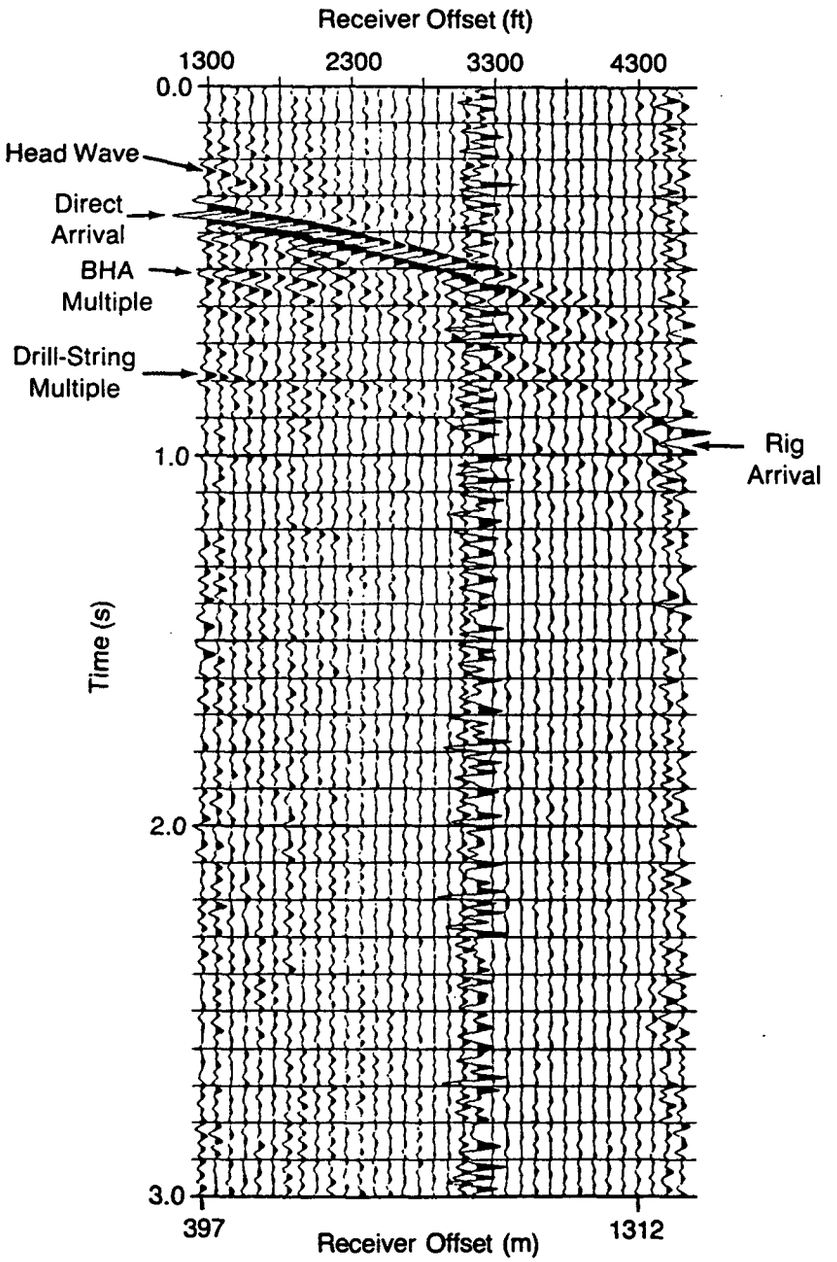

Figure 3-11. a) Wavefield data recorded when the drill bit was drilling at a depth of 3290 ft (1003m) on a vertical well.

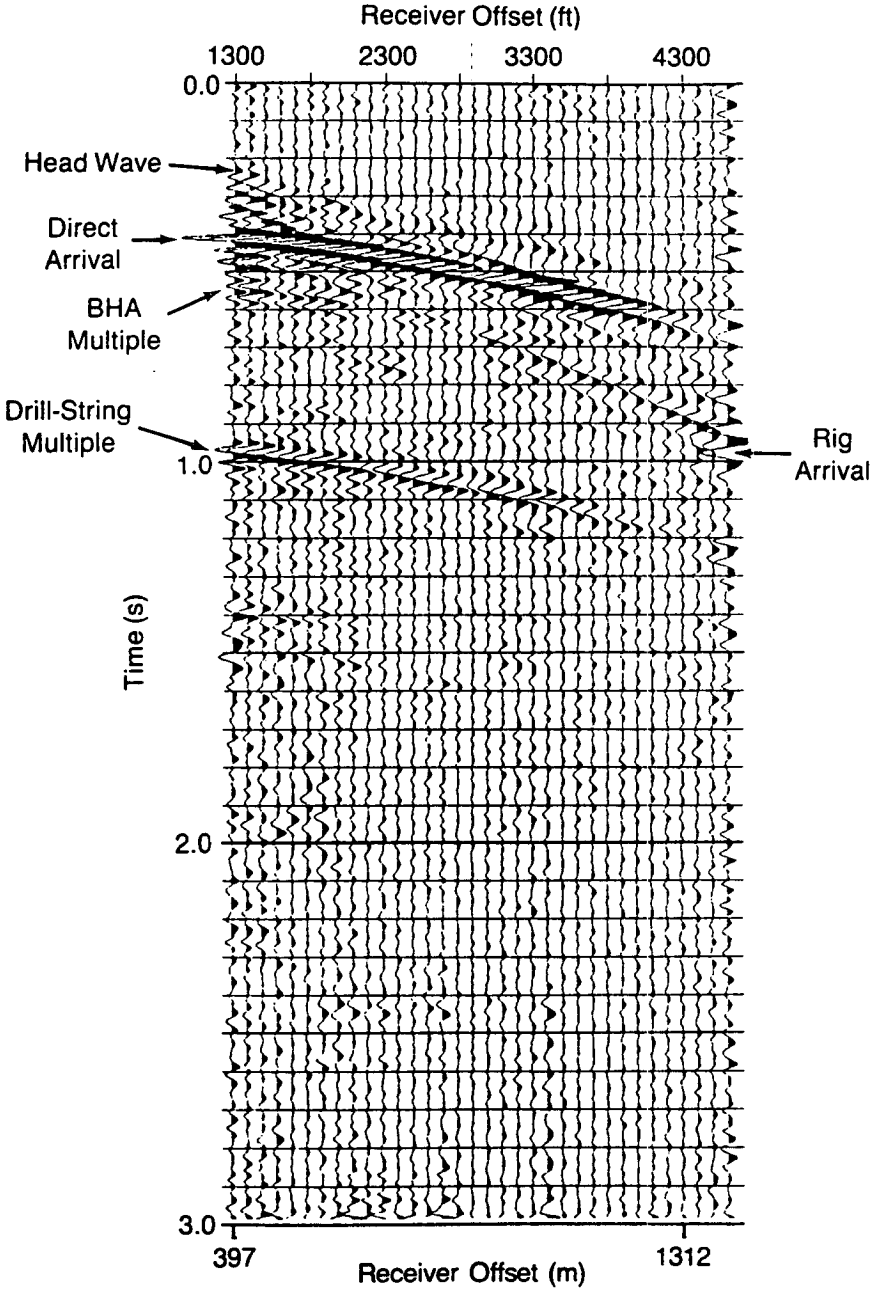

Figure 3-11. b) Wavefield data recorded when the drill bit was drilling at a depth of 4440 ft (1353m) on a vertical well.

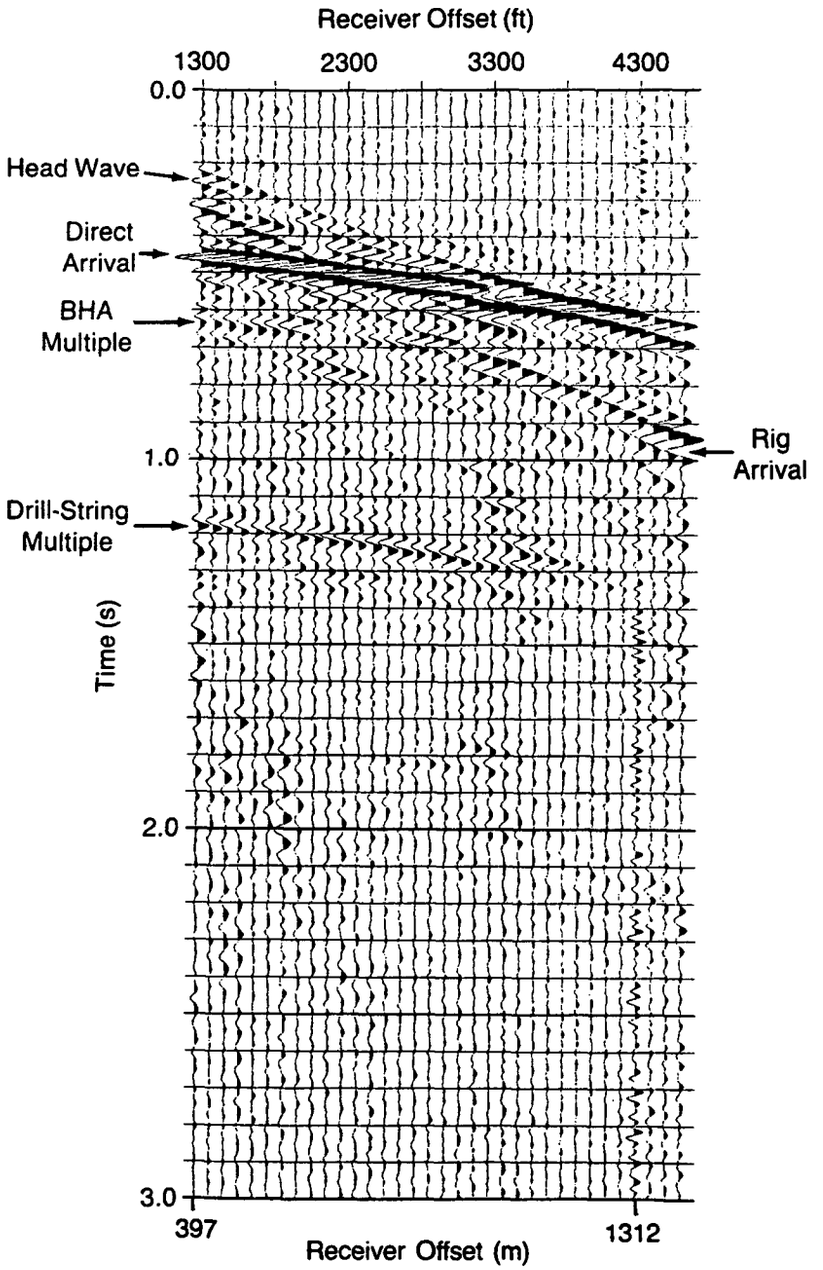

Figure 3-11. c) Wavefield data recorded when the drill bit was drilling at a depth of 5717 ft (1743m) on a vertical well.

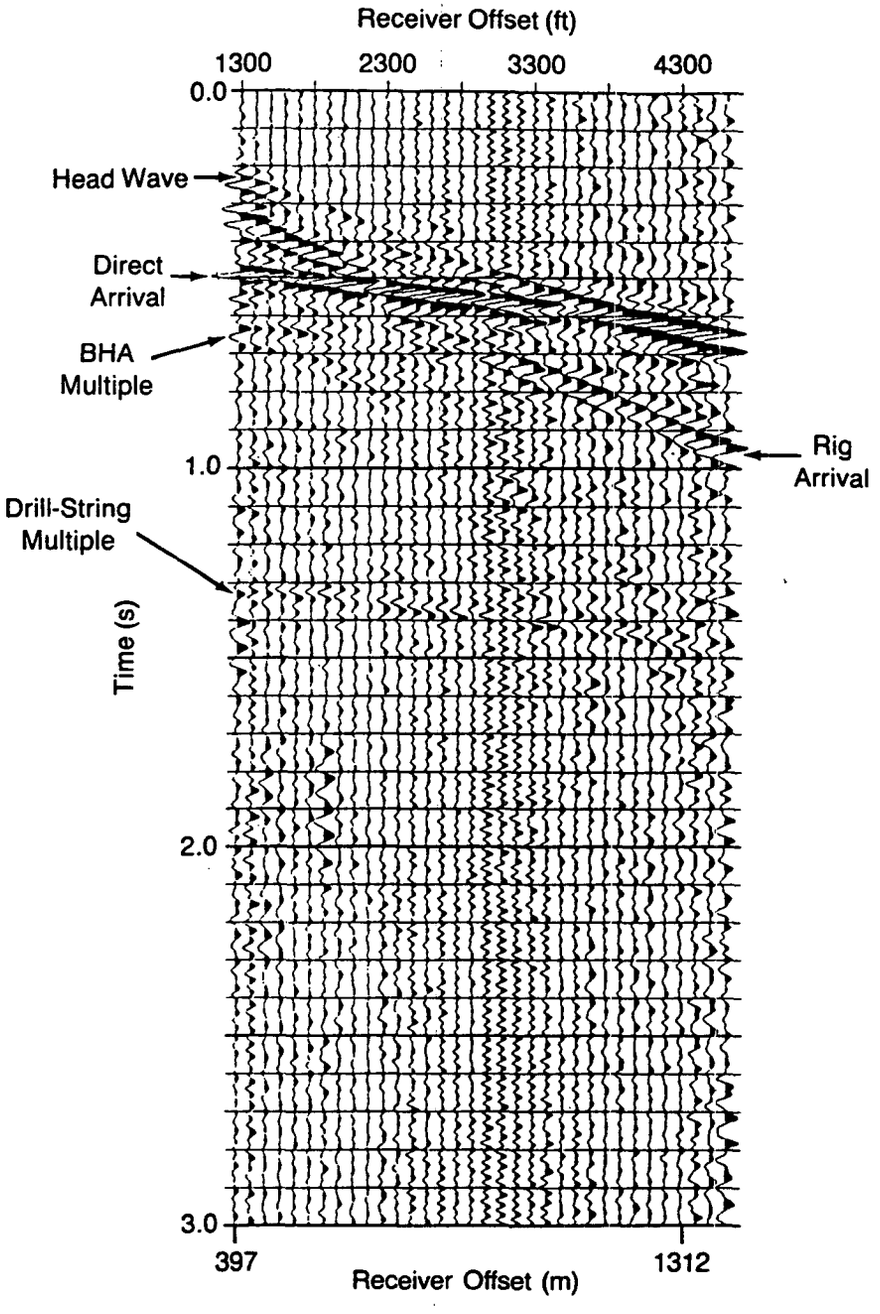

Figure 3-11. d) Wavefield data recorded when the drill bit was drilling at a depth of 6515 ft (1986m) on a vertical well.

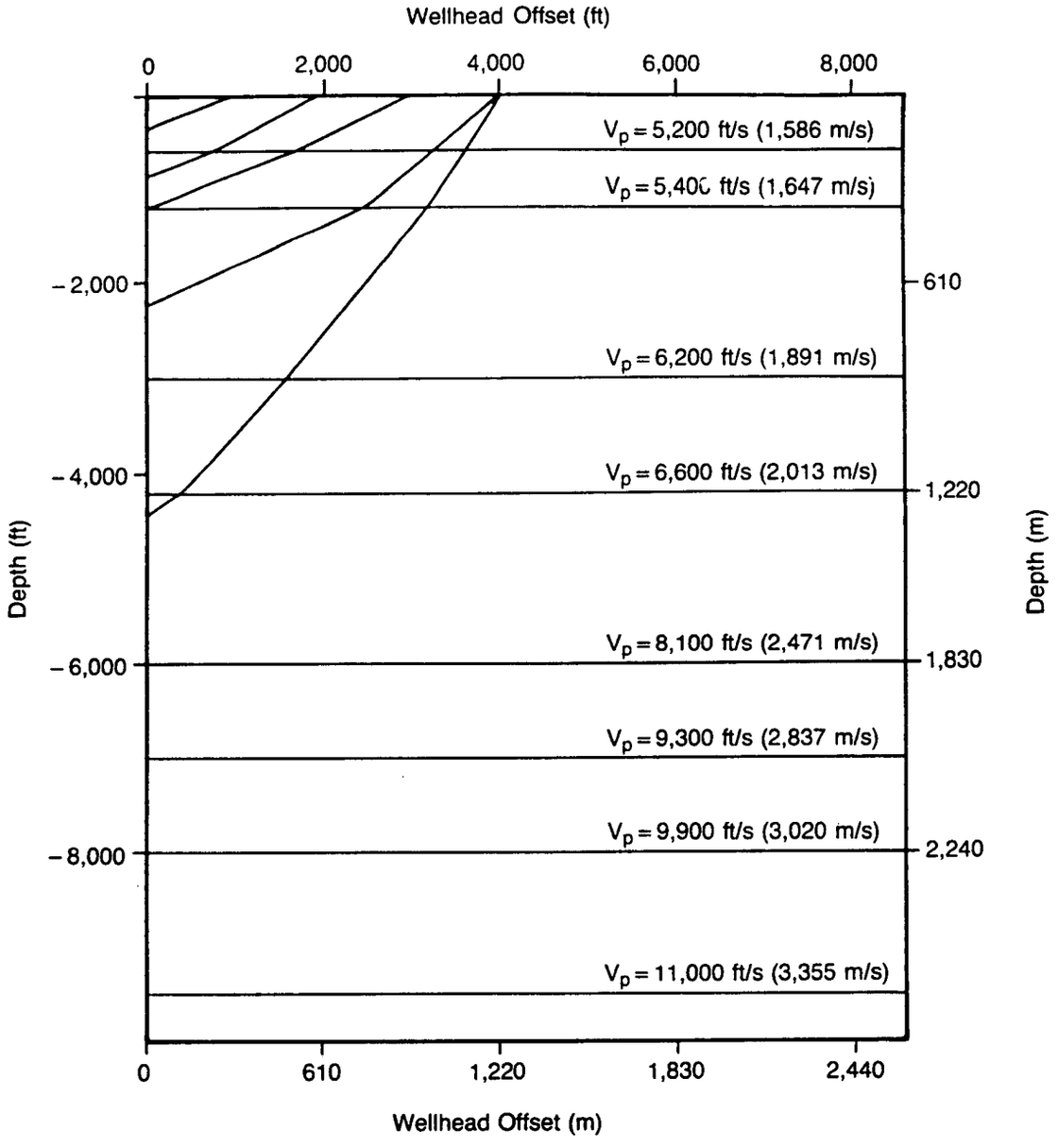

Figure 3-12. P-wave velocity model corresponding to the data in Figure 3-11.

This moveout is equivalent to the moveout with offset that would be observed in a walkaway VSP.

Figure 3-13a through 3-13d show synthetic P-wave direct arrivals corresponding to the depths in Figure 3-11. The synthetics were computed by raytracing from the drill bit to the surface through the velocity model, convolving the data with a 30 Hz Ricker wavelet, and advancing the arrival times by z/v_{DS}, to account for the traveltime in the drillstring. The synthetic correlation times and moveouts give good agreement with the correlation times and moveouts of the real data.

The BHA and drillstring multiples arrive later than the P-wave direct arrival with correlation times, t_{BHA} and t_{DS}, given by:

$$t_{BHA} = t_D + 2z_{BHA}/V_{DS} \tag{3-8}$$

and

$$t_{DS} = t_D + 2z/V_{DS} \tag{3-9}$$

Obviously, the drillstring and BHA multiples have the same moveout with offset as the P-wave direct arrival, since they come from the same source depth. In the data examples shown in Figure 3-11, the BHA length was not documented. Assuming a 130 ms delay from the direct arrival, the BHA length is about 1000 ft (305m). The delay of the drillstring multiple increases in proportion to increasing drillstring length just as did the drillpipe multiple in Chapter 1. The measured traveltimes of the drillstring multiples correspond within 30 ms of the theoretical traveltimes.

Unlike the hyperbolic moveout with offset of the direct and drillstring multiple arrivals, the rig arrivals in Figure 3-11 exhibit nearly linear moveout with receiver offset. These arrivals travel with a phase velocity between 4500 and 6000 ft/s (1372 and 1830 m/s), and a group velocity of between 4000 and 4800 ft/s (1219 and 1463 m/s). The most likely travelpath for these arrivals is a near-surface P refraction

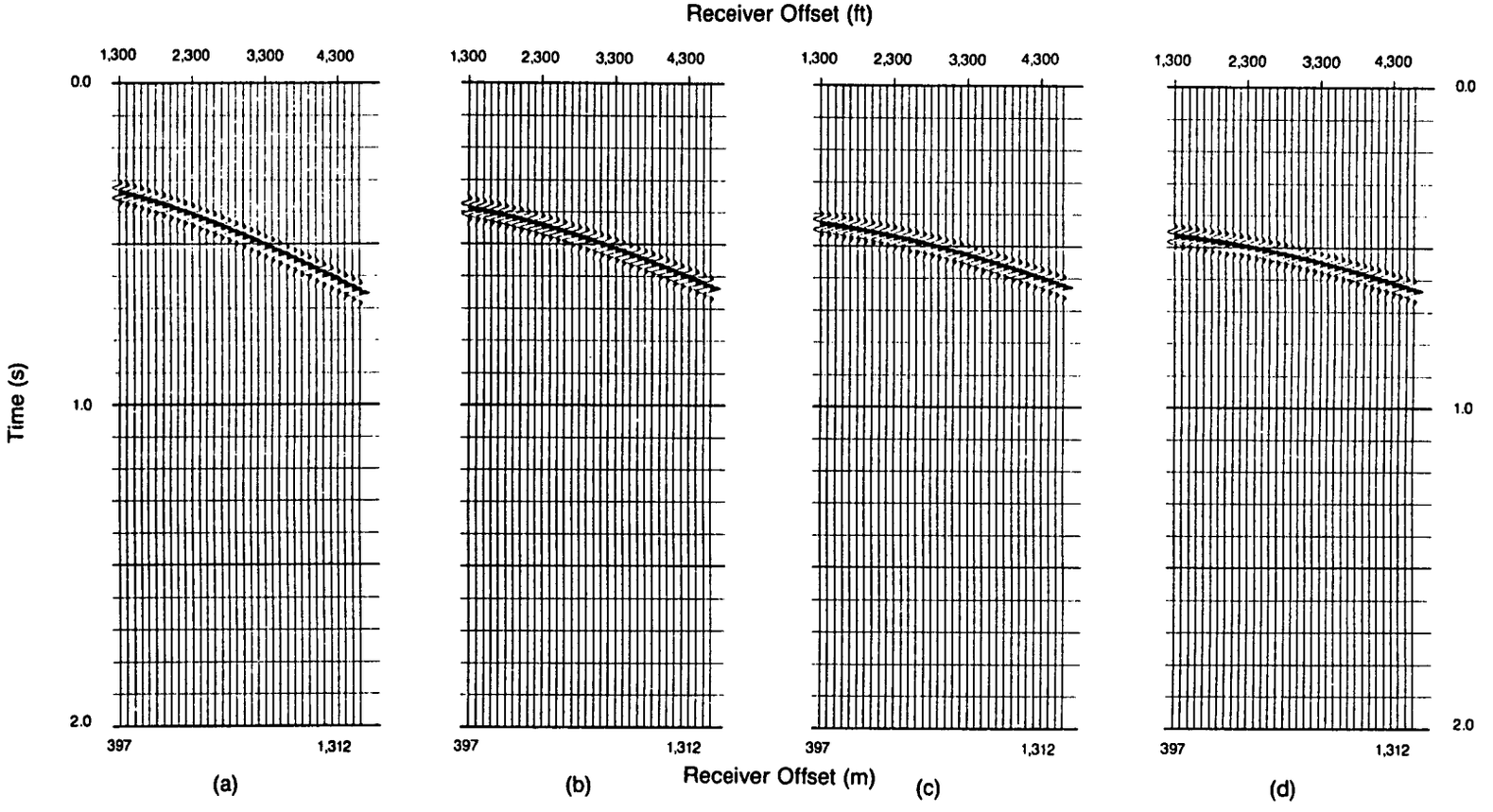

Figure 3-13. Synthetic P-wave direct arrivals corresponding to the data in Figure 3-11.

or a wide-angle P reflection off a near surface layer. The group velocities are somewhat lower than the group velocities observed in the 'first breaks' from conventional surface seismic shot records in the region, which are generally about 5200 ft/s (1585 m/s). The low group velocities may be due to the delay from the top of the drillstring to the bottom of the rig mast (Chapter 2). Since the rig arrival secondary source position is nearly colocated with the pilot sensor, the correlation times of the rig arrival are virtually identical to the earth traveltime.

Like the rig arrivals, the head wave arrivals labeled in Figure 3-11 exhibit nearly linear moveout with wellhead offset. They can be distinguished from the rig arrivals based on their correlation time. The correlation time of the head wave is nearly coincident with the rig arrival time at the near receiver offsets, but by an offset of 2300 ft (700m), the head wave correlation time is more than 100 ms earlier. Since no arrival from the drill rig can occur before the first break time, this arrival must come from another source point. The head wave arrival can preceed the first-break rig arrival because its source position is along the drillstring. As discussed in Chapter 1, the correlation time of an arrival from the drill bit through the earth to an earth receiver is advanced by the traveltime from the bit through the drillstring to the top of the drillstring. For the case of an arrival apparently radiated from the drillstring, the correlation time is advanced from its traveltime through the earth by z_H/V_{DS}, where z_H is the distance from the radiation depth to the pilot sensor at the top of the drillstring.

Assuming a horizontally layered earth with a velocity, v(z), that can vary with depth, the head wave traveltime at a particular receiver location is related to the traveltime of a plane wave in the earth. If (x = 0, z = 0) is the head wave intersection with the drillstring, then following Claerbout (1985), the correlation time is given by:

$$t(x,z) = px + \int_0^{z_H} \left[\frac{1}{V^2(z)} - p^2 \right]^{1/2} dz - \frac{z_H}{V_{DS}} \qquad (3\text{-}10)$$

where $p = \sin\varphi_c/V_f = 1/V_{DS}$, and z_H is the vertical distance from the depth of the head wave intersection with the drillstring to the surface. At the near receiver offsets, the head wave correlation times observed in Figure 3-11 coincide with head wave source points along the drillstring computed from Equation 3-10 of 500 to 1500 ft (150 to 450m).

The head wave arrival can be distinguished from point sources along the drillstring based on moveout with offset. If these arrivals were point sources along the drillstring, they would exhibit hyperbolic moveout like the direct arrival. The apparent velocities of the head wave arrival in Figure 3-11 is 5800 ft/s (1768 m/s) at geophone offsets less than 2700 ft (823m). This apparent velocity is more than 1000 ft/s less than the apparent velocity from a point source at the head wave source point in the drillstring.

Assuming a homogeneous earth, the head wave moveout with offset, $\Delta t_H/\Delta x$, is:

$$\Delta t_H/\Delta X = 1/V_f \cos\theta_c \qquad (3\text{-}11)$$

Due to the distributed nature of the head wave source position along the drillstring, the apparent velocity is less than the formation velocity. By contrast, a wave arriving at the surface from a point source at depth always exhibits an apparent velocity that is higher than the formation velocity. Solving for the formation velocity in Equation 3-11 yields:

$$V_f = \left(\frac{(1+4(\Delta t_H/\Delta X)^{-2})^{1/2} - 1}{2(\Delta t_H/\Delta X)^{-2}} \right)^{1/2} \qquad (3\text{-}12)$$

Thus, even without the correlation time of the head wave arrival, we can estimate the formation velocities along the drillstring by the head wave moveout with offset. Using Equation 3-12, a formation velocity of 6350 ft/s (1936 m/s) is estimated. These formation velocities are encountered somewhat deeper than the emenation depths predicted by the correlation times. This discrepancy could be due either to the inaccuracies of a straight raypath assumption or the presence of formation velocities at shallow depths that are higher than those modeled.

This example illustrates the highly variable nature of head wave behavior and emphasizes that the presence of head waves at the surface is strongly influenced by the surface receiver offset and the formation velocities adjacent to the drillstring. Figure 3-14 shows the occurrence of head waves on a vertical well as a function of offset, depth, and formation velocity at depth (assuming straight raypaths). Given a velocity function that increases with depth, the receiver offset will be somewhat less than those depicted in Figure 3-14, and an individual offset can record several head wave arrivals from difference source depths. Near offsets receive head waves from drillstring depths corresponding to shallow, low velocity formations and deep high velocity formations. Longer receiver offsets record head waves over a wider range of drillstring depths for lower velocity formations, but they do not receive head waves for very high formation velocities at most drillstring depths of interest.

The moveout differences between the head wave/rig arrivals and the direct arrivals from the bit can be used to separate the arrivals by beamforming a group of receiver arrays. Any beamformer that 'looks' down, into the earth, with improve the S/N of the direct arrivals from the drill bit relative to the lower apparent wavelength arrivals. A simple downward-looking beamformer is an array of geophones oriented toward the drill rig. Besides attenuating the head waves/rig arrivals an array of geophones attenuates incoherent noise from the drill rig (Chapter 2). If multiple receiver offsets are recorded individually, more sophisticated beamformers that

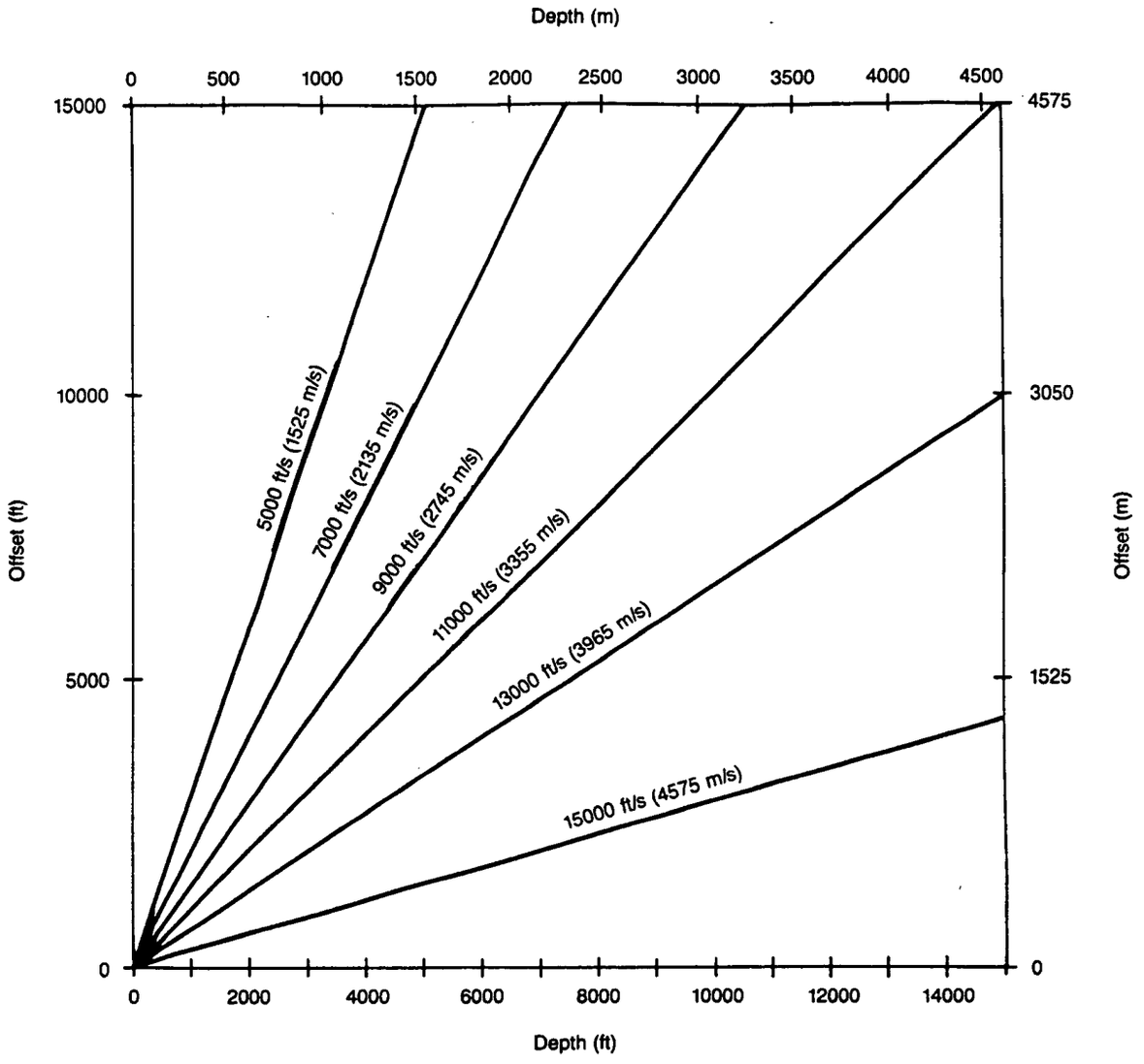

Figure 3-14. Head wave arrival intersection with the drillstring and with the surface as a function of formation velocity. A vertical borehole and a homogeneous earth have been assumed.

incorporate time delay and amplitude as well as moveout can be used (Seeman and Horowicz, 1983). Alternatively, as shown in Figure 3-14, it may be possible with a knowledge of v(z) to place the receivers so as to avoid recording head waves altogether.

3.6 Identification and Separation of Arrivals Based on Moveout With Depth

Figure 3-15 shows a series of correlated drill bit wavefields from a geophone array located 2532 ft (772m) from the wellhead. The data were recorded on a vertical well drilled in sediments similar to the well where the data in Figure 3-11 were acquired. The geophone array consisted of forty-eight 10 Hz geophones oriented toward the wellhead with a total aperture of 300 ft (91m). This array attenuated the low apparent velocity head wave and rig arrivals observed in Figure 3-11 while preserving the higher apparent velocity direct arrivals at most depths. The correlated traces in Figure 3-15 were computed over recording times ranging from 10 minutes at shallow depths to over 1 hour in the deeper section. The data have had reference deconvolution applied (Chapter 1) and have been bandpassed from 13 to 50 Hz. The arrivals identified in Figure 3-11 are also labeled in Figure 3-15. In addition, an event reflected from below the drill bit is labeled. Each of the arrivals has a characteristic moveout as a function of drill bit depth.

Assuming a straight raypath between the drill bit and the surface receiver, the moveout with depth of the drill bit direct arrival in a vertical borehole is:

$$\frac{\Delta t_d}{\Delta z} = \frac{\cos\phi}{V_{\Delta z}} - \frac{1}{V_{DS}}, \qquad (3\text{-}13)$$

and the moveout of a reflection from a horizontal interface just beneath the drill bit is approximately given by:

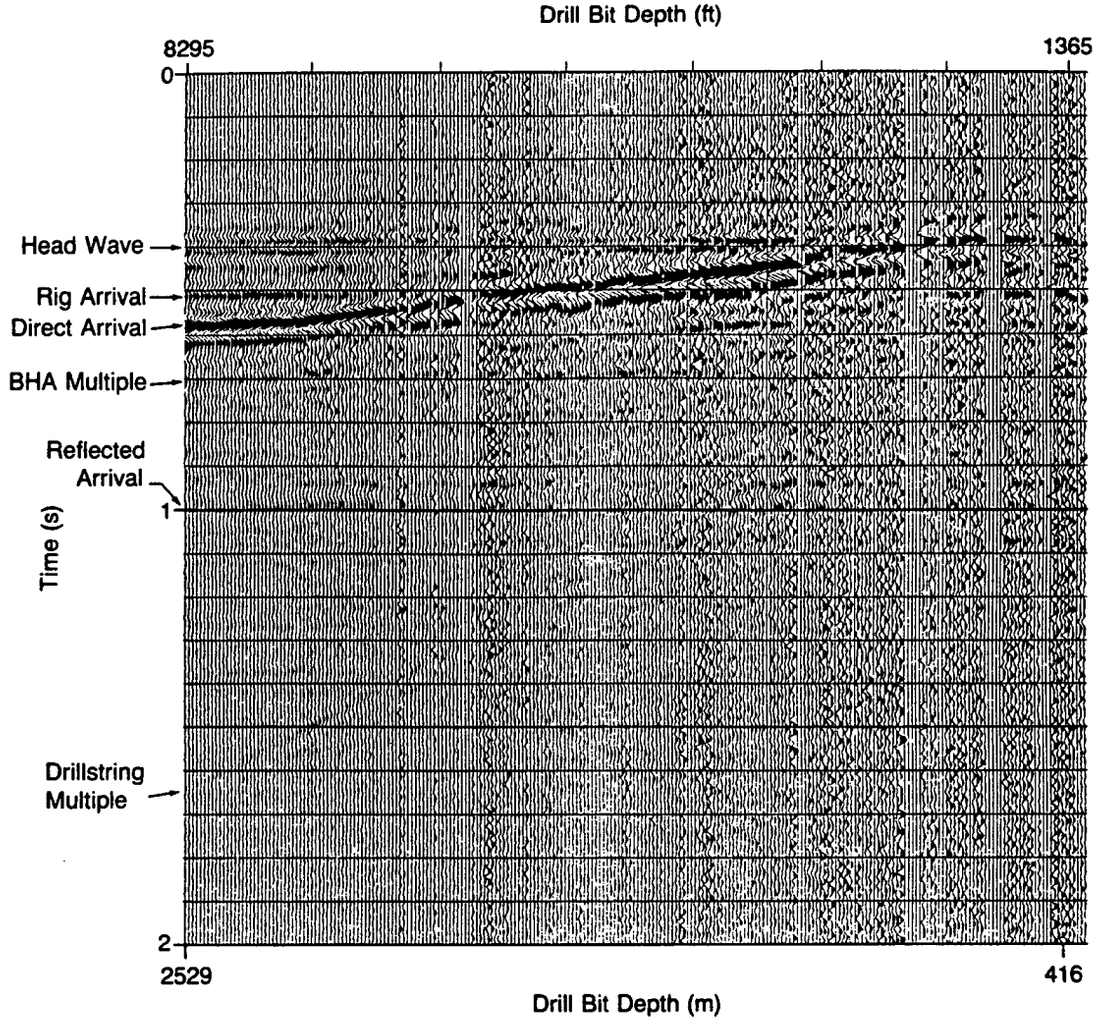

Figure 3-15. Drill-bit wavefields from a geophone group located 2532 ft (772m) from the wellhead. The traces represent data samples at 30 ft (9.1m) intervals from 1245 to 8295 ft (379 to 2528m).

$$\frac{\Delta t_r}{\Delta z} \sim -\frac{\cos\phi}{V_{\Delta z}} - \frac{1}{V_{DS}} \qquad (3\text{-}14)$$

where $\Delta t/\Delta z$is the moveout, $V_{\Delta z}$ is the formation interval velocity (assumed constant) over a small depth range Δz, and ϕ is the take off angle of the ray with respect to the vertical. The corresponding moveout equations for a conventional VSP omit the term $1/V_{DS}$ (Chapter 1). Therefore, the moveout of the correlated P-wave direct arrival over depth is always less than the moveout of an equivalent VSP direct arrival, and the negative moveout of the reflection arrivals is always greater than the corresponding negative moveout of equivalent VSP reflection arrivals. Moreover, the direct arrival can exhibit zero, or even negative moveout with depth (if ϕ or $V_{\Delta z}$ becomes large); whereas, an arrival from a reflection below the drill bit always exhibits negative moveout. In Figure 3-15, the direct arrival exhibits positive moveout and the drill-bit reflections exhibit negative moveouts. This is consistent with the expected formation P-wave velocities in the vicinity of the borehole (which are similar to those depicted in Figure 3-12).

The BHA multiple arrival in Figure 3-15 exhibits a moveout with depth that mimics the P-wave direct-arrival moveout since the BHA multiple occurs at a constant time lag relative to the direct arrival given by Equation 3-8. In Figure 3-15, the BHA length was approximately 800 ft (244m), which resulted in t_{BHA} = 100 ms. Like earth-path multiple arrivals in conventional VSP, the BHA multiples can be attenuated through deconvolution of the direct arrival (Hardage, 1985).

In Figure 3-15, the drillstring multiple arrival exhibits a moveout that is approximately double that of the direct arrival. Referring to Equation 3-9, the moveout of the drillstring multiple relative to the direct-arrival moveout is:

$$\frac{\Delta t_{DS}}{\Delta Z_{DS}} = \frac{2}{V_{DS}} . \qquad (3\text{-}15)$$

In Figure 3-15, the head wave arrival time exhibits no change as the depth of the drill bit increases. Since the intersection of the head wave with the drillstring is the same regardless of the depth of the drill bit, its drillstring-to-receiver path does not change with drilling depth. Thus the head wave arrival exhibits zero moveout as a function of drilling depth in a series of cross-correlation functions. Another way to describe this phenomena is that the head wave traveling in the earth is the longitudinal wave traveling up the drillstring, which is the same wave that the pilot signal records. As the drill bit moves deeper, both the head wave arrival recorded by the geophone array and the drillstring arrival recorded by the pilot sensor are delayed by the same factor, and therefore the moveout of the head wave arrival is zero regardless of the receiver offset, the borehole deviation, or the formation velocity. The depth at which the head wave intersects the direct arrival determines the intersection depth of the head wave and the drillstring. The particular head wave radiated from this depth does not exist above this depth and thus head wave arrivals behave as step functions over depth. In Figure 3-15, the head waves recorded at this receiver location intersected the drillstring slightly above 3000 ft (914m).

Rig-generated arrivals also have zero moveout with depth. As discussed in Section 3.4, the longitudinal wave that the pilot sensor records propagates into the earth after traveling past the pilot sensor, up the drilling lines, and into the rig mast. Therefore, the cross-correlation arrival time does not change with the length of the drillstring, and like the head wave arrivals, rig-generated arrivals also exhibit zero moveout as a function of drill bit depth. Unlike the step-function behavior of the head wave arrival, the rig arrival is continuous over depth.

Separation of Wave Modes Based on Moveout With Depth

The moveout differences between the different arrivals in Figure 3-15 suggest that conventional VSP wavefield separation techniques (Hardage, 1985) can be used to extract the primary drill bit direct and reflected arrivals. Since the rig and head wave

arrivals have zero moveout with depth, a filter rejecting events that appear to move along the depth axis with infinite apparent velocity (zero spatial frequency) will attenuate these arrivals. A filter applied to reject events with an apparent velocity that is related to the direct-arrival apparent velocity by Equation 3-15 would reject first order drillstring multiple arrivals.

To remove the rig and head wave arrivals in Figure 3-14, a median filter was chosen because of its ability to pass step functions (Hardage, 1985) like the head wave arrival. Figure 3-16 shows the zero moveout arrivals in Figure 3-15 enhanced with a 55 trace median filter, and Figure 3-17 shows the residual after subtracting the enhanced data in Figure 3-16 from the original data in Figure 3-15. 55 traces (1680 ft, 512m) was the average apparent wavelength of the direct arrival in Figure 3-15 at the low end of the frequency spectrum (13 Hz). Inspection of Figure 3-16 shows that some direct arrival energy has been retained. Consequently, a portion of the direct arrival has been removed in the residual, particularly at the deepest depths where the formation velocities (and thus the apparent velocities) of the direct arrival were highest. By contrast, the reflected arrivals and drillstring multiple arrivals have not been affected by the median filtering, as the apparent wavelengths in Figure 3-15 are very low. Since the ultimate goal of VSP wavefield separation is typically the 'upgoing' reflected energy, the attenuation of the direct arrival in Figure 3-17 is not a major concern unless a 'downgoing wave' deconvolution filter (Hardage, 1985) is to be obtained from the direct-arrival wavelets. In this case the presence of overlapping rig and head wave arrivals of similar moveouts may make it difficult to obtain a good estimate of the direct arrival wavelet. Consequently, it may be necessary to deconvolve the upgoing reflections with a filter derived from the reflected arrivals as in conventional surface seismic deconvolution.

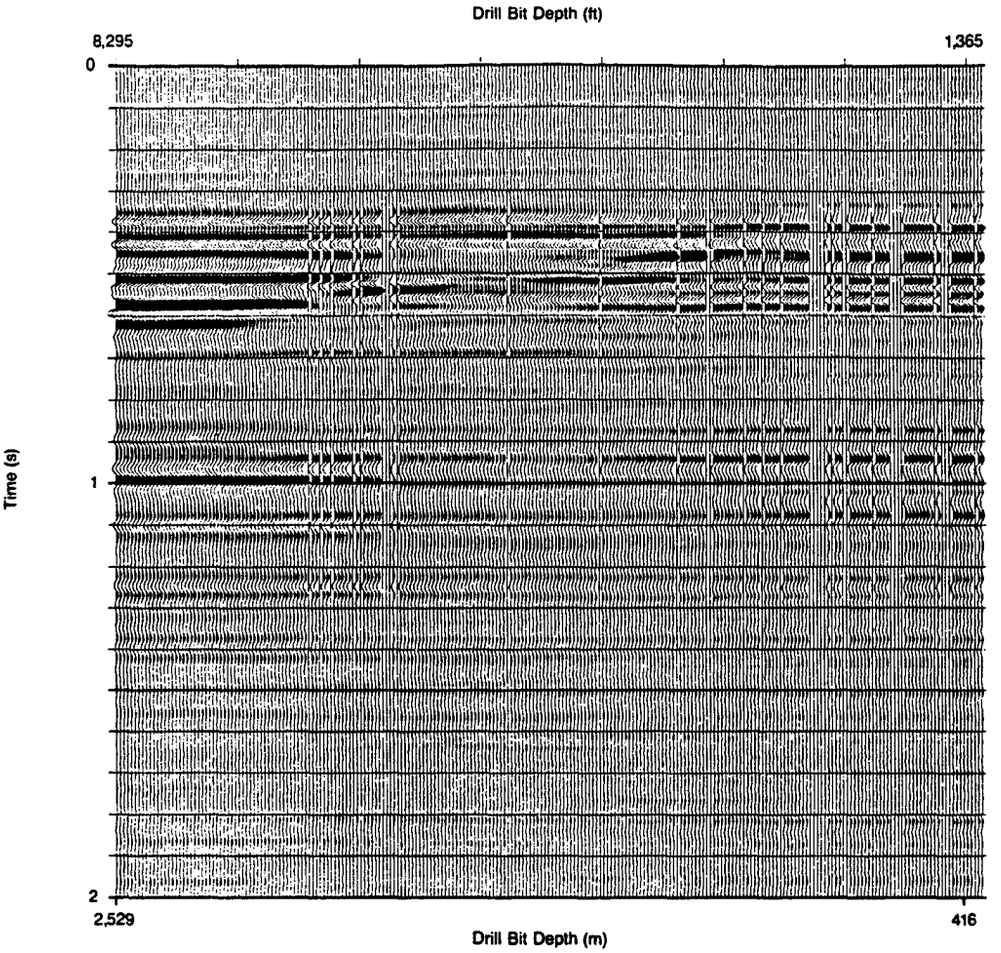

Figure 3-16. Drill bit wavefields corresponding to the data in Figure 3-15 after enhancing arrivals that have zero moveout with drill bit depth using a 55 trace median filter.

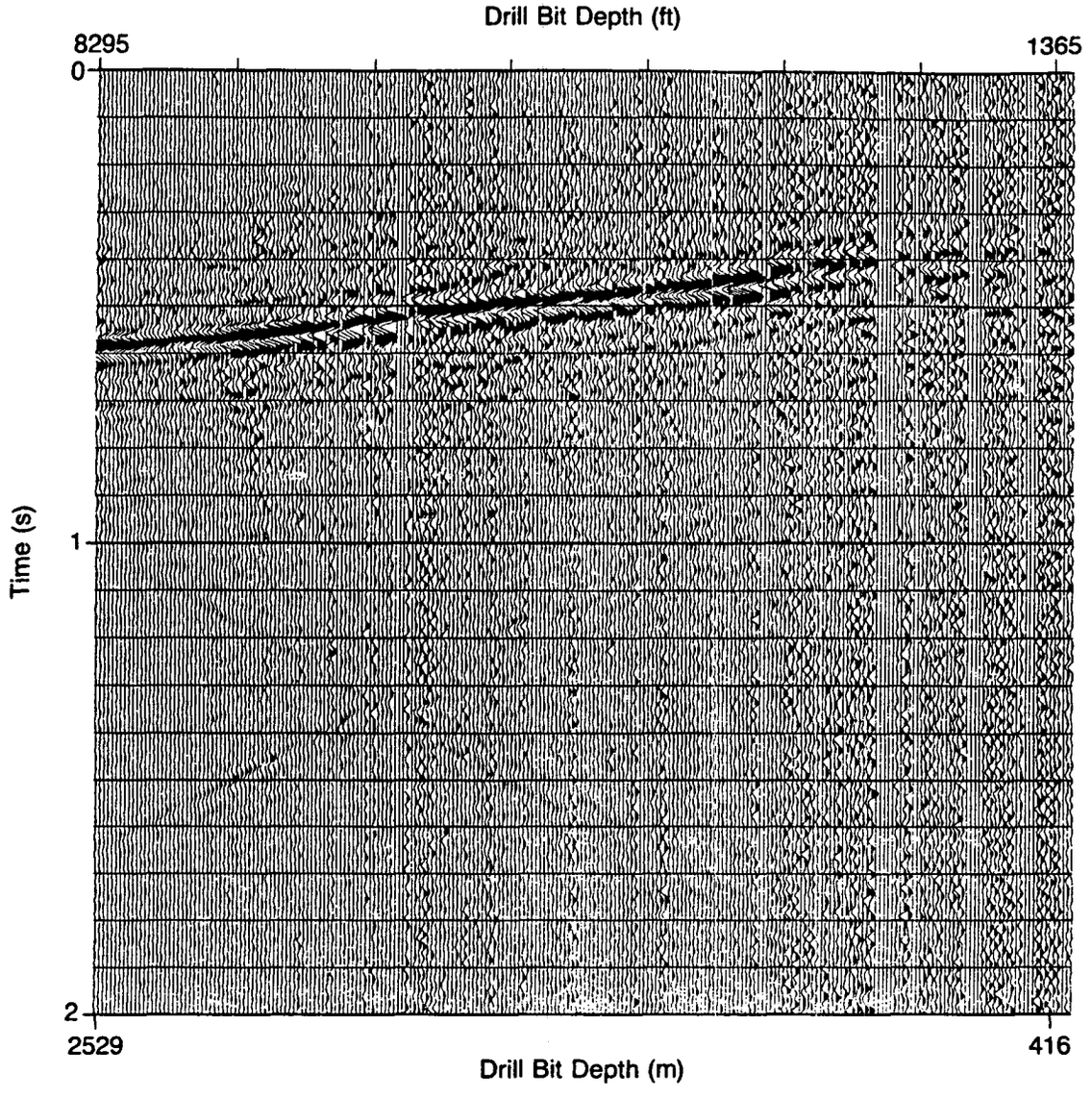

Figure 3-17. Residual after subtracting Figure 3-16 from Figure 3-15.

3.7 Conclusions

The following wave modes are radiated into the earth and received by surface receivers when a drill bit creates axial impacts at the bottom of a borehole.

1) P and SV body waves radiated away from the point of impact. In the far-field, the P-wave amplitudes are largest along the borehole axis, and progressively weaken away from the axis until no P-waves are radiated perpendicular to the axis. The SV waves have a radiation pattern rotated 90° from the P-wave radiation pattern. The SV displacement amplitude are approximately three times larger than the P-waves amplitude at an angle of 45° from the borehole axis. The radiation patterns have symmetry across a plane perpendicular to the borehole axis and also symmetry of rotation about the borehole axis. When axial symmetry is assumed, no SH waves are radiated by the axial drill bit impacts.
2) Rig-generated arrivals originate at the drill bit, travel up the drillstring into the rig mast, and then into the earth where they travel via predominantly near-surface paths to surface receivers.
3) Head wave arrivals are present when the formation velocity adjacent to the drillstring is less than the longitudinal wave velocity in the drillstring. These head waves propagate as plane waves in the earth, making a wavefront angle with respect to the borehole axis defined by Equation 3-4. The head wave wavefronts are nearly parallel with the borehole axis when the formation velocity is very low, and are nearly perpendicular to the borehole axis when the formation velocity approaches the drillstring velocity.
4) Multiple body wave arrivals are radiated at the drill bit when the longitudinal wave traveling in the drillstring undergoes one or more reflections at the various drillstring discontinuities.

These arrivals has a characteristic traveltimes and moveouts in drill-bit cross-correlation functions that are dependent upon the formation velocities near the borehole, the receiver offset from the drill bit, and in some cases, the depth of the drill bit. The differences in the spatial characteristics of these arrivals in time versus offset and depth provide a means by which they can be identified and separated using spatial filtering techniques.

The drill-bit radiation pattern is particularly well suited for applications such as P-wave velocity surveys and P-wave zero offset imaging in vertical boreholes. Deviated borehole P-wave velocity surveys and reflection imaging around the borehole can be accomplished, provided that some of the surface receivers are deployed to avoid the P-wave radiation null zone. In a vertical well, shear wave velocity surveys and shear/converted wave images are obtainable provided the receiver is offset from the borehole. Shear wave surveys on a vertical well are not obtainable at very near offsets and thus vertically-incident shear wave velocity surveys will be very noisy. In a horizontal well, shear waves will be recorded vertically above the drill bit which opens up a large area of investigative possibilities. However, vertically-incident P-wave velocity surveys are not desirable given the drill-bit radiation pattern in horizontal wells. Drill bit impacts are also a good source of shear wave energy and a low-level source of P-wave energy for cross-borehole applications between vertical wells.

Chapter 3: References

Claerbout, J.F., 1985, Imaging the earth's interior, Blackwell Scientific Publications, 398 p.

Crampin, S., 1985, Evaluation of anisotropy by shear wave splitting, Geophysics, 50, 142-151.

Hardage, B.A., 1981, An examination of tube wave noise in vertical seismic profiles, 46, 892-903.

Hardage, B.A., 1985, Vertical Seismic Profiling Part A: Principles, 2nd edition, Pergammon Press, 509 p.

Heelan, P.A., 1953, Radiation from a cylindrical source of finite length: Geophysics, 18, p. 685-696.

Kennedy, W., Wiggins, W., and Aronstam, P., 1988, Swept-frequency borehole source for inverse VSP and cross-borehole surveying, Soc. of Expl. Geophysicists, 58th Annual Meeting Expanded Abstracts, 1, 158-160.

Lee, M.W. and Balch, A.H., 1982, Theoretical seismic wave radiating from a fluid-filled borehole, Geophysics, 47, p. 1308-1320.

Paulsson, B.N.P., 1988, Three component downhole seismic vibrator, Soc. of Expl. Geophysicists, 58th Annual Meeting Expanded Abstracts, 1, 139-142.

Samec, P. and Kostov, C., 1988, Full waveform modeling of a downhole source radiation pattern using the finite element technique, Soc. of Expl. Geophysicists, 58th Annual Meeting Expanded Abstracts, 1, 143-145.

Samec, P., 1989a, Modeling of downhole sources radiation pattern using the finite element method, Paper G, Stanford Rock Physics Annual Report.

Samec, P., 1989b, Stanford University (personal communication).

Seeman and Horowicz, 1983, Vertical Seismic Profiling: Separation of upgoing and downgoing acoustic waves in a stratified medium: Geophysics, 48, 5, 555-568.

White, J.E. and Sengbush, R.L., 1963, Shear waves from explosive sources: Geophysics, 28, 1001-1019.

White, J.E., 1965, Seismic Waves: Radiation, Transmission, and Attenuation, New York, McGraw-Hill Book Company, 302 p.

Winbow, G.A., 1989, Seismic sources in open and cased boreholes, Presented at the 59th Ann. Int'l. Meeting of the Soc. of Expl. Geophys., 1, 8-10.

APPENDIX 3-A

THEORETICAL CYLINDRICAL WAVE PROPAGATION

The general solution for axially-symmetric wave propagation around a vertical borehole in cylindrical coordinates is White (1965):

$$\Phi = [A_1 H_0^{(1)}(mx) + A_2 H_0^{(2)}(mx)]e^{-ilz}e^{i\omega t},$$

$$\Theta = [B_1 H_1^{(1)}(kx) + B_2 H_1^{(2)}(kx)]e^{-ilz}e^{i\omega t}, \qquad (3\text{-}1A)$$

$$l = \frac{\omega}{c}, \quad m = \omega\left(\frac{1}{\alpha^2} - \frac{1}{c^2}\right)^{1/2}, \quad k = \omega\left(\frac{1}{\beta^2} - \frac{1}{c^2}\right)^{1/2},$$

where α is the compressional velocity of the formation, β is the shear velocity of the formation, c is the propagation velocity in the borehole (which will be defined as the longitudinal wave velocity up the drillstring (15600 ft/s) (4758 m/s)), x is the perpendicular distance from the borehole axis, ω is angular frequency, H_0, and H_1 are modified Hankel functions as described by White (1965), and Φ and Θ are scalar potentials satisfying the wave equation.

The arguments of the Hankel functions H_0 and H_1 in Equation 3-1A will be real provided that $\beta < c$ and $\alpha < c$. If $\beta < c$ and $\alpha > c$, then the argument of H_1 will be real and the argument of H_0 will be imaginary. If both α and β are greater than c, then both arguments are imaginary. This last case ($\alpha > c$, $\beta > c$) is the condition used to define tube wave propagation in a fluid-filled borehole. When a longitudinal wave is propagating up a steel drillstring, both arguments are generally real.

White noted that Hankel functions of large, real arguments can be approximated as:

$$H_0(mx) \cong \left(\frac{2}{\pi mx}\right)^{1/2} e^{i(mx-\pi/4)},$$

$$H_1(kx) \cong \left(\frac{2}{\pi kx}\right)^{1/2} e^{i(kx-3\pi/4)}, \qquad (3\text{-}2A)$$

and Hankel functions of large, imaginary arguments take the form:

$$H_0(imx) \cong A_1 e^{-mx},$$

$$H_1(ikx) \cong B_1 e^{-kx}, \qquad (3\text{-}3A)$$

where, $m = |\omega| \left(\frac{1}{c^2} - \frac{1}{\alpha^2}\right)^{1/2}$, $k = |\omega| \left(\frac{1}{c^2} - \frac{1}{\beta^2}\right)^{1/2}$.

Using these approximations, the far-field solution for wave behavior around a cylindrical borehole can be split into two conditions that depend upon whether the arguments are real or imaginary (i.e., upon the compressional and shear velocities, α and β, of the formation surrounding the borehole and the velocity of propagation up the borehole, c).

Condition 1: $\beta < \alpha < c$

If both the compressional and shear velocities are less than the propagation velocity up the drillstring, then in the far-field, the potentials Φ are Θ for waves traveling in the +z direction (upwards) become:

$$\Phi \cong \frac{1}{(xm)^{1/2}} e^{-imx} e^{-ilz} e^{i\omega t}$$

$$\Theta \cong \frac{1}{(xk)^{1/2}} e^{-ikx} e^{-ilz} e^{i\omega t} \qquad (3\text{-}4A)$$

These potentials define head waves that propagate away from the borehole as plane waves making an angle, φ_c, with respect to the perpendicular to the borehole axis. For the compressional potential, Φ,

$$\varphi_c = \sin^{-1}\left(\frac{\alpha(z)}{c}\right), \tag{3-5A}$$

and for the shear potential, θ,

$$\varphi_c = \sin^{-1}\left(\frac{\beta(z)}{c}\right). \tag{3-6A}$$

The compressional potential, Φ, defines a head wave that propagates into the earth at the compressional velocity, whereas the shear potential, θ, defines a head wave that propagates at the shear velocity.

As Equation 3-4A shows, the head wave amplitude decreases as $x^{-1/2}$ away from the borehole. Equation 3-4A also shows that the head wave amplitude increases as α and β approach c, the velocity of propagation in the drillstring. In the near-field, the Hankel functions approach a constant value, and the expressions in Equation 3-1A become:

$$\begin{aligned} \Phi &\cong e^{-ilz}e^{i\omega t} \\ \Theta &\cong e^{-ilz}e^{i\omega t} \end{aligned} \tag{3-7A}$$

Both of these potentials define a displacement in the z direction, which travels with a velocity c, and as depicted in Figure 3-6, the wavefront bends in toward the normal to the borehole axis as r decreases.

Condition 2: $\beta < c < \alpha$

If the compressional velocity is greater than the velocity of the longitudinal wave traveling up the drillstring, then the argument of the zero order Hankel functions, H_0, in Equation 3-3A is imaginary, and the compressional potential in the far-field becomes:

$$\Phi \cong H_1 e^{-mx} e^{-ilz} e^{i\omega t} \qquad (3\text{-}8A)$$

where, $m = |\omega| (1/c^2 - 1/\alpha^2)^{1/2}$

and a guided wave traveling up the borehole is activated. This guided wave travels up the borehole with a velocity equal to the longitudinal wave velocity in the drillstring. Due to its exponential decay away from the borehole wall, this wave does not propagate appreciably into the earth. The shear potential Θ is the same as in Equation 3-4A, and shear head waves are radiated into the earth as before.

CHAPTER 4

COMPARISON AND APPLICATION CASE STUDIES OF DRILL-BIT SIGNAL UTILIZATION

4.1 Comparison Between Drill-Bit VSP and Conventional VSP

4.1.1 Introduction

As shown in the previous chapters, in addition to the primary direct and reflected arrivals the correlated drill-bit signals contain many arrivals that are not observed in conventional VSP data. Compensation techniques such as reference deconvolution, component filtering, and zero-moveout median filtering are utilized to correct for these differences. In this section we discuss a case history that investigates the similarities and differences between 'compensated' drill-bit correlations and conventional VSP data acquired in the same borehole. The traveltimes are compared to evaluate the utility of the drill-bit direct arrival as a velocity survey replacement. The processed reflection images are also compared to evaluate the utility of the drill-bit VSP as a subsurface imaging method.

4.1.2 Data Acquisition

A well in the Sabine Uplift region of west-central Louisiana was used to compare drill-bit data with conventional VSP data. Drill-bit VSP data were recorded from 1370 to 2600m in a clastic and carbonate zone. The geophone array deployed on the surface consisted of twenty-four 10 Hz vertical geophones with a total array length of 36m. The array center was 778m from the wellhead. The 10m recording times used to generate the correlation functions ranges from 25 to 75 minutes in the shallow logging section to 240 minutes in the deep section.

After the well was completed, a conventional VSP survey was conducted using an airgun suspended in a pit. The airgun was located at the same wellhead offset as the geophone array used to record the drill-bit signals. However, due to logistical

difficulties in locating the airgun source near the geophone-array azimuth, the airgun was positioned on the opposite side of the wellhead (approximately along strike). Since the geology in the region was essentially flat, the non-reciprocal source and receiver positions were not expected to result in major differences between the data acquired. The direct-arrival traveltime differences due to lateral velocity variations were expected to be less than 1 ms, as checkshot surveys on nearby wells showed under 3 ms of discrepancy from well to well. An LRS 1300 3-component downhole receiver was used to record the VSP data. The downhole receiver occupied the same depth zone over which the drill-bit signals had previously been recorded. To maintain equivalence in receiver antenna patterns only the vertical component was processed for comparison.

4.1.3 Total Wavefield and Direct Arrival Traveltime Comparison

Figure 4-1 shows the compensation-processed drill-bit correlations and the conventional VSP data. Compensation processing consisted of: 1) reference deconvolution (Chapter 1), 2) a 99-trace median reject filter applied to attenuate the head waves, rig arrivals, and drillstring multiple arrivals (Chapter 3), and 3) correction for the time shift in the correlations due to travel in the drillstring (Chapter 1). The compensated correlations were bandpassed from 14 to 56 Hz and a surgical mute was applied before the direct arrival. Every other drill-bit VSP trace is shown to emulate the 20m VSP sampling interval. The VSP data are displayed after the same bandpass filtering and surgical muting.

Both data sections exhibit a dominant P-wave direct arrival. The events following the direct arrival have a different character. The drill-bit data have a more random appearance; whereas the conventional VSP appears more organized. In the conventional VSP data direct-arrival reverberations continue for about 200 ms past the first break time. This is believed to be due to the residual bubble-pulse and pit-interaction reverberations of the airgun source (Dragoset, 1990). The more random

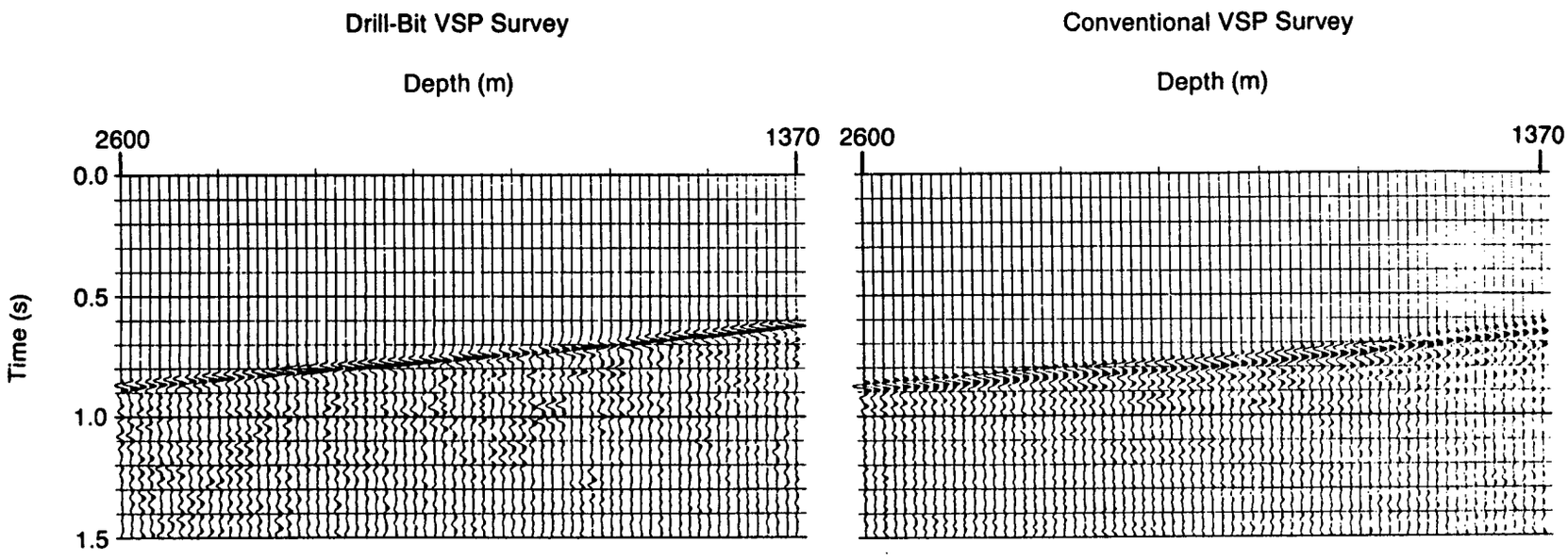

Figure 4-1. Comparison of compensation processed drill-bit VSP data and conventional VSP data.

appearance of the drill-bit data is probably due to the effects of the zero-moveout median rejection filter. The zero moveout filter removes the low spatial frequencies from the f-k spectrum, enhancing the higher apparent velocity evanescent energy.

The direct-arrival wavelets in Figure 4-1 have very different phase characteristics. The correlated drill-bit direct-arrival wavelet appears to be nearly symmetrical whereas the impulsive airgun VSP wavelet looks more front-loaded. This character is consistent with the nature of the trace extraction processes which theoretically have zero phase and minimum phase outputs, respectively. If we assume that the correlated drill-bit wavelet is zero phase and the airgun VSP wavelet is minimum phase then the timing of the wavelet peak in the correlated drill-bit wavelet should compare to the airgun VSP first break time. Figure 4-2 shows a comparison of the traveltimes using this comparison criteria. The time picks were interpolated between samples using a 99-point sinc(t) function, resulting in a resolution of 0.1 ms.

The traveltimes in Figure 4-2 generally correspond within 2 ms or 0.3 percent of the total traveltime. The maximum observed difference was slightly over 5 ms. These differences are comparable to the traveltime difference observed when impulsive-source checkshot times are compared with vibroseis-source checkshot times (Manzur, 1989). When comparing impulsive-source data to correlative data traveltime differences can be caused by the fact that the wavelet peak times of the correlative source are more influenced by the minimum-phase earth impulse response filter than the onset time of the impulse source.

The correlated drill bit direct arrival wavelet, w(t), can be represented as:

$$w(t) = DS(-t) * K(t-t_{da}) * DS'(t) * E(t) , \qquad (4\text{-}1)$$

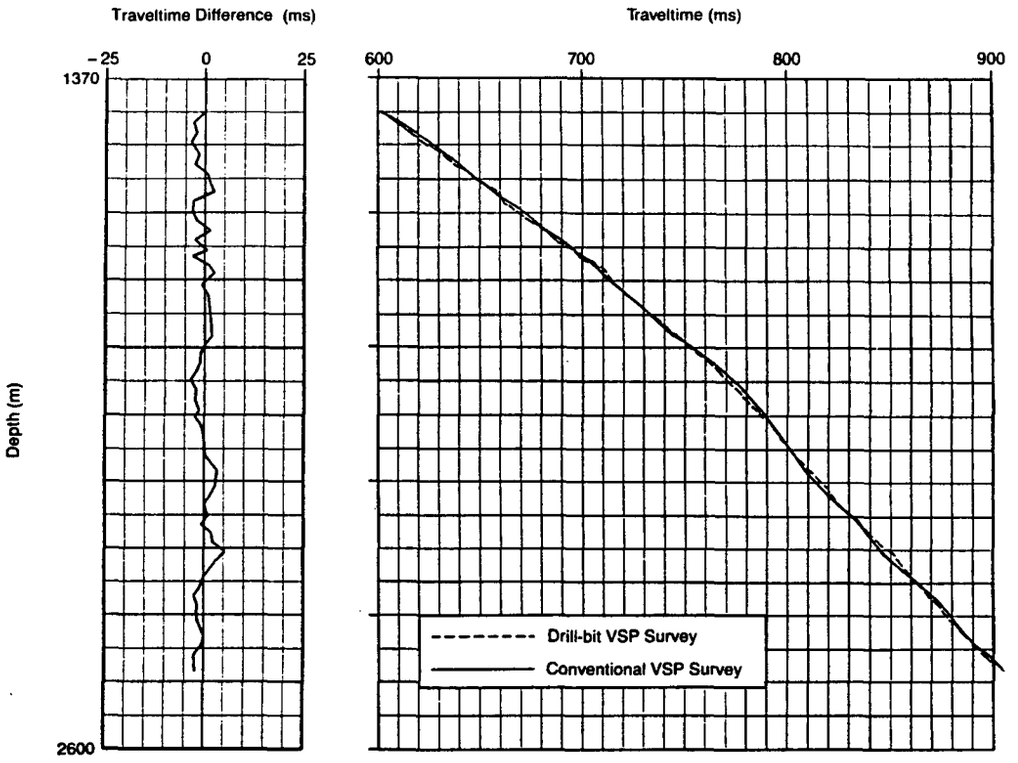

Figure 4-2. Comparison of direct-arrival traveltimes computed from drill-bit VSP data and conventional VSP data. The drill-bit VSP traveltimes were measured from the direct-arrival wavelet peak in Figure 4-1. The conventional VSP traveltimes were measured from the first-break times in Figure 4-1.

where:

$DS(-t)$ = The particle velocity response of the top of drillstring recording to an impulse at the drill bit

$K(t-t_{da})$ = The zero-phase Klauder wavelet representing the autocorrelation of the drill bit source signature (assumed wideband)

t_{da} = The Klauder wavelet peak time

$DS'(t)$ = The drillstring multiples recorded by the surface receiver

$E(t)$ = The earth filter.

If the drillstring and the Earth were all pass, pure delay filters, the timing of the direct arrival wavelet would be equal to the timing of the Klauder wavelet, which would be equivalent to the onset time of an impulsive source. However, the filtering of the drill bit signal in both the drillstring and the earth can bias the wavelet peak time array from the Klauder wavelet peak time.

Both short-period multiples and absorbtion can change the phase of the correlated wavelet and alter the timing of the wavelet peak. A study by Stewart, et al (1989) demonstrated time drifts caused by multiples of up to 0.2 ms/1000 ft. The effects of absorbtion are to delay the Klauder wavelet peak time by an amount, T_{gbias}, where:

$$T_{gbias} \cong T_{RE} - T_{RDS} , \tag{4-2}$$

and T_{RE}, T_{DS} are the rise times of the earth Q filter and the drillstring Q filter respectively. The rise time of a constant Q filter was defined by Kjartannson (1979) as the difference between the 90 percent and 10 percent values of the constant Q filter impulse response. For a particle velocity detector, the rise time, T_R, is:

$$T_R \cong 0.298t/Q , \tag{4-3}$$

where t is the traveltime of the arrival. With estimates of both drillstring and earth Q and traveltime, the time bias introduced by absorbtion can be estimated from Equations 4-2 and 4-3. In the traveltime comparison shown in Figure 4-2, the average formation Q was thought to be somewhere between 50 and 200. These Q values would theoretically alter the traveltime by a very small (<1 ms/1000 ft) amount.

Other factors that can contribute to time differences between the two techniques include:

1) Dispersion
2) Differences in source and receiver positions
3) Source and receiver array effects
4) Crossing arrivals in drill bit data. (For example, the head waves and rig arrivals in drill-bit data could interfere with the direct arrival creating a false wavelet peak.)
5) Differences between drillers depth and wireline depth (on this well the difference was less than 2m)
6) Uncertainty of drillstring velocity calculated in Chapter 1

From the many sources of traveltime difference, it is unlikely that direct correspondence between these two techniques can be achieved. More realistically, we estimate that 1 percent absolute uncertainty and 1 to 2 ms of random uncertainty will always exist in the correspondence between impulsive and correlative picked times. As typically 20 to 40 ms of two-way time mistie can exist between well-log-derived formation tops and seismic reflections (Goins, 1987), the correspondence is generally adequate for time-to-depth uses of the drill-bit data. The 1 to 2 ms of random traveltime uncertainty means that simple interval velocity calculations from the data are only reliable (within 10 percent) over depth intervals greater than about 60m. More sophisticated techniques (Godkin, 1985; Salo and Schuester, 1988)

incorporating the multiplicity of raypaths that traverse an interval could be used to obtain more reliable velocity estimates over finer intervals.

4.1.4 Comparison of Reflection Images

Reflected arrivals were extracted from the total wavefield data by performing conventional VSP wavefield separation and deconvolution (Hardage, 1985) on the total wavefield data sets shown in Figure 4-1. The deconvolved reflected events were transformed the data to common reflection point using a 'VSP-CDP' transform (Wyatt and Wyatt, 1981). The VSP-CDP transform converts the traveltime versus depth coordinates of VSP data into coordinates of two-way traveltime versus subsurface reflection point (in terms of wellhead offset). The specific implementation consisted of raytracing through a velocity model defined by the direct arrival traveltimes to associate a particular subsurface reflection point with the source (or receiver depth) and the surface receiver (or source) offset. The common reflection points were collected in 25 ft (7.6m) bins, moveout corrected (using the traveltimes computed from the raytracing), and summed. Each of the common reflection points were then converted to two-way vertical time using the integrated velocity model.

The mapping processing of the VSP-CDP transform can best be understood with a simple model. Using straight raypaths and horizontal reflectors we can write the subsurface reflection point wellhead offset, X_{CRP}, in terms of the source (or receiver) depth, Z, the surface receiver (or source) offset, X, and the vertical distance, Z_r, of the reflector below Z as:

$$X_{CRP} = X\, Z_r/(Z + 2Z_r) \qquad (4\text{-}4)$$

If Z = 0, this equation reduces to: $X_{CRP} = 1/2X$; the common-midpoint-stack used in conventional surface seismic processing. Equation 4-4 shows that deeper reflections are located farther from the wellhead.

Equation 4-4 also shows that the subsurface coverage along a given reflector changes as Z approaches Z_r. For $Z << Z_r$ the subsurface point is a constant independent of the source depth (and approximately equal to 1/2X). For $Z >> Z_r$, Equation 4-4 reduces to:

$$X_{CRP} = X Z_r/Z \tag{4-5}$$

In this case, the subsurface point is strongly dependent upon Z, resulting in a relatively wide range of subsurface coverage for a narrow range of source (or receiver) depths. Consequently, when interpreting VSP-CDP transforms the eye is often drawn to the high coverage/low fold traces near the borehole where $Z_r << Z$.

Figure 4-3 illustrates the VSP-CDP transforms of the drill bit and conventional VSP data. Overall, the VSP-CDP images are similar and compare favorably with published VSP-CDP transform data (VanderPoel and Cassell, 1989) in terms of their ties. The principal reflectors at 1.3, 1.43, 1.5, and 1.58s tie very well. However, there are some differences in the reflection images. For example, the drill-bit VSP-CDP image exhibits a strong reflection at 1.175s. On the conventional VSP-CDP image this reflector is virtually non-existent. The reflector package between 1.6 and 1.7s is more continuous in the conventional VSP-CDP than in the drill-bit VSP-CDP. In addition, the reflectors that tie exhibit some phase differences.

The differences in the VSP-CDP images are probably attributable to some of the causes enumerated for discrepancies between the direct-arrival traveltimes. In particular, the presence of different crossing arrivals, and different levels of noise are probably responsible for the observed differences in reflector continuity. Besides the delay and moveout differences between drill-bit head waves and rig arrivals, and airgun VSP tube wave arrivals, the radiation patterns of the airgun source was expected to behave quite differently from the radiation pattern of the drill bit source

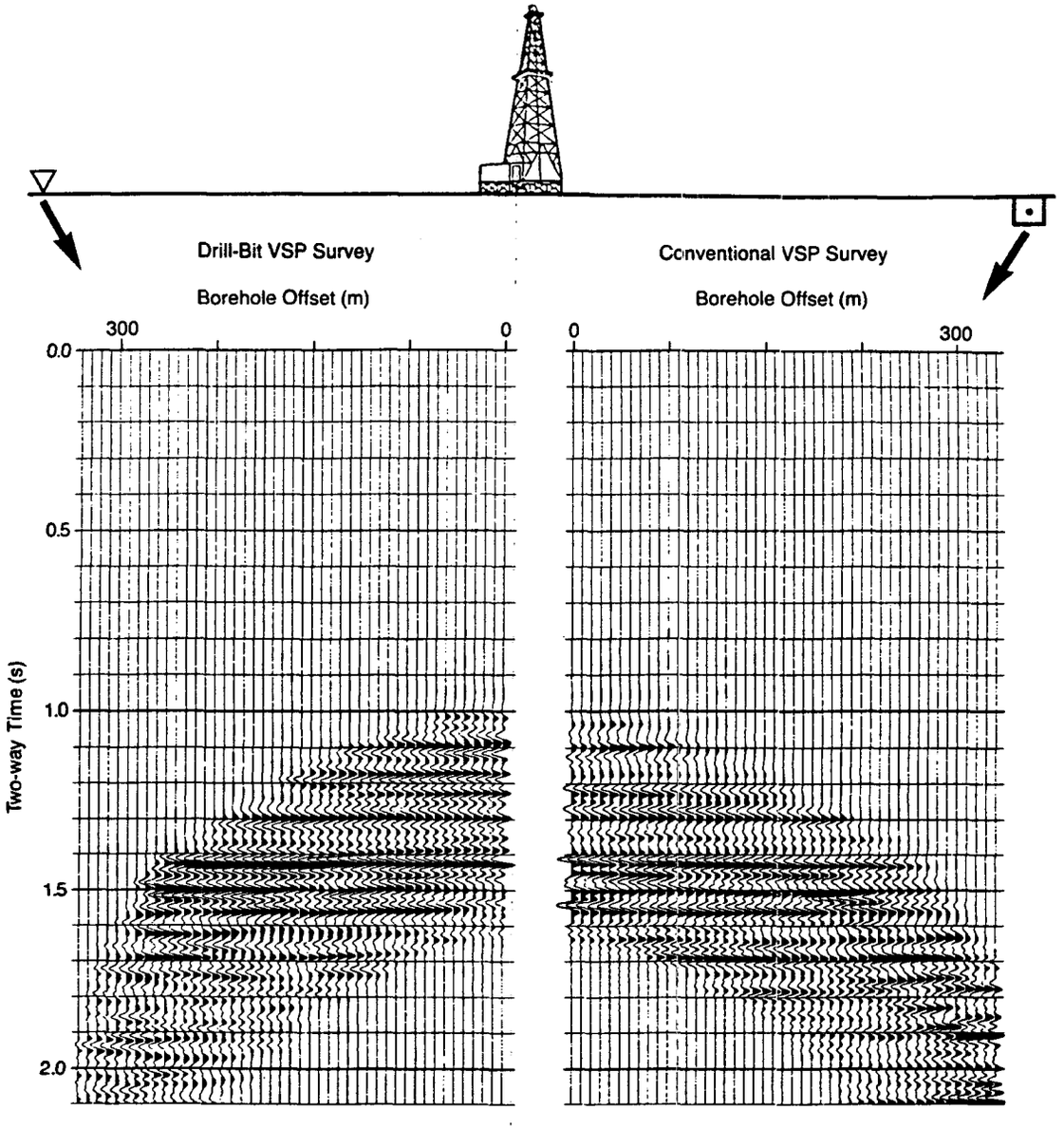

Figure 4-3. Comparison of the subsurface reflection images generated using a VSP-CDP transform from drill-bit VSP data and from conventional VSP data.

proposed in Chapter 3. The airgun source theoretically behaves as a purely dilatational source (White, 1965), generating compressional waves with an omnidirectional radiation pattern. Whereas the drill bit is expected to generate shear as well as compressional energy. Consequently, shear-corrected arrivals would be expected to contribute more to the total response of the drill bit data than to the airgun VSP data. The wavelet phase differences in the images are probably due to the major wavelet differences observed in the direct arrivals. The major differences in the direct-arrival wavelets created very different deconvolution operators (Hardage, 1985), which would be expected to behave very differently when applied to the upgoing reflection arrivals.

An improved comparison would probably have been obtained using a conventional VSP vibroseis energy source colocated with the drill-bit surface array. This would have reduced the wavelet differences and the source radiation differences substantially and eliminated the subsurface differences. In addition, the use of a longer surface array in the drill-bit data would have improved the S/N of primary drill-bit arrivals to crossing rig and head wave interference. However, like the traveltime differences, direct correspondence between a drill bit and a conventional VSP reflector image is difficult to obtain.

Summary

This case study illustrated that the processed drill-bit direct-arrival traveltimes and reflection images were comparable to conventional VSP traveltimes and reflection images. Traveltimes corresponded within 0.3 percent, and major reflection packages tied. The study also illustrated many possible causes for the lack of direct correspondence between the techniques. Although improved correspondence could have been obtained on this test well through better data acquisition parameters, identical results are very difficult, if not impossible to achieve.

4.2 Comparison of Drill-Bit Reflection Images With Conventional Surface Seismic Reflection Data

4.2.1 Introduction

A comparison of a drill-bit reflection image with conventional surface seismic reflection data was made on a well located in the Gulf Coast region of East Texas. This location was chosen to evaluate the ability of the drill-bit data to detect reflections associated with a zone of abnormal pressures. In the Gulf Coast region, the most common mechanisms for abnormal pressuring (Bruce, 1984) are: gravitational loading, smectite-illite transformation, and aquathermal pressuring. The top of the abnormal pressure is often expressed as a rapid increase in interval velocity associated with a higher density resistive cap containing abnormal amounts of limey or calcareous sands (Pennebaker, 1968; Reynolds, 1970). The abnormal pressure zone itself has lower interval velocities. These velocity contrasts often result in reflections that can be identified on surface seismic data. The timing of these reflections can be used to predict the onset depth of abnormal pressure. This information can aid the driller in selecting casing depths and mud programs. The reflections from a downhole source or receiver provide an improvement over surface seismic reflection data in that the fresnel zone is reduced (Hardage, 1985) and the reflection image (assuming horizontal reflectors and a receiver offset close to the wellhead) corresponds to reflections from sequences penetrated by the drill bit.

4.2.2 Data Acquisition and Drill-Bit Data Processing

Figure 4-4 shows a map view of the well location the surface seismic line and the surface geophone array location used to record the drill-bit data. The geophone array consisted of forty-eight 10 Hz vertical geophones spanning a total distance of 400 ft (122m). The drill-bit signals were logged from 3000 to 8526 ft (915 to 2600m) over a period of approximately 7 days. The seismic data were acquired using a dynamite source with an unknown receiver geometry. Figure 4-5 shows the processed

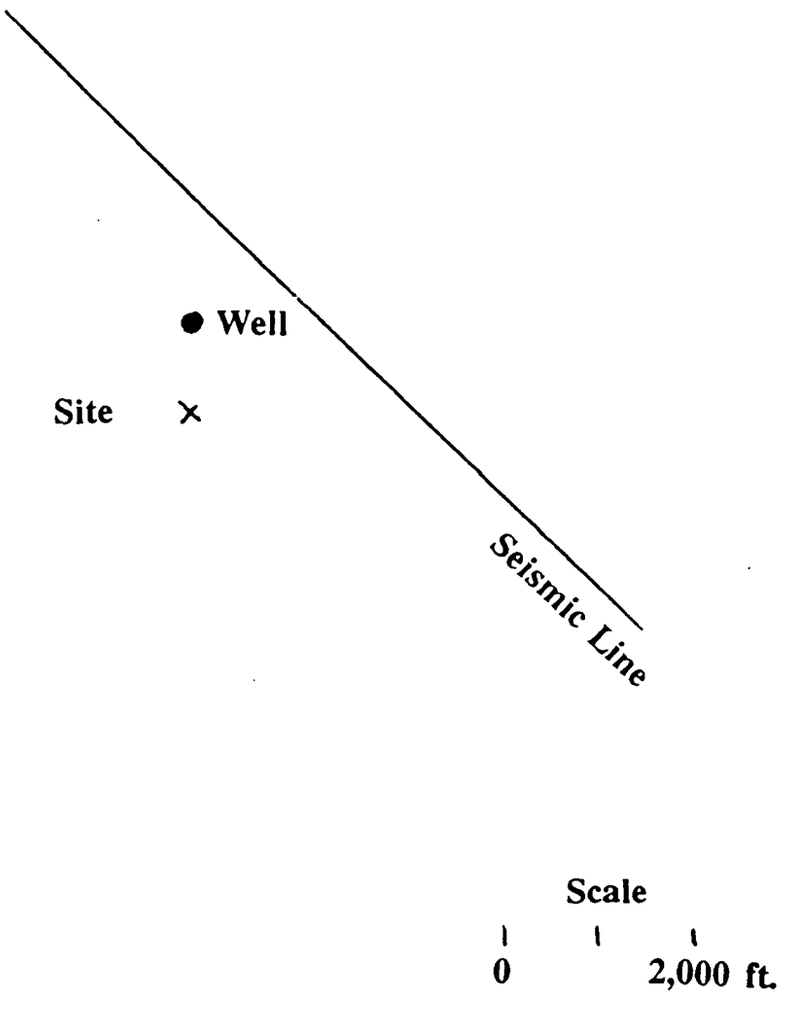

Figure 4-4. Prospect map.

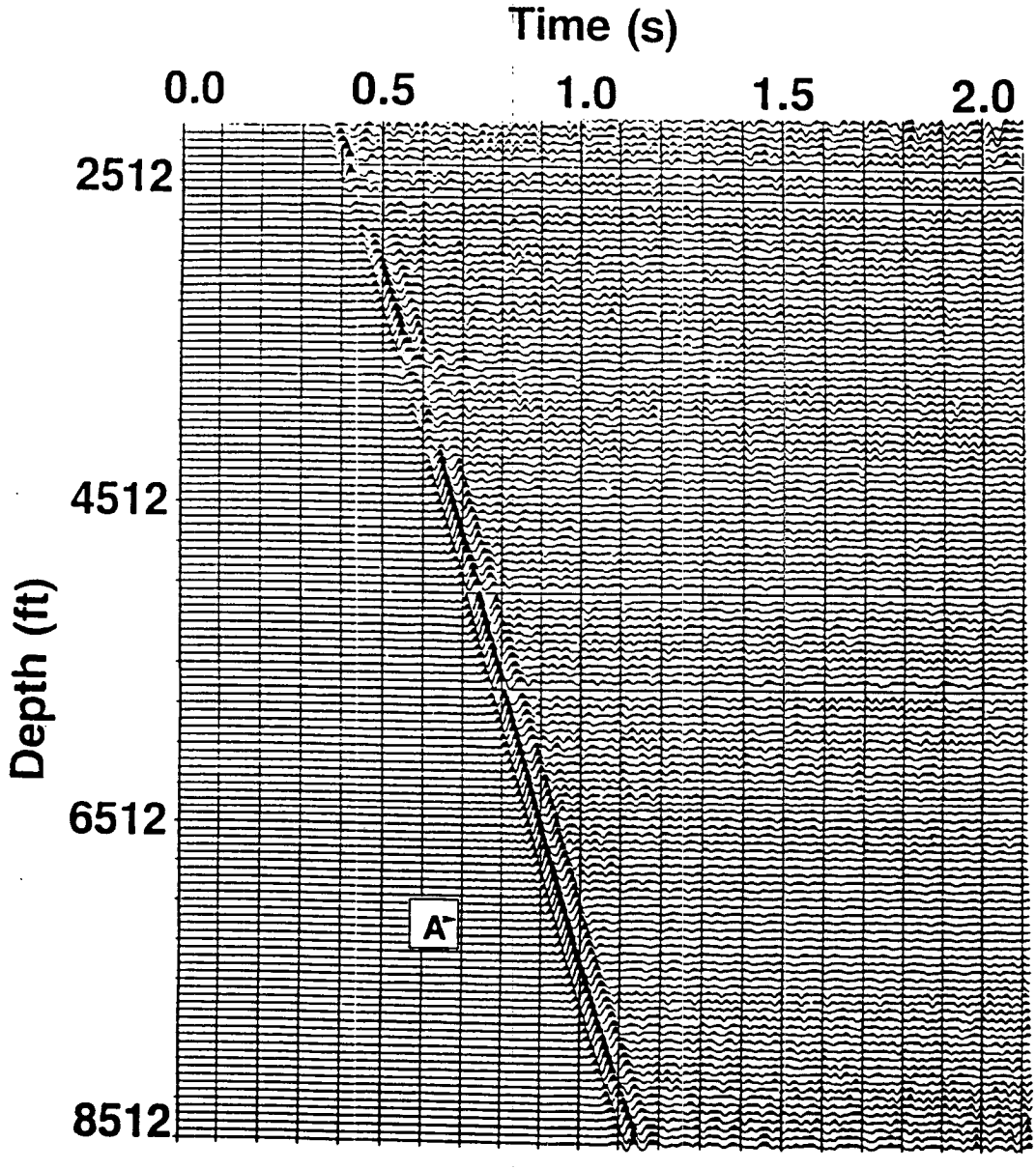

Figure 4-5. Compensation-processed drill-bit wavefield. Depth A is the onset of an abnormal pressure zone.

drill-bit 'VSP-equivalent' wavefield. The data processing employed to generate the display consisted of cross-correlation over 10m of drill-bit moveout (the average recording time for each 10m interval was 30 minutes), reference deconvolution (Chapter 1), zero-moveout interference removal (using a 60-trace median filter), correction for drillstring traveltime (Chapter 2), and resampling to 50 ft (15m) depth intervals. Finally a surgical mute was applied before the direct arrival and the muted data were bandpass filtered from 10 to 45 Hz. (The frequency content of the seismic data in the region was typically less than 40 to 50 Hz (Manzur, 1989).) The depth resampling was done by vertically stacking the correlated traces over a 50 ft (15m) window centered at the depths displayed. This process resulted in attenuation of some of the higher frequency signals, but had little effect in the seismic band of interest ($<$45 Hz).

The principal arrival observed is the P-wave direct arrival from the drill bit. There are several traces, particularly above 4500 ft (1372m), where the direct arrival is not apparent. The absence of direct arrival energy in these zones was primarily due to equipment problems. Besides the direct arrival, there appears to be some residual rig generated and head wave arrivals traveling with a moveout of 15600 ft/s (4758 m/s). Also evident are reflected arrivals with negative moveout of a magnitude comparable to the direct-arrival moveout. Based on an increase observed in the penetration rate (Jorden and Shirley, 1966), the onset of abnormal pressure was interpreted to be at 8112 ft (2470m), designated by A. Many of the traces also appear to contain narrowband signals. These narrowband signals may be due to residual incoherent rig noise from the rig engines and the mud pumps (Chapter 2).

4.2.3 Comparison of Drill-Bit Reflections With Surface Seismic and Sonic Log Data

Figure 4-6 show a portion of the surface seismic data, the sonic log, and the reflection image obtained from the drill-bit wavefield. The drill-bit reflection image was obtained by performing conventional VSP wavefield separation and direct-arrival

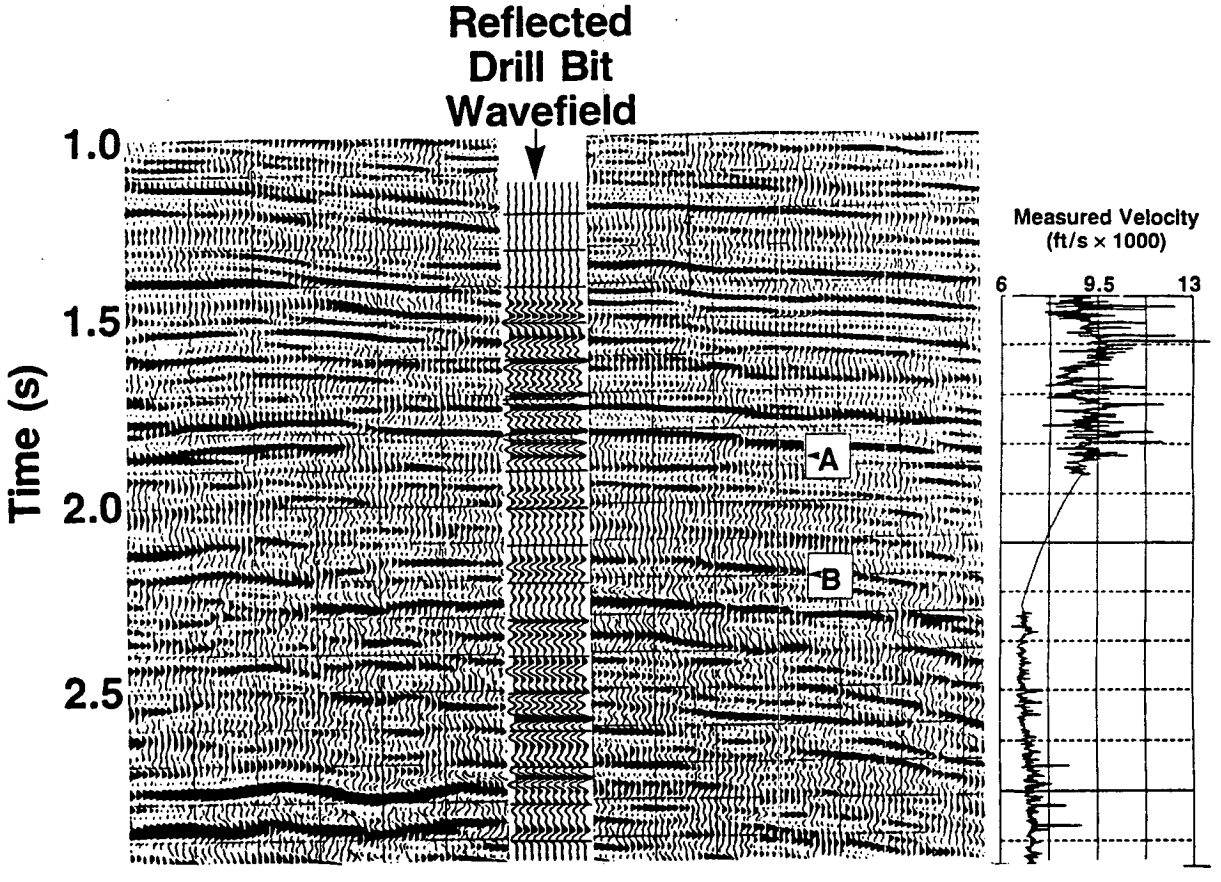

Figure 4-6. Correlation of the adjacent seismic line, the corridor stack of the drill-bit reflected wavefield and the sonic log. B is the interpreted bottom of the abnormally pressured zone.

deconvolution (Hardage, 1985) on the drill-bit wavefield displayed in Figure 4-5. The residual reflected arrivals were aligned to two-way vertical times using the cosine-corrected one-way times of the direct arrival wavelet peak. The reflected data were then corridor-stacked (Hardage, 1985) using a 200 ms window past the direct arrival. The corridor-stack window was tapered to include over 1000 ms past the direct arrival below 6500 ft (1980m). The data was displayed with a 0.8s agc.

The surface seismic data were processed with an unknown sequence. They were believed to have been wavelet processed to zero phase. Typical seismic lines in the area have a CDP interval of 220 ft (67m) (Manzur, 1989). The sonic log reportedly had operational problems below 7800 ft (2380m), resulting in a loss of transit-time information throughout much of the abnormally-pressured zone.

The reflection immediately above the top of the abnormally pressured zone corresponds to increases in formation velocity on the sonic log. This reflection is apparent on both the surface seismic data and on the reflected drill-bit wavefield. In addition, the base of the abnormally pressured zone (B) ties well. The other reflected arrivals compare less favorably. In particular the major reflector at about 2.27s on the surface seismic data has a very different expression on the drill-bit reflection data.

The lack of reflector correspondence between these techniques may be associated with the lack of continuity on most of the reflections observed on the surface seismic reflection data. Except for the reflection immediately above A, the reflectors have low S/N and are highly discontinuous. Assuming flat reflectors, the drill-bit reflections at A and above cover a very small region very near the well. In this zone, the corridor stack represents reflectors that originate just ahead of the drill-bit positions. As shown in Section 4.1, the longer traveltimes represent reflectors progressively farther from the borehole. The maximum reflection point is less than 450 ft (137m) from the wellhead. By contrast, the surface seismic reflection points are anywhere from 1000 to 1200 ft (305 to 366m) from the drill-bit VSP reflection

points. Other potential causes for the lack of correspondence were listed in Section 4.1. In particular, the reflections from well ahead of the drill bit would be expected to have lower S/N due to the increased travelpath lengths.

4.3 Measure-While-Drill (MWD) Velocity Survey From an Offshore Platform

Abstract

Two drill-bit surveys were acquired on highly deviated wells drilled from a platform located offshore from the California coast. Seafloor hydrophones were used to record the drill-bit signals on the two surveys. The first survey was performed to test whether the technique would work in an offshore environment, since previous surveys had been confined to land wells and transition zones. On the first survey, drill bit generated direct and reflected events were observed in the cross-correlated data. The direct-arrival traveltimes were within 1 percent of the traveltimes from a conventional vertically-incident velocity survey performed after drilling was completed. Based on these results, a survey on a second well was performed, utilizing the MWD velocity survey capabilities to monitor the vertical position of the bit on the seismic time section. With the MWD velocity survey, improved confidence in the well course was obtained.

4.3.1 Introduction

Seismic reflection data are often used by drillers and geologists to predict formation tops. The locations of formation tops define casing and coring depths, mud programs, hole deviations, and total well depth (TD). A common problem faced in predicting formation tops from seismic reflection data is the conversion from two-way traveltime to subsurface depth. Typically, a time-versus-depth relationship is determined from nearby wells where sonic logs and velocity surveys have been performed. This velocity information is extrapolated to the proposed well location using the seismic reflection data.

On rank wildcats or in areas with lateral velocity gradients, there may be significant uncertainty in the extrapolated time-versus-depth relationship. Target depths can be in error by several hundred feet, resulting in added drilling costs and risks. Depth uncertainty could be reduced if a velocity survey were performed while the well was being drilled. Target depth predictions could be updated and the drilling plan could be modified resulting in more efficient and less risky drilling. An offshore case study demonstrating the use of drill-bit signals for MWD purposes is described in this section.

4.3.2 Velocity Problem

Figure 4-7 shows typical interval velocities encountered in this area. The interval velocities range from about 5500 ft/s (1676 m/s) near the ocean bottom to more than 10000 ft/s (3352 m/s) at depth. The interval velocities increase with depth except between 3000 and 4000 ft. The presence of trapped gas in this zone creates a velocity inversion with measured formation velocities as low as 4500 ft/s (1372 m/s) directly beneath the platform where the gas column is over 1000 ft (305m) thick. As the height of the gas column decreases (away from the platform), the interval velocities increase by 30 percent to over 6000 ft/s (1829 m/s). Due to the variation in the height of the gas column, average velocities to depths below the trapped-gas zone vary by as much as 15 percent across the field.

Because of the large lateral velocity gradient, depth conversion of the deeper seismic data is uncertain and cannot be extrapolated from one well to another. Consequently, deviated well courses are projected onto the seismic data with some uncertainty. On development wells drilled from this platform there was a potential uncertainty in plotting the bit position onto the surface seismic of 8 percent below the gas-charged zone.

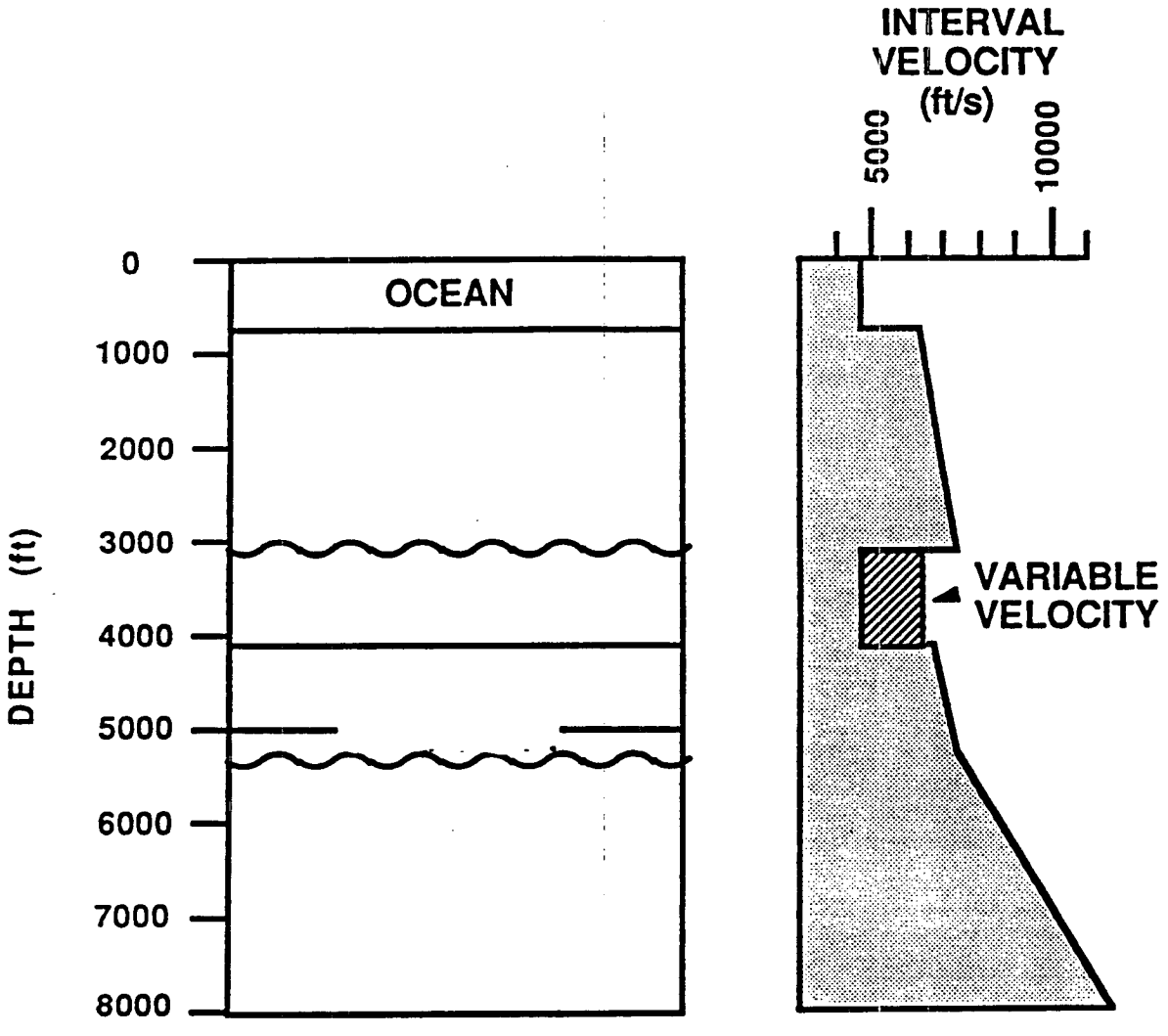

Figure 4-7. Typical interval velocities for the formations present at study wells 1 and 2. The interval velocities are highly variable ranging from 4500 ft/s to 6000 ft/s (1370 to 1829 m/s) between 3000 and 4000 ft.

4.3.3 Survey Layout and Drill-Bit Data Collection

Figure 4-8 shows the well courses for the two development wells where drill-bit data was recorded. The first survey, performed on study well 1, was an initial test of the drill-bit VSP concept in an offshore environment. The second survey, performed on study well 2, was used as an MWD velocity survey to reduce the uncertainty in drill bit position on the seismic time section. The drill bit wavefields were recorded using a pilot sensor deployment similar to land rigs, but in place of land vertical geophone arrays, hydrophones were deployed on the ocean bottom. A cable containing three hydrophones spaced at 1500 ft (457m) intervals was deployed by navigating a work boat away from the platform along the proposed well course. The cable was spooled off the end of the boat and anchored to the seafloor with heavy chains. An ocean-bottom deployment scheme was used rather than sea-surface deployment to ensure that the hydrophones did not move during the period of drill-bit signal logging. The ocean-bottom deployment scheme also improved the S/N over conventional sea-surface deployment. Not only was the noise from ship traffic and wave action reduced, but the shorter travelpaths from the drill bit to the hydrophones reduced the attenuation of the drill bit signals caused by spherical spreading and absorbtion. The hydrophones were specially constructed for the high ambient pressures of deep water. They were pressure rated for use at depths of up to 6000 ft (1830m). Ocean-bottom geophones were not used due to lack of availability and logistical problems in deployment.

Figure 4-9 shows a map view of the hydrophone positions on the ocean bottom. The positions were determined by firing a short grid of airgun pops above the assumed hydrophone position. The traveltimes of the direct water arrival from the shotpoints to each hydrophone were used to triangulate on the actual hydrophone positions. The location of the cable was determined to be about 20 degrees south of the intended cable position above the study well 1 well course. This departure was

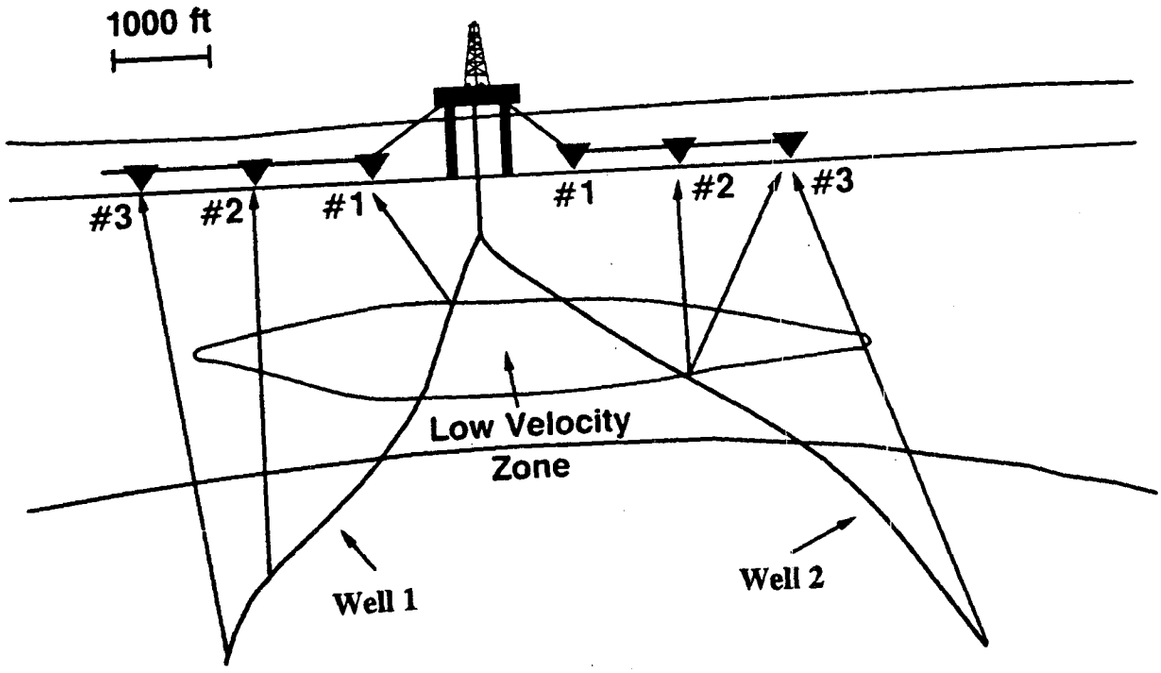

Figure 4-8. Well courses for study wells 1 and 2 along with direct arrival raypaths from the bit to the surface.

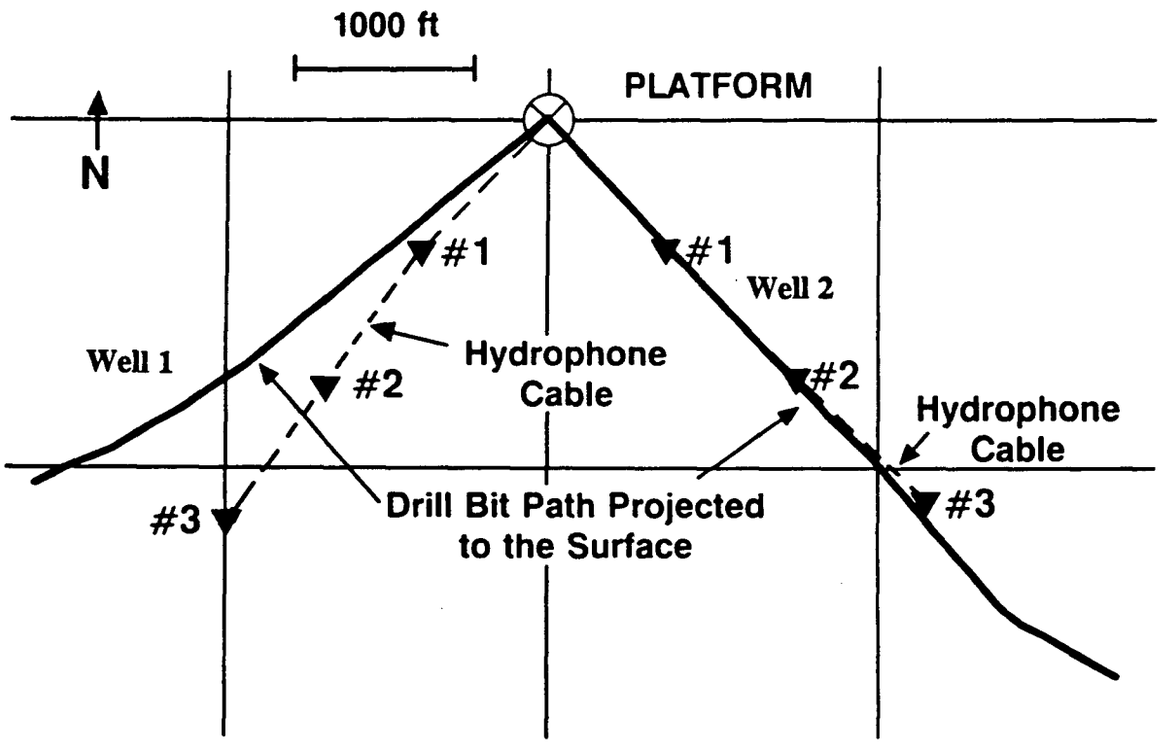

Figure 4-9. Map view of hydrophone locations along with well courses for study wells 1 and 2.

due to a lack of navigation equipment aboard the cable deployment vessel. On study well 2, the use of navigation equipment resulted in the correct positoning of the cable in a vertical plane above the proposed well course. Judging from the position of the deployment vessel, the hydrophones sank vertically to the bottom and were not strongly affected by currents. Total deployment and location time was under 5 hours. The well continued to drill during this period.

Drill-bit signals were recorded continuously on these study wells from intermediate casing through the end of drilling. On study well 1 this resulted in logging from a measured depth (MD) of 2850 ft (869m) to an MD of 8576 ft (2614m). On study well 2 the logging was from an MD of 5395 ft (1645m) to an MD of 10458 ft (3188m). Cross-correlation functions were computed over successive depth intervals of 30 ft (9.1m). After cross-correlation, compensation processing consisting of reference deconvolution (Chapter 1), an 8 to 35 Hz bandpass filter, and drillstring delay correction were applied to each trace.

A section of data from study well 1 is shown in Figure 4-10. The data quality from study well 2 was comparable. Like the surface seismic data in the area, the drill-bit data are low frequency, presumably due to wave propagation in unconsolidated sediments with a low quality factor. The drill-bit direct-arrival is the first event in Figure 4-10. The traveltime of this arrival is used to generate the time-versus-depth relationship and average velocities. At hydrophone site 1, the direct arrival is strongest at the shallowest depths. Due to attenuation caused by spherical spreading and absorbtion, the amplitude of the direct arrival decreases as the drill bit moves away from the hydrophone. At hydrophone site 2, the direct arrival is apparent only below 4000 ft (1220m) (MD) possibly due to the radiation pattern of the drill bit (Chapter 3). Referring to Figure 4-11 and assuming straight raypaths, the P-wave direct arrival at site 2 emerges within 10 degrees of a null in the radiation pattern at drill-bit depths above 4000 ft (1220m), so its radiated amplitude is less than

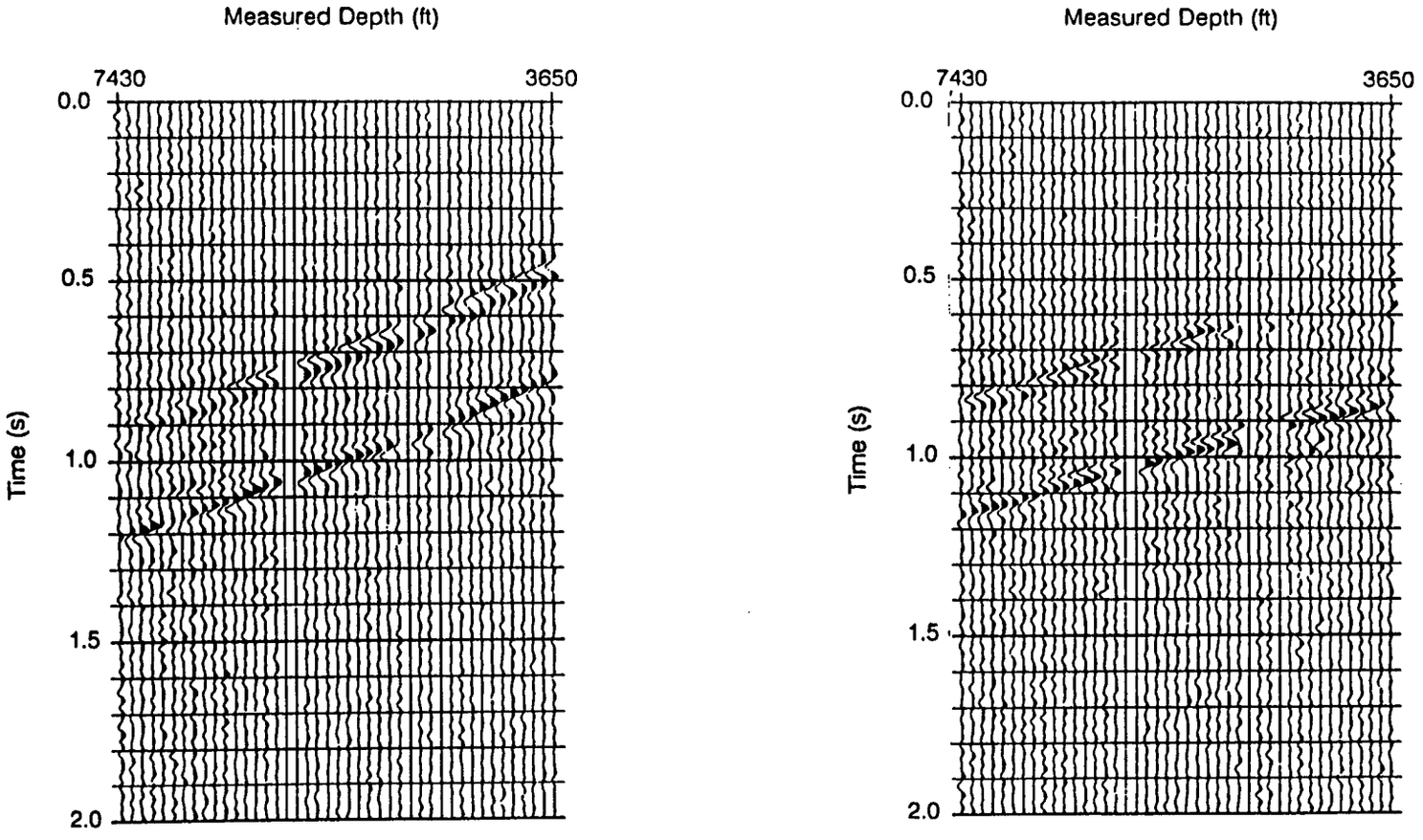

Figure 4-10. Drill bit wavefields from hydrophone 1 (left) and 2 (right) at study well 1. The data are shown like a VSP display, sampled at 90 ft (27m) depth intervals over a limited section of the well.

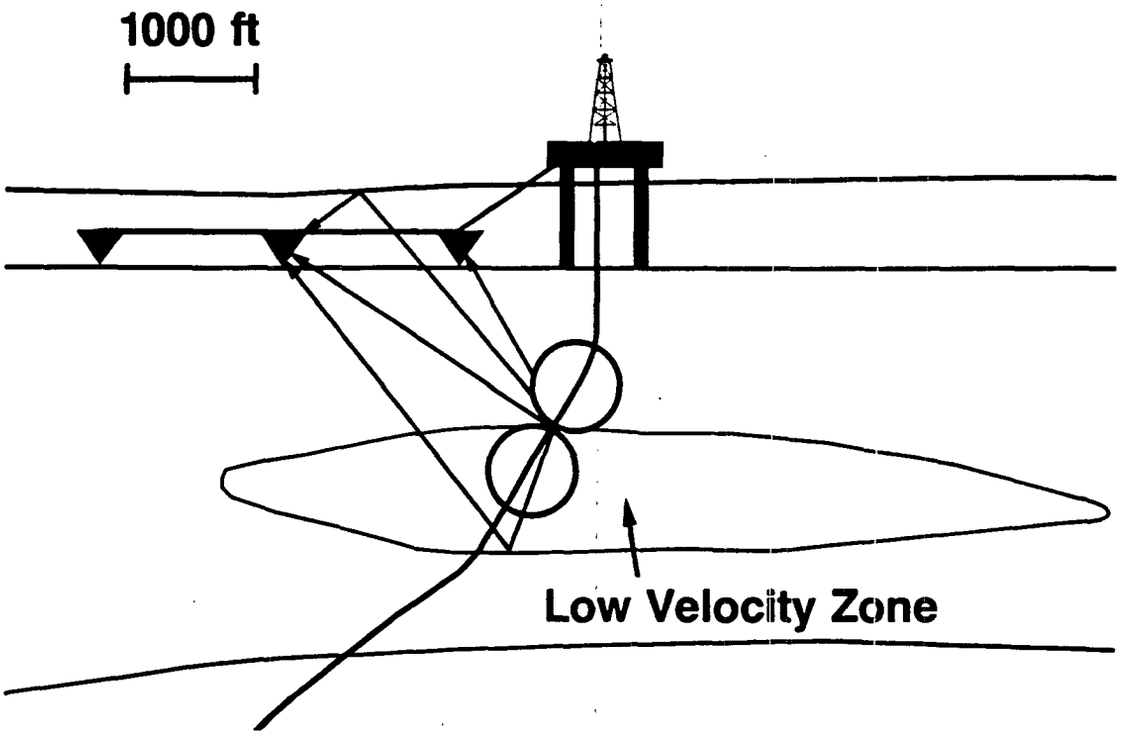

Figure 4-11. Raypaths of various arrivals identified in Figure 4-10. The circles show the theoretical P-wave radiation pattern of the drill bit on study well 1. The drill bit radiates most of the P-wave energy along the axis of the borehole. No P-wave energy is radiated perpendicular to the borehole axis.

20 percent of the radiated amplitude along the borehole axis. As the drill-bit depth increases, the direct-arrival raypath to site 2 emerges closer to the borehole axis, and a P-wave direct arrival becomes discernable.

The arrival following the direct arrival at a time lag of approximatly 310 ms is a water-top multiple. The water-top multiple travels directly up to the sea surface where it reflects and travels back down to the ocean bottom as shown in Figure 4-11. The sea surface reflection reverses the polarity of the arrival on the hydrophone recording. Conventional offshore seismic acquisition typically places the source and receiver at most 30 ft (9m) below the sea surface. Hence the water top multiples have a short period, with a delay of less than 15 ms. In ocean bottom recordings, the water-top multiples are longer period and can have a significantly different travelpath than the direct arrival.

The radiation pattern of a drill bit in a deviated borehole also predicts that P-wave reflected energy radiated by the drill bit will be stronger 'ahead' of the bit path than behind it. Thus, on study well 1, site 2 should record more reflected drill bit energy than site 1. Referring to Figure 4-10, there is a distinct reflected arrival at site 2 that appears to intersect the direct arrival at 4000 ft (1220m) MD. The reflected arrival is not apparent on the data from site 1. This reflector is thought to be the base of the gas-charged low velocity zone.

4.3.4 Comparison Between TOMEX Traveltimes and Conventional Velocity Survey Traveltimes

Figure 4-12 shows a comparison of traveltimes computed from the drill bit VSP velocity survey and traveltimes from a conventional airgun velocity survey on study well 1. Tool and hole problems prevented conventional logging of the entire well, so a direct comparison could be made only over a limited portion of the well. The traveltimes were measured by picking the peak of the drill-bit direct-arrival wavelet and the onset of energy in the direct-arrival wavelet from the conventional airgun

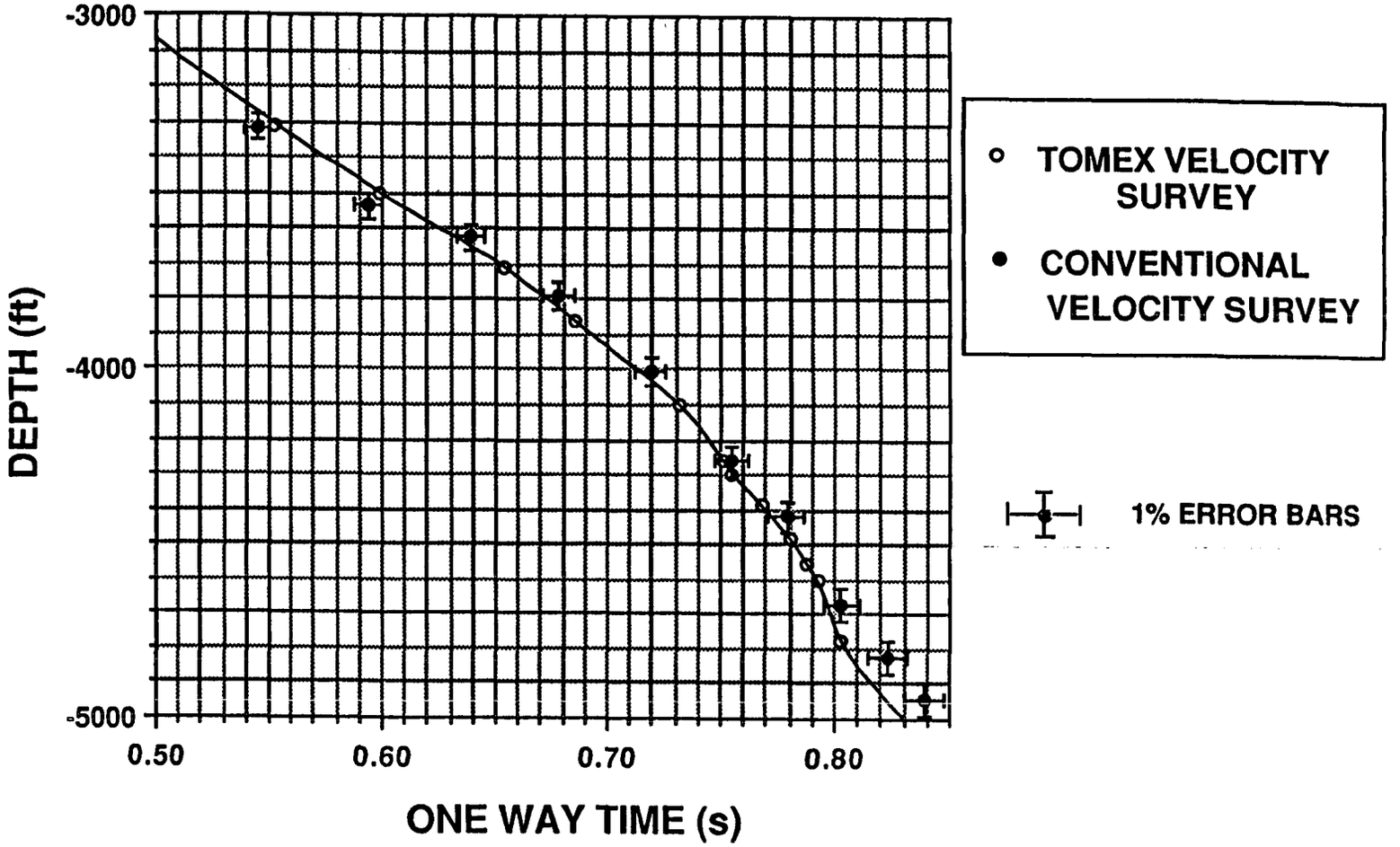

Figure 4-12. Comparison between drill bit and conventional velocity survey traveltimes. Conventional data could be obtained over only a limited portion of study well 1 due to wireline problems in the deeper section.

direct arrival. The drill-bit direct arrival traveltimes were corrected to vertical traveltime by assuming a straight raypath between source and receiver. These vertical traveltimes were then datum corrected from ocean bottom to sea level using the replacement velocity of seawater. The conventional velocity survey was acquired with the airgun positioned at the sea surface vertically above the receiver, and no raypath or datum corrections were necessary.

The traveltime differences in the two measurements are generally less than 1 percent, resulting in a depth discrepancy of less than 50 ft (15m). These differences are comparable to the traveltime differences observed when dynamite source first-break times are compared to correlated vibroseis peak times (Section 4.1). The differences are also comparable to the typical 20 to 40 ms of mistie observed when formation tops derived from well logs are calibrated to seismic reflection two-way times (Goins, 1987). Besides the potential causes for traveltime differences obtained in Section 4.1, differences in travelpath could cause a potentially large mistie in this example. The misplacement of the ocean-bottom hydrophones for the drill-bit data, away from the proposed well course, introduced the potential for traveltime differences caused by ray refraction differences and anisotropy as well as differences caused by lateral velocity gradients.

4.3.5 MWD Velocity Survey Results: Study Well 2

The results on study well 1 indicated that the drill-bit direct-arrival traveltimes had sufficient accuracy to be used as a real-time MWD velocity survey on study well 2. Figure 4-13 is a display of the proposed well course for study well 2 overlain on the surface seismic data. Like all wells deviated off this platform, study well 2 had poor velocity control below the gas-charged zone. The potential depth/time error at the target depth was $\pm$200 ft/80 ms. The goal of the drilling was to pierce the target on the downthrown side of the fault shown in Figure 4-13, as close to the fault as possible. The fault was defined primarily by the seismic, and the velocity uncertainty

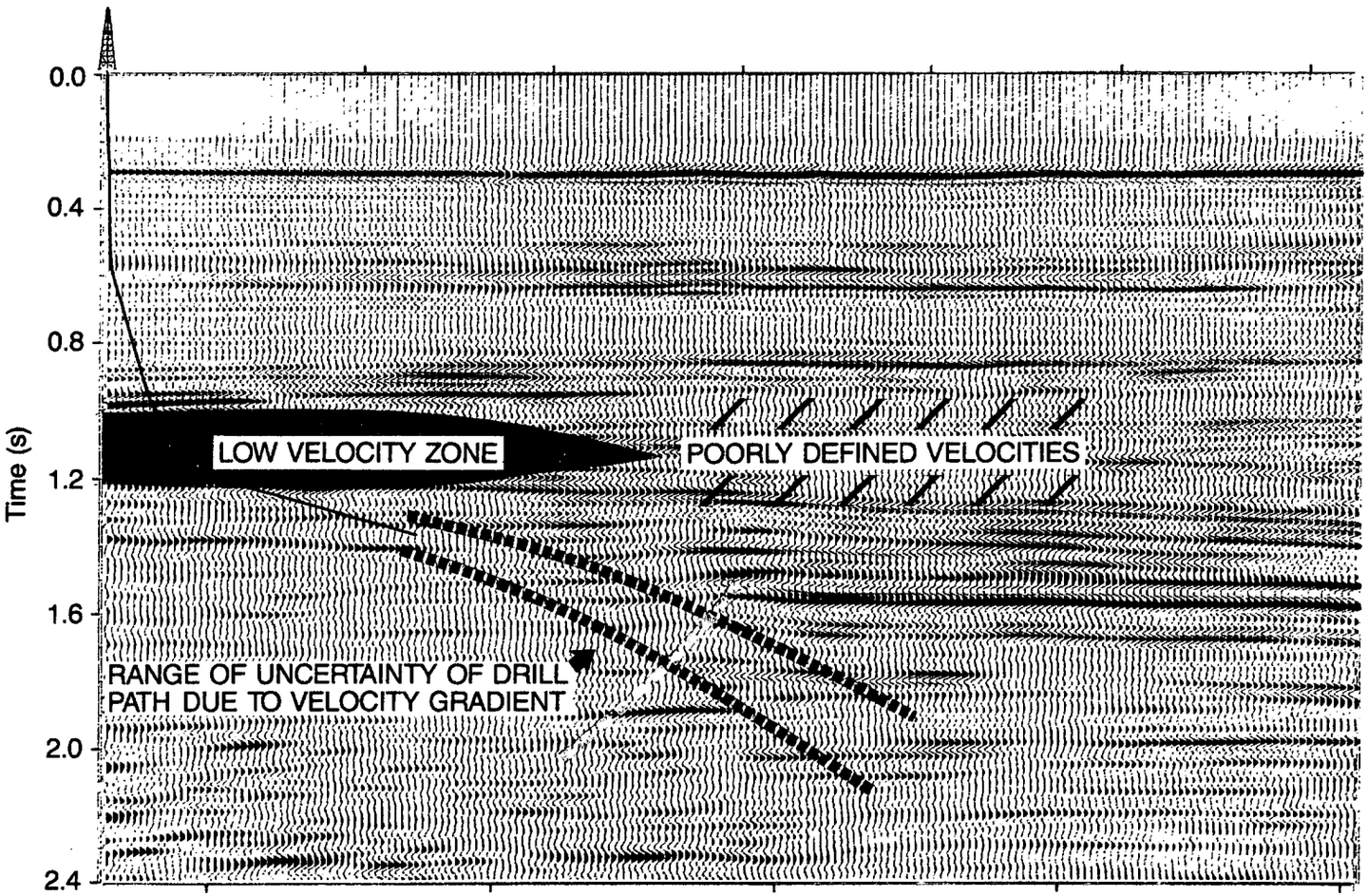

Figure 4-13. Seismic line taken from 3-D seismic cube along study well 2 well course. The target is on the downthrown side of a fault. The potential uncertainty in the well course caused by the poorly defined velocities in the gas-charged sediments is shown in blue.

created a potential uncertainty in the drill bit path shown by the blue dashed lines in Figure 4-13. If the bit came in on the lower of the blue dashed lines, the fault would be crosses below the target and the pay zone would be missed altogether. If the bit came in on the upper of the blue lines, the fault would be crossed well above the target, and the pay zone would have been penetrated far away from the fault.

The MWD velocity survey data provided by the drill-bit signals was utilized in the following manner. Vertical two-way traveltime versus subsea depth pairs were transmitted from the wellsite to the production office twice daily. Using the lateral position coordinates of the drill bit as determined from an MWD gyroscopic survey, the drill-bit position was plotted as a point on the seismic time section. Figure 4-14 shows the location of the drill bit course on the seismic data using the drill-bit velocity survey data. The uncertainty in the well course with respect to the traveltimes of the reflection data was reduced by 75 percent and the depth of the target was encountered within 5 ft (1.5m) of the desired pierce point. As it turned out, the anticipated well course on the surface seismic data was very close to the well course encountered.

4.3.6 Summary

Drill-bit data acquired on two offshore wells demonstrated the feasibility of recording drill-bit signals in an offshore environment and the utility of drill-bit data as an MWD velocity survey data that could be used to steer the drill bit. The presence of gas charged sediments above the target created a thick low velocity zone that varied laterally away from the center of the field. Since the extent and the magnitude of the low velocity zone could not be anticipated from surface seismic data, well courses and interpreted structures below the low velocity zone had large uncertainties even after several velocity surveys had been run on other wells. The drill-bit MWD data reduced these uncertainties.

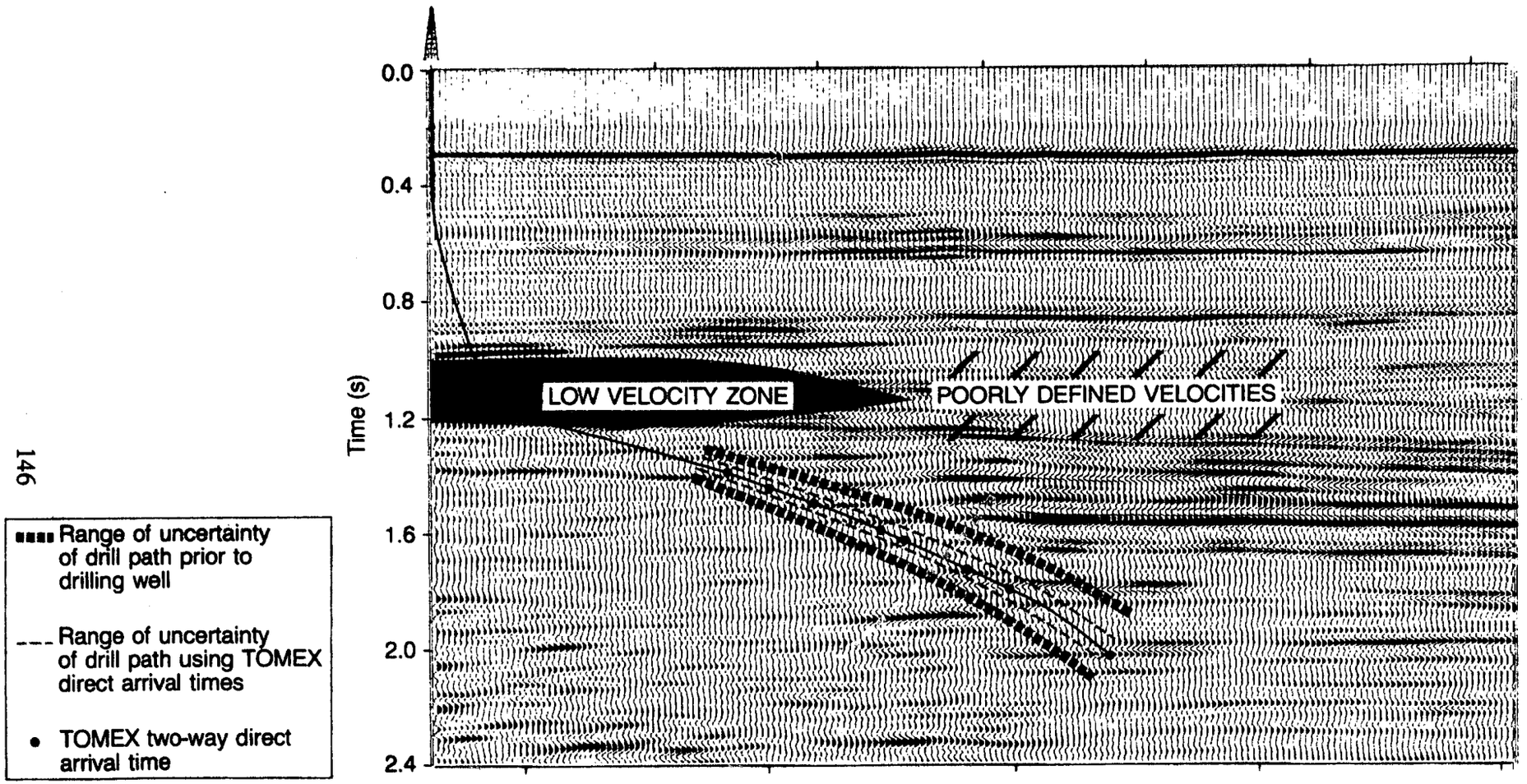

Figure 4-14. Study well 2 well course and uncertainty plotted on seismic two-way time section using drill-bit MWD velocity survey times. The uncertainty in the well course was reduced by 75 percent.

Chapter 4: References

Aki, K. and Richards, P.G., 1980, Quantitative seismology, theory and methods, W.H. Freeman and Co.

Bruce, C.H., 1984, Smectite dehydration-its relation to structural development and hydrocarbon accumulation in Northern Gulf of Mexico Basin, Am. Assn. Petr. Geol., 53, 73-93.

Dragoset, W.H., 1990, Air-gun array specs: a tutorial, Geophysics: The Leading Edge, 9, 1, 24-32.

Godkin, C., 1985, Traveltime inversion of multi-offset vertical seismic profiles, MIT Reservoir Delination-Vertical Seismic Profiling Consortium Annual Report, paper 6.

Goins, N.R., 1987, Velocity surveys in deviated wells, Oil and Gas Journal, October 12, 53-56.

Hardage, B.A., 1985, Vertical seismic profiling, Part A: Principles, Geophysical Press.

Jorden, J.R. and Shirley, O.J., 1966, Application of drilling performance data to overpressure detection, Journal Pet. Tech., 1387-1394.

Manzur, A., 1989, personal communication.

Pennebaker, E.S., 1968, Seismic data indicate depth, magnitude of abnormal pressure, World Oil, 166, 73-78.

Reynolds, E.B., 1970, Predicting overpressure zones with seismic data, World Oil, 171, 73-78.

Salo, E.L. and Schuster, G.T., 1989, Traveltime inversion of both direct and reflected arrivals in vertical seismic profiling data, Geophysics, 54, 1, 49-56.

VanderPoel, N.J. and Cassell, B.R., 1989, Borehole seismic surveys for fault delination in the Dutch North Sea, Geophysics, 54, 9, 1091-1100.

White, J.E., 1965, Seismic waves: radiation, transmission, and attenuation, New York, McGraw-Hill Book Company.

Wyatt, K.D. and Wyatt, S.B., 1981, The determination of subsurface structural information using the vertical seismic profile, presented at the 51st Annual Meeting, Soc. Expl. Geophy., Los Angeles, California.